

Contributions to Models of Single Neuron Computation in Striatum and Cortex

Dissertation
zur
Erlangung des akademischen Grades
Doktor-Ingenieur (Dr.-Ing.)
der Fakultät für Informatik und Elektrotechnik
der Universität Rostock

vorgelegt von
Youwei Zheng
geb. am 14.07.1986 in Shanghai, China
verteidigt am 13.11.2015
abgegeben am 01.05.2015

Gutachter
Prof. Adelinde Uhrmacher (Universität Rostock)
Dr. Lars Schwabe (Xplosion Interactive GmbH)
Prof. D. James Surmeier (Northwestern University)



Selbständigkeitserklärung

Ich, Youwei Zheng, erkläre hiermit, dass ich die vorliegende Dissertation selbstständig, ohne die unerlaubte Hilfe und nur unter Vorlage der angegebenen Literatur und Hilfsmittel angefertigt habe.

----- (Unterschrift)

Rostock, November 18, 2015

Acknowledgement

First and foremost, the deepest gratitude goes to my principal advisor, Prof. Lars Schwabe, for the freedom, the trust and the support he offered me during the entire course of my PhD study, no matter where I was and when I needed him. He has always encouraged me to follow my heart, pursue interdependent collaboration and perform independent research.

Next, I am equally indebted to Prof. Joshua L. Plotkin, who, shared the excitement of my two-year modeling exploration in the striatal electrophysiology. He has been there, while the “chilly” Chi-Town’s blizzard was blowing outside, as an advisor, a colleague and a friend. The appreciation extends to Prof. James Surmeier, who opened to me the door of a successful atmosphere of doing science at the first place.

Also, I thank Dr. Nicolas Le Novère for his generous help and tutoring during my visit in Cambridge. In particular, I am grateful to him for guiding me into the research of Basal Ganglia and Systems Biology. A special acknowledgment must go to Dr. Michele Mattioni, his former PhD student, who had been a brother to me and always did his best to patiently answer my technical questions.

Besides, I would like to express my sincere gratitude to the colleagues in the dIEM oSiRiS. I thank Prof. Adeline Uhrmacher for always understanding my decisions for external visit and supervising the final completion of the thesis. I am thankful to Sigrun Hoffmann for her genuine kindness and support in all sorts of administrative matters from the first minute of my scientific journey.

Finally, I am incredibly indebted to my wife, the mother of my two lovely and precious children, Dr. Yanjiao Cai, who has always been of great support since the very beginning. Her encouragement, quiet patience and unwavering love have been undeniably the fundamentals upon which the past five years of my life have been built.

Abstract

Single neurons are bioelectrical transformers that continuously convert input spike trains encoding sensory perception alongside internal states of the brain into output spike series. The essence of this computational transformation is nonlinearity, realized by a cascade of nonlinear components within the neuronal circuits: dendrite, spine, synapse and synaptic plasticity. A deeper understanding is required of how a single neuron utilizes its nonlinear subcellular computational devices at different neuroanatomical scales to generate complex neuronal dynamics. The results presented in this thesis focus on single neuron computation.

In particular, compartmental models of cortex and striatum are accurately formulated and firmly grounded in the experimental reality of electrophysiology to address two questions:

- i) how striatal projection neurons implement location-dependent dendritic integration to carry out association-based computation. A new multi-compartmental model is introduced to replicate the regenerative characteristics of distal dendrites observed in the experiment. By applying the model to a new set of stimulation protocols, I find that single neuron's richness in associative information processing comes from the interplay between proximal and distal dendrites. This behavior is governed by two cellular anatomical ingredients which are the delicate tapering of single dendritic branch and the length of spine neck;
- ii) how cortical pyramidal neurons strategically exploit the type and location of synaptic contacts to enrich its computational capacities. A new model is validated by the glutamate uncaging experiment that reveals the difference between evoked EPSPs by axo-spinous and axo-shaft synapses. The model prediction demonstrates that distal axo-shaft synapses can gate nonlinear dendritic computing with higher threshold and drive somatic potential with higher gain. The results shade light on the preserved functional role of subcellular components on neuronal computation across different brain regions.

In another separate investigative pursuit, the emphasis is on addressing the question: how point neuron models respond to converging presynaptic inputs to form synaptic patterns, given diverse configurations of input statistics and various kinds of learning rules which are known as spike-timing-dependent plasticity (STDP)? I characterize the potential effects of action potential (AP) dynamics on STDP by exploring a new phenomenological model that incorporates an AP-dependent learning window. The simulation indicates that AP duration is another key factor for insensitizing the postsynaptic neural firing and for controlling the shape of synaptic weight distribution.

Abstract

The models developed in this thesis are not designed to accomplish good performance in model parameter estimation or either modeling formalism, but to predict particular aspects of single neuron computation that involves re-assembling nonlinear fundamental units of neuronal information processing. The results provide strong and testable predictions, which if experimentally validated, could offer new insights into the functional roles of elementary computational units of the brain such as shaft synapses that have not yet been investigated.

Zusammenfassung

Neuronale Zellen transformieren kontinuierliche Signale in diskrete Zeitserien von Aktionspotentialen und kodieren damit Perzeptionen und interne Zustände. Diese Transformationen sind inhärent nicht-linear und werden durch eine Verkettung der Berechnung von einzelnen nicht-linearen Elementen realisiert: Dendriten, Spines und Synapsen. Ein tieferes Verständnis dieser nichtlinearen Prozesse ist notwendig, um die komplexe dynamische Prozesse zu verstehen. In dieser Arbeit ist der Fokus auf den Berechnungen durch einzelne Nervenzellen.

Im Speziellen, werden Kompartiment-Modelle formuliert von Nervenzellen im Kortex und Striatum, die elektrophysiologisch fundiert sind, um spezifische Fragen zu adressieren:

- i) Inwiefern implementieren Projektionen vom Striatum ortsabhängige dendritische Integration, um Assoziationens-basierte Berechnungen zu realisieren? Dazu wird ein neues detailliertes Kompartiment-Modell eingeführt, das experimentelle Ergebnisse reproduziert. Das Modell wird dann verwendet, um die Antworten zu bisher noch nicht experimentell verwendeten Stimulationsprotokollen vorherzusagen. In diesen Studien wurde herausgearbeitet, dass die Interaktion zwischen – bezogen auf den Zellkörper – nahen und fernen Stimulationsorten ausschlaggebend ist. Geometrische Eigenschaften wie die Länge der Spines sind hier zentrale Einflussgrößen;
- ii) Inwiefern nutzen kortikale Zellen den Typ und den Ort, um die durch sie realisierten Berechnungen zu optimieren? Ein neues Modell wurde erarbeitet und dann durch neue Experimente validiert. Das Modell sagt vorher, dass vom Zellkörper entfernte Stimulationen nichtlineare Summationsprozesse mit einem höheren „Gain“ aktivieren können. Diese Simulationsergebnisse legen nahe, dass sub-zelluläre Prozesse einen signifikanten Einfluss auf neuronale Berechnungen haben.

In einer weiteren Studie, die Neuronenmodellen ohne räumliche Ausdehnung beschreiben, wurde untersucht, inwiefern die durch Spike-timing abhängige Plastizität induzierten Änderungen an den synaptischen „Gewichten“ durch die detaillierte Dynamik des postsynaptischen Aktionspotentials beeinflusst werden. Hier wurde ein neues phänomenologisches Modell exploriert. Es konnte gezeigt werden, dass diese Dynamik einen vermutlich bisher ungeahnt großen Einfluss auf die Ensemblestatistik der synaptischen Gewichte der Nervenzellen hat.

Abstract

Alle in dieser Arbeit entwickelten Modelle haben nicht das Ziel, experimentelle Ergebnisse im Detail zu reproduzieren, indem Modellparameter anhand von Daten gefittet werden. Ziel war es, bestimmte Aspekte von experimentellen Daten zu reproduzieren, um Vorhersagen für Experimente abzuleiten und somit Einsichten in die funktionalen (nicht-linearen) Elemente der Verarbeitungsketten zu gewinnen.

Contents

1	Introduction	1
1.1	Motivation and Addressed Questions	1
1.2	Background from Neuroanatomy and Neurophysiology	2
1.3	Road-map of this Dissertation	9
2	Modeling Methods for Neuronal and Synaptic Dynamics	10
2.1	Models of Neurons	10
2.2	Models of Synaptic Kinetics	16
2.3	Models of Bidirectional Synaptic Plasticity	20
2.4	Models of Dendritic Spines	29
3	Extrapolating the Predictions of STDP Models to Disease States	37
3.1	Background and Motivation	38
3.2	Bayesian Network and STDP models	40
3.3	Results	44
3.4	Inference with proposed Bayesian Network	45
3.5	Discussion and Future Vision	48
4	Adapting the Ensemble of Synaptic Weights via STDP by Changing the Action Potential Shape	49
4.1	Background and Motivation	50
4.2	Formulation of dSTDP model	54
4.3	Results	57
4.4	Discussion	68
5	Exploring the Consequences of State Transition in Striatal Principal Neurons by Detailed and Reduced Approaches	70
5.1	State Transitions in Striatal Principal Neurons	71
5.2	The Detailed Compartmental Model	72
5.3	The Reduced Compartmental Model	85
5.4	Discussion	92
6	Differential Spine and Shaft Computations in a Pyramidal Neuron Model	94
6.1	Experimental Background and Modeling Motivation	95

6.2	Model Description	96
6.3	Results	96
6.4	Discussion	105
7	Concluding Remarks	106
7.1	Summary	107
7.2	Towards a Versatile Model of SPN	108
7.3	Synaptic Plasticity and Dendritic Plateau Potentials	114
7.4	Cellular Implementation of Bayesian Computation	116
	Bibliography	118

Chapter 1

Introduction

1.1 Motivation and Addressed Questions

Computational neuroscience is a branch of brain science that uses mathematical modeling to provide either an account or a prediction of the behaviors observed in the corresponding neurobiological system. In this dissertation, the system of interest is individual neurons of different types and the motivation is to better understand how a *single neuron* utilizes its five born-with nonlinear computational devices at different cellular levels and neuroanatomical scales to integrate presynaptic input sequences and generate complex patterns of postsynaptic output spikes. A simulation approach using particular sets of the methods developed by the community of computational neuroscience is adopted throughout to tackle the scientific questions of interest, with the theme of the thesis diverging into two major parts:

In one of the parts, I am interested in studying the cellular mechanisms of two neurophysiological phenomena, building models that can provide reasonable accounts for the experimental observations, and exploring by performing simulations the potential consequences of the modeled mechanistic underpinnings. The model predictions not only provide deeper insights into the inner-working of the studied systems, but also serve as precursors that can offer much clear directions or expectations on the further experiment designs that are of relevance. In order to achieve such a goal, a compartmental modeling approach is exploited, because it permits realistic simulation exploration by taking into account sufficient neuroanatomical and neurobiophysical details together with the desired experimental protocols. For the particular scientific questions in this part, I selected two experimental observations that have been recently published: i) synaptically-evoked plateau potential seen in the principal neurons of a brain region called striatum (SPN: Striatal Principal Neuron) [Plotkin et al., 2011]; ii) the differences found in the evoked EPSPs by the axo-spinous and the axo-shaft synapse in the Layer II pyramidal neurons of another brain region named cortex (CL2PN: Cortical Layer 2 Pyramidal Neuron) [Araya et al., 2006a]. I utilize the built-models then to address two questions that relate to *single neuron* computation: i) how regenerative characteristics of distal dendrites can potentially enable SPNs to efficiently carry out context-dependent information processing in the striatum; ii) how the

axo-spinous and axo-shaft synapse can enrich the computational power of CL2PNs by exerting complementary contributions in the cortex. The developed compartmental models are validated by experimental data and aim at better capturing how the neuronal dendrites, dendritic spines and synaptic components can implement elementary computations within a single neuron.

In the other part, I am intrigued to investigate the emergent properties and functional consequences of *single neuron* computation given a model neuron receives thousands of presynaptic inputs which is experimentally infeasible. For this purpose, a detailed compartmental approach would be computationally too demanding, therefore I adopted a framework developed by [Song et al., 2000] using simplified phenomenological models that neglect in large the biophysical details of a real neuron. The particular neuroscientific questions addressed in this part are: i) how the alteration in the neuronal output dynamics is attributable to the change of the input statistics given spike-timing dependent synaptic plasticity (STDP) [Abbott and Nelson, 2000]; ii) how the outcome of STDP learning can be shaped by an intrinsic neuronal attribute: the duration of action potential. The linkage of the phenomenological models studied in this part to the compartmental models in the other one will be discussed in the final chapter to showcase how these two seemingly diverged approaches converge to a few common contributions to acquiring a deeper comprehension about single neuron computation across different brain regions.

1.2 Background from Neuroanatomy and Neurophysiology

1.2.1 Primer on Neuroanatomy

Brain circuits integrate sensory information, control motor behavior and realize high-level cognitive performance. These functions are implemented by three primary brain divisions: cerebral cortex, basal ganglia and thalamus. The cerebral cortex (the upper portion of cerebrum) is the main integration center which makes sense of particularly all the environmental data that comes into the brain (green-line circled area in Fig. 1.1). For example, the sub-region called somatosensory cortex, located in the parietal lobe, primarily processes neural information sent from the receptors via sensory nerves. The thalamus, an egg-shaped structure sitting right in the middle of the brain, serves as a router that sorts all kinds of senses and distribute them to the designated brain regions (blue-line circled area in Fig. 1.1). The basal ganglia (the base portion of cerebrum) is located below the cerebral cortex, which comprises multiple subcortical nuclei (pinked area in Fig. 1.1), involves complex interaction between inhibitory and excitatory nuclei and controls a wide range of motor functions through the connectivity between cortex and thalamus (see the next section for more details). The striatum, the major focus of this thesis, serves as the principal recipient of input reaching the basal ganglia and thus provides the key substrate for parallel neural integration of information across corticostriatal and thalamostriatal circuits. Besides, striatum is as well the major recipient of dense dopaminergic innervation and therefore responsible

for integrating glutamatergic inputs from cortex and thalamus in tandem with dopaminergic modulation. Its normal neuronal function of discharging action potentials and synaptic function of responding to glutamatergic afferents is crucial for evolutionarily conserved procedural learning and motor planning. In this dissertation, simulation studies are carried out to investigate the profound anatomically-related functional consequences of the location-dependent synaptic integration of corticostriatal contacts (proximal vs. distal dendrite) and the type-dependent of thalamostriatal connections (axo-spinous vs. axo-shaft).

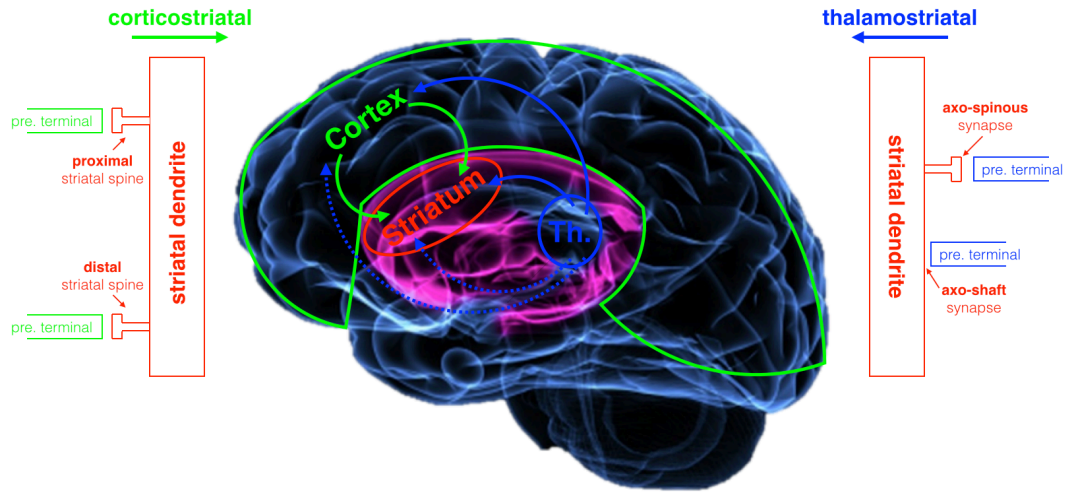


Figure 1.1: **Brain mapping and connectivity between cortex, thalamus and striatum.**

The figure presents an illustrative painting of anatomical connectivity between three brain regions. The excitatory presynaptic terminals from the cortex (green-circled) typically arrive on the striatal spines, of both proximal and distal dendritic locations (left panel). In contrast, the thalamic (blue-circled) postsynaptic axons target the striatal dendrites with the synaptic contacts established, on both dendritic spines and shafts (right panel). The annotation is drawn upon the original background picture, taken from [Kumar and Kotaleski, 2014].

1.2.2 The Importance of Striatum

To undertake both glutamatergic and dopaminergic integrative tasks, the striatum evolutionarily developed a specific type of GABAergic neuron: the striatal projection neuron (SPN), which comprises 95% of the total striatal cell population. Striatum is of paramount importance for the basal ganglia, because it organizes the two gateways to the downstream effectors. SPNs that straightforwardly innervate the GPi/SNr complex (two major output-nuclei of the basal ganglia: internal globus pallidus and substantia nigra reticulata, as depicted in Fig. 1.2), establish the gateway to the “direct” pathway (dSPN) and those innervating the external globus pallidus (GPe) open the gateway to the “indirect” pathway (iSPN). The prevailing model illustrated that these two pathways *separately* control the outgoing information of the basal ganglia: dSPNs gate thalamocortical circuits by flashing a “go” signal whereas iSPNs flash a “no-go” signal by dis-inhibiting the output nuclei. This model is recently enhanced by a piece of *in vivo* evidence from [Cui et al., 2013], which showed

beautifully that dSPNs and iSPNs are concurrently active at movement initiation.

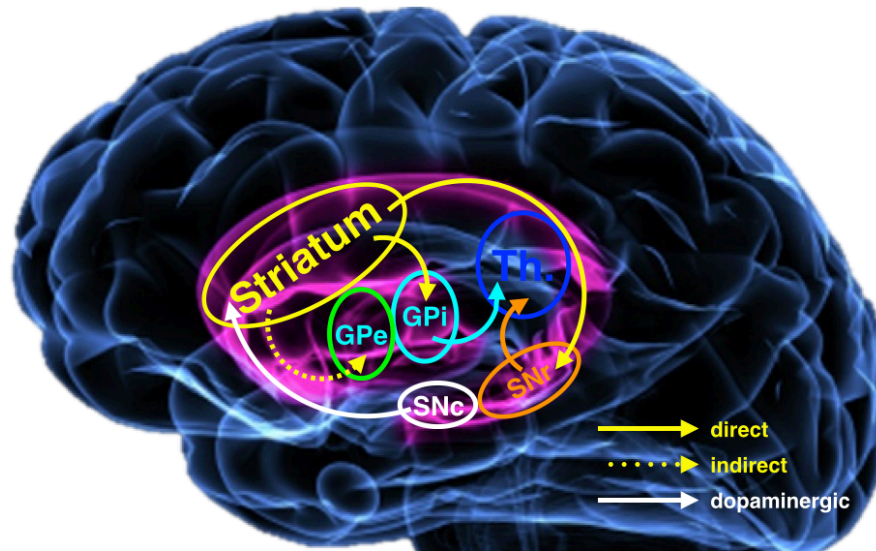


Figure 1.2: The complex interaction between the nuclei within the basal ganglia.

The internal loop of the basal ganglia illustrates three pathways that are of symbolic importance to the striatum-related functions. The striatum connects to SNr (substantia nigra pars reticulata) and GPi (internal globus pallidus) via direct pathway (solid yellow), to external globus pallidus (GPe) establishing one piece of indirect pathway (dashed yellow) and receives dopaminergic innervation (solid white) from SNc (substantia nigra pars compacta).

The importance of the striatum is also highlighted by various neurological diseases of basal ganglia in which the striatum is obviously involved, including Parkinson's, Huntington's and schizophrenia. The neurological pathology of those diseases often manifest themselves as an alteration in dopaminergic afferents to the striatum. In Parkinson's disease, for instance, the alteration leads to a depletion of striatal dopamine and hence results in an imbalance of the combined output by the direct and indirect pathways. More specifically, two neuronal integrative properties of SPNs are impaired: i) the loss of dopaminergic innervation leads to hyper-activity in iSPNs and hypo-activity in dSPNs so that indirect pathway becomes too strong and direct pathway is not strong enough. As a consequence, movement is suppressed by a strong net "no-go" signal delivered by the indirect pathway which disinhibits the output of GPi/SNr complex; ii) dopaminergic dysfunction is associated with the impairment in synaptic integration across corticostriatal and thalamostriatal circuits. It has been shown that hypo-activity in dSPNs is partly caused by the inability to undergo long-term depression (LTD), which is designed to balance the excitatory drive onto iSPNs [Lerner and Kreitzer, 2012]. Taken together, modeling of the electrical property of SPNs are desperately needed not only for having computational models to test experimental hypothesis but also for exploring the possible consequences of disease-induced and pathway-specific physiological alterations.

1.2.3 The Nonlinear Building Blocks of Computation in the Brain

If say our brain is a computer, the question “what is the elemental computational block of the brain” is poorly-formulated compared to a digital one nowadays, and the answer to that question is still rigorously under exploration and hotly open to debate. For over the past six decades since the enunciation by [McCulloch and Pitts, 1943] that the single neuron represents the elementary computational unit of the brain, the principles of neurocomputing have been characterized mainly at the level of individual neurons or neural networks formed by single neurons. The reason for that notion to have prevailed over almost half of the century was simple: First, the noble prize awarded discovery by [Hodgkin and Huxley, 1952] demonstrated the essence of computation: nonlinearity through the interaction between sodium and potassium channels; Second, the invention of the first transformative resistor in the end of 1947 not only has been revolutionizing our fashion of living and our way of using the biological brain until today, but also reinforced the central idea that the complex brain function has to be a result of a cascade or a network of nonlinear elements with naturally-adaptive dynamic nonlinear thresholds: **the neuron**, an electrically excitable nerve cell that can generate action potentials and transmit nervous information through electrical and chemical signals (Fig. 1.3, upper center).

Two neurons mostly communicate via a chemical synapse that comprises a terminal of the presynaptic axon which releases the neurotransmitter, a synaptic cleft and a postsynaptic collection of receptors which receive the transmitted molecule. One single neuron integrates thousands of synaptic inputs from the presynaptic counterpart and then processes this converged information to generate output spikes. Early models of neurons implemented such integration by assuming that each synaptic input represents a linear and passive weight. Indeed, one of the major synaptic receptors, amino-3-hydroxy-5-methyl-4-isoxazolepropionic acid receptor (AMPA), generates nearly instantaneous and passive response depending on the input strength of the presynaptic host. However, it didn't take long for experimentalists to recognize that a synapse is not merely a passive weight-holder, but as well a nonlinear device which is capable of encoding the current state of the neuron by another type of receptor, known as N-methyl-D-aspartate receptor (NMDAR) [Nowak et al., 1984]. The dynamics of NMDAR channels are both input-sensitive, depending on the amount of the neurotransmitter released from the presynaptic terminal, and voltage-dependent, gated jointly by the extracellular concentration of magnesium and the level of membrane potential at the synaptic site [Jahr and Stevens, 1990]. In addition, the biological synapse changes the “weight” nonlinearly on a short timescale depending upon the past history of the spike trains delivered to the synaptic site, thereby constantly redistributing the synaptic efficacy between two neurons [Markram and Tsodyks, 1996] and reading out differently an identical presynaptic neural code [Gerstner et al., 1997]. In contrast to the static synapse, the inherent dynamics of the nonlinear synapse enriches neural networks with a very diverse class of computations on spatiotemporal patterns [Maass and Sontag, 2000] or even dominates synaptic responses to behaviorally relevant natural stimulation patterns [Dobrunz and Stevens, 1999]. In this context, another computational layer of the brain [Zador, 2000] can be indepen-

dently added by the nonlinear synaptic device: **the synapse**, a biophysical conjunction that is specialized to pass electrical and chemical signals between neurons (Fig. 1.3, lower center).

Neurons are distinct from other sphere-shaped or disk-shaped cells, they have a main body (soma), a long slender nerve fibre extended from the soma (axon) and branched protoplasmic protrusions that extrude from the soma (dendrites). Interestingly, most of the synaptic potentials arise not from the main body but from dendritic trees, and then journey along to the soma and the axon. Despite long-held suspicions, the dendrite had a very dull image and was once thought to work in the neural metropolis merely as the bean counter who adds passively the total amount of synaptic beans delivered, until the very beginning of the new era in dendritic biology [Barinaga, 1995]. First, Nobel laureate Bert Sakmann and his postdocs listened carefully to the dendrites through multiple patch clamps and showed that the finely tapered dendritic network is not an *Einbahnstraße* conveying only synaptic messages to the cell body but a two-way *Autobahn* that also back-propagates the signal from soma to the dendritic tip [Stuart and Sakmann, 1994] and elevates dendritic intracellular calcium concentration [Spruston et al., 1995]. Second, active sodium and calcium channels can be recruited to engage in the dendritic integration of synaptic events and participate to boost the diminished impact of many distant synapses on the neuronal output [Magee and Johnston, 1995]. Third, thin dendrite can explode in the local dynamic spike-initiation zone and *spike*, amplifying the somatic voltage in a significantly nonlinear fashion [Schiller et al., 2000]. Fourth, the spatiotemporal sequence of the presynaptic input dotted on the dendritic trunk can underlie our sensory detection of moving objects, such as near or far and left or right etc. Single dendrite can carry out such processing by synaptic sequencing and dendritic discrimination [Branco et al., 2010], thereby serving as the computational primitive for encoding and manipulating sequences. Those findings all had remarkable consequences on the subsequent experimental explorations of dendritic nonlinearity. Importantly, the recent empirical evidence had let the dendrite shed its historical character as a dull linear counter and become a favorite candidate of computational subunits within the single neuron [Polsky et al., 2004]. If the essence of computation is symbolized by the S-shaped sigmoidal function, the single neuron was then fortunate to possess a chain of bidirectional sigmoidal computational primitives: **the dendrite**, the surrounding cytoplasm branched from the soma in complex patterns that serve to receive electrical signals from other neurons and propagate them actively back to the soma (Fig. 1.3, lower left).

The fundamental electronic unit of any modern digital device is the transistor. The neuron cannot be a transistor as it is not having just “three” antennas but connected with too many nerve fibers from all parts of the brain. Likewise is the dendrite. The synapse could *base* a current induced by the conductive pores of biochemical ion channels and *emit* a sizable dendritic postsynaptic potential, however, individual synapse cannot efficiently *collect* the electric energy and function as a voltage-divider even in a simplest serial circuit of dendritic branch. Early in 1888, the great Ramón y Cajal had discovered that the site of synaptic contact from the presynaptic cell is not directly located onto the surface of

the dendrite but onto a tiny membrane protrusion that sticks out from the dendritic shaft [Yuste, 2015]. The discovery of the dendritic spine has since fascinated the physicist, the electrical engineer and the neuroscientist, because: First, the electrical model of a spine realizes the most rudimentary functionality expected from a voltage-separator, by which the levels of membrane potential in the spine head and the dendritic shaft can be relatively independently regulated by the neck in a purely current-based system [Gulledge et al., 2012]. Second, the high degree of spine compartmentalization guarantees a restricted biochemical signaling that permits stimuli-specific pattern recognition and learning [Lee et al., 2009]. Third, the spine is a variable resistor, which can transform its neck resistance to operate with a wide range of impedance levels, thereby providing a structural basis for synaptic efficacy [Matsuzaki et al., 2004] and underlying receptor expression [Matsuzaki et al., 2001]. Fourth, the transformative variable resistor of spine neck could indeed function theoretically as a voltage-divider in the neuronal circuit and such divisive process may be optimized for generating maximal amplification either locally in the spine head or globally in the soma [Segev and Rall, 1988]. Nowadays, as the elementary building block, thousands of transistors are assembled onto one single board of integrated circuits and it might be no wonder that our brain is ubiquitously presented with such neuronal “transistor”: **the spine**, a small membranous protrusion from the dendrite that act to receive single or multiple axonal terminals from other neurons and provide a dendritic neuronal substrate for synaptic strength storage (Fig. 1.3D, upper left).

Synaptic transmission is not linear and the short-term plasticity dominates the neural code used in the signaling between two neurons on short time scales due to for example, uncertainty in the neurotransmitter release [Tsodyks and Markram, 1997]. If neurons, synapses and dendrites can all accomplish their assigned batches of brain computation, how is then the computed result saved and retrieved the next time with less neural effort? *“the persistence or repetition of a reverberatory activity tends to induce lasting cellular changes that add to its stability.”* In 1949, Donald Hebb conjectured that repetitive interexchange of neural activity leaves and consolidates a trace at the synaptic location where the computation occurs [Hebb, 1949]. The first shred of evidence of such speculated synaptic modification was after 25 years obtained by [Bliss and Lomo, 1973] who demonstrated for the first time that synapses do modify, in a long-term manner. Later, the work from another Nobel laureate Eric Kandel on one of the simplest brain but the largest neuron in the animal kingdom revealed that it was indeed the modified synaptic connection between the sensory and motor neurons that were responsible for long-term memory storage and long-term differential behaviors of *Aplysia* [Bailey and Kandel, 2008]. Moreover, Hebbian notion of synaptically-controlled association “firing together wire together” was confirmed by experimental pairing of synaptic input and action potential output signals [Magee and Johnston, 1997]. Furthermore, suggested by network simulations, the nonrandom connectivity map formed by the evolved synaptic weight may reflect sensory coding. Unidirectional strong connections can store input patterns presented in the temporal scheme and bidirectional stable associations are established to memorize the rate-coded stimuli [Clopath et al., 2010]. If the biological

neural network implements in part the biologically-inspired back-propagation algorithm used in the artificial neural network, the error correction is computed with diverse computational parameters of multiple dimensions [Markram et al., 2011]. None of them appeared to be fit-able into linear models and this complicated nonlinear function of learning rate that awaits theoreticians to formulate its general principles is: **synaptic plasticity**, a plastic attribute of a synapse that can either increase or decrease its response to the incoming electrical and chemical signals (Fig. 1.3, right panel).

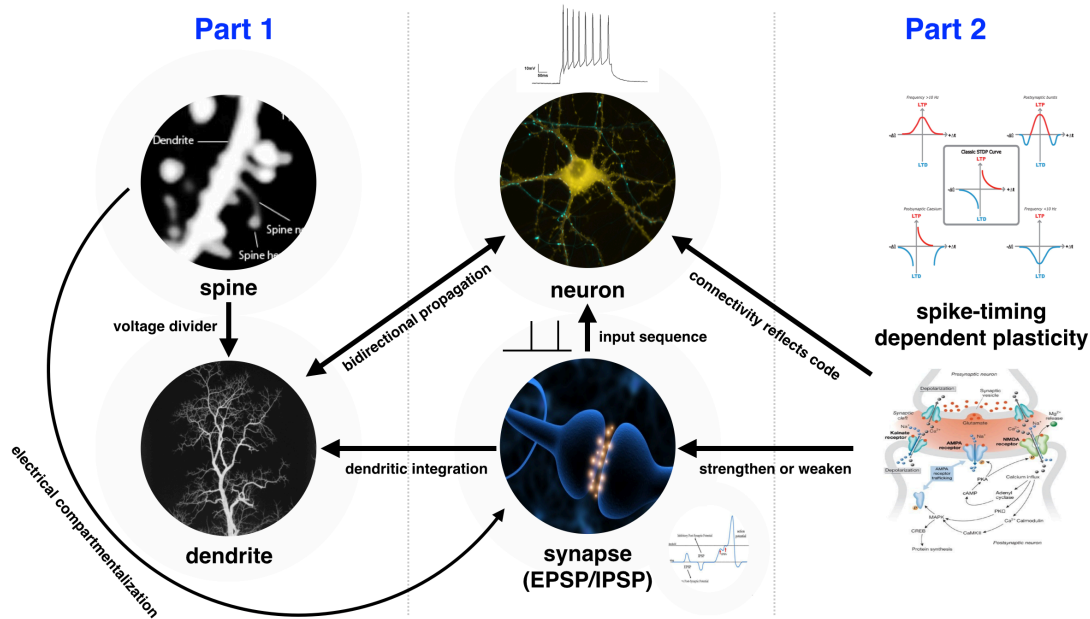


Figure 1.3: The five nonlinear elementary elements of brain computation.

This figure illustrates an inventory of the cellular components that function cooperatively to realize single neuron computation and their relations to the two parts of the thesis.

1.3 Road-map of this Dissertation

The following chapters are adapted from the papers that were published during the completion of the thesis. Each chapter starts with a preamble together with the particular domain knowledge and the modeling motivation by the time the research was initiated, and then lays out the major results. The last chapter summarizes the main contributions of each study and discusses the openings for future works.

Chapter 3: Extrapolating the Predictions of STDP Models to Disease States

This chapter features a workflow that extracts qualitative findings from simulation results and an attempt to represent new knowledge using Bayesian inference. The particular example considered here is the potential effects of various phenomenological STDP models on a single model neuron in the condition of paroxysmal brain activity such as epileptic seizures. The content is adapted from [Zheng and Schwabe, 2011a].

Chapter 4: Adapting the Ensemble of Synaptic Weights via STDP by Changing the Action Potential Shape

This chapter proposes a novel phenomenological STDP model that depresses the synapse using an AP duration dependent LTD window and induces the potentiation of synaptic strength when presynaptic spikes arrive before and during a postsynaptic AP (dSTDP). The model produces a unimodal distribution of synaptic weights and regulates the postsynaptic spiking in a way that the neuronal response is sensitive to the signal but resistant to the noise. The content is adapted from [Zheng and Schwabe, 2013b] and [Zheng and Schwabe, 2014].

Chapter 5: Exploring the Consequences of State Transition in Striatal Principal Neurons by Detailed and Reduced Modeling Approaches

This chapter aims at realistic implementations of single neuron computing in a striatal neuron. Compartmental models are built to validate *in-vitro* experimental data and then used to simulate the functional consequences of the spatiotemporal synaptic signals impinging on the proximal and distal dendrites.

The content is adapted from [Zheng and Schwabe, 2013a] and [Zheng et al., 2014].

Chapter 6: Differential Spine and Shaft Computations in a Pyramidal Neuron Model

This chapter presents a pyramidal neuron model that accurately replicates the *type*-dependent synaptic integration observed in [Araya et al., 2006a], axo-dendritic vs. axo-spinous synapses. The results demonstrate that distal axo-dendritic synapses can gate nonlinear dendritic computing with higher threshold and drive somatic potential with higher gain.

The content is adapted from an accepted manuscript [Zheng and Schwabe, 2015].

Chapter 7: Concluding Remarks

Chapter 2

Modeling Methods for Neuronal and Synaptic Dynamics

2.1 Models of Neurons

The core of modeling the basic electrical dynamics of individual neurons is anchored in the models of passive membrane. The complex interplay of diverse ion mechanisms results in a voltage difference across the membrane, with the inside potential conventionally denoted being negative relative to the outside. The neuronal membrane that separates the intercellular material from the extracellular environment is a lipid bilayer, which can be modeled as a capacitor, that usually has a constant capacitance C_m . In addition, this bilayer functions in part as a resistor whose passive component usually has a resistance R_m . Thus, based on the conceptualization of a lipid bilayer, the simplest model of a passive membrane is a linear electrical circuit with a capacitor and a resistor connected in parallel (Fig. 2.1). Injecting a time-dependent current I_{inj} into this RC circuit causes a voltage change inside the membrane, that is attributable to the respective resistive and capacitive currents. The resulting membrane potential u can be mathematically described by Eq. 2.1:

$$C_m \frac{du}{dt} + \frac{u - u^{\text{rest}}}{R_m} = I_{inj} \quad (2.1)$$

where u^{rest} represents the resting potential of the membrane. By re-arranging the term and using the membrane time constant τ_m as the production of resistance R_m and capacitance C_m , Eq. 2.2 is obtained, which is the form more commonly used in the simulation studies.

$$\tau_m \frac{du}{dt} = -(u - u^{\text{rest}}) + R_m I_{inj} \quad (2.2)$$

2.1.1 Point Models

Models that describe the dynamics of membrane potential using a single variable u for denoting the membrane potential, are called point models. Often, those models involve no spatial variables, and thus are also referred to as isopotential models. In what follows, I recapitulate three major formalisms that are widely used in modeling individual point neurons.

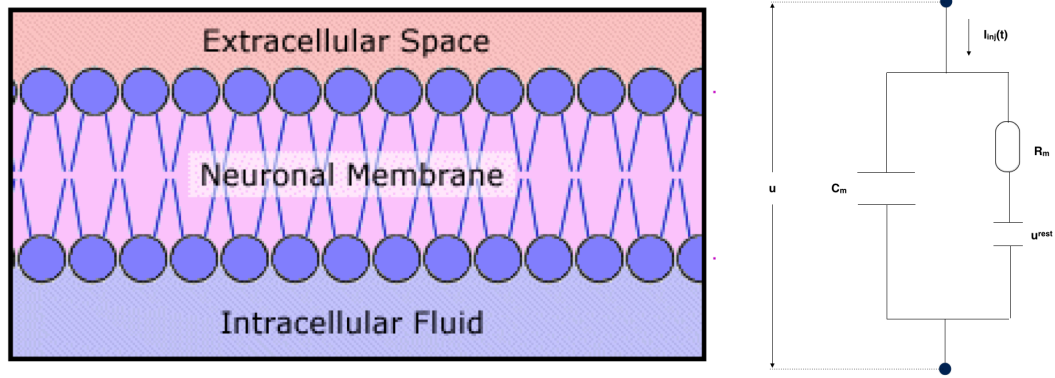


Figure 2.1: Simple RC circuit model of neuronal membrane.

The left panel illustrates a biological neuronal membrane and the right presents the simple RC circuit that models the essential voltage dynamics across the membrane.

Integrate-and-Fire (IaF) Formalism

A model, that takes IaF formalism, does not incorporate the biophysical mechanisms that contribute to the formation of an action potential and its corresponding shape (e.g., the amplitude and the duration). In an IaF model, individual action potential is only described as an electrical pulse. Each pulse arriving onto the postsynaptic neuron from a presynaptic one, causes an electrical response which can either be excitatory or inhibitory postsynaptic potential (EPSP or IPSP), depending on the nature of presynaptic signaling neuron. The “faked” action potential is triggered in an IaF model when the membrane potential reaches a *threshold* value. Therefore, an IaF model can be understood intuitively as a passive membrane model (Eq. 2.2) combined with an artificial spiking threshold. For a constant input current, it can be expected that an IaF model would spike linearly and regularly with a fixed inter-spike interval as plotted in Fig. 2.2A.

Everything in an IaF model described above is linear except at the threshold. However, its linear nature can't account for a large body of *nonlinear* subthreshold responses. For this purpose, a more generalized idea of IaF formalism was proposed to describe the dynamics of membrane potential u_m by introducing nonlinear terms in the differential equation, such as $F(u_m)$ in Eq. 2.3:

$$\tau_m \frac{du}{dt} = F(u) + R_m i_{inj} \quad (2.3)$$

One of the best-studied functions in the field of computational neuroscience is the exponential function. For example, an Adaptive Exponential Integrate-and-Fire Model (aEIF) was shown to reliably predict in-vitro recorded neuronal activity [Brette and Gerstner, 2005]. The nonlinear function $F(u)$ can be then formulated with an abstract form as described in Eq. 2.4 which has a linear part that is identical to the term used in an IaF, and a nonlinear component by which the curve bends rapidly near the spiking threshold:

$$F(u) = -(u - u^{rest}) + c_0 \exp(u - V_{th}) \quad (2.4)$$

where c_0 is some coefficient and V_{th} is the threshold. As a consequence, given an identical input current, aEIF model elicits spikes with an adaptive mechanism, extending the inter-spike interval (Fig. 2.2B). It is worth mentioning that the championship model of the international competition launched by International Neuroinformatics Coordinating Facility that predicted correctly 59.6% and 81.6% of the spike times of two neuronal recordings, was implemented by adopting a very similar modeling strategy with a moving threshold [Kobayashi et al., 2009].

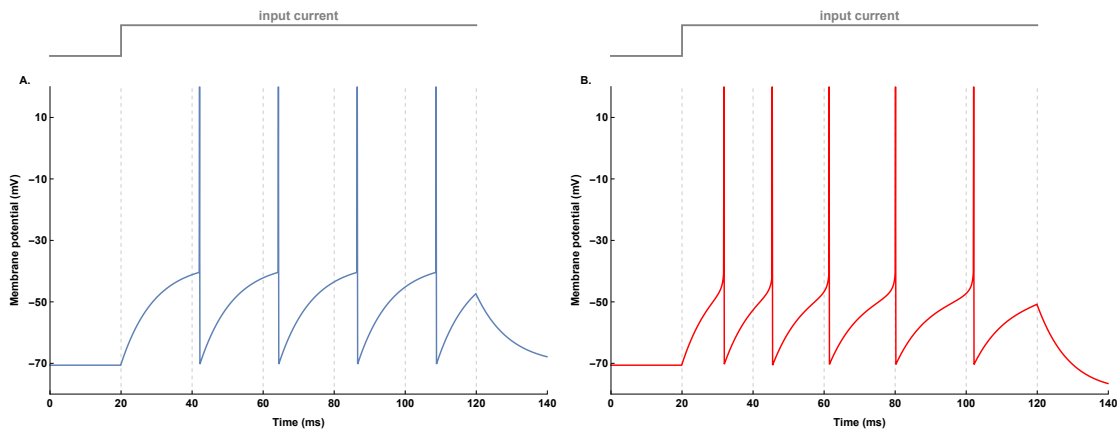


Figure 2.2: **Differential spiking behaviors given identical current injection.**

A. The IaF model generates regular spiking.

B. In contrast, the aEIF model elicits spikes that are adapting to the injected current.

The neuron model is adapted from [Brette and Gerstner, 2005] and the simulation is performed using the Brian Simulator [Goodman and Brette, 2008].

Izhikevich Formalism

The classic one-dimensional IaF model is one of the most widely used formalism in the community of computational neuroscience. It works as a simple integrator and can exhibit tonic spikes with constant firing frequency as shown in Fig. 2.2A. However, it is probably the worst model to use in simulations because it cannot replicate many prominent features of spiking neurons. Adding another dimension to it, the adaptive IaF does endow the model with spike-frequency adaption as shown in Fig. 2.2B. Nevertheless, aEIF model still lacks a number of fundamental properties of spiking neurons. Real biological neurons feature rich firing patterns and complex spiking dynamics as reviewed in [Izhikevich, 2004], including regular tonic spiking, burst spiking, spike frequency adaptation, inhibition-induced spiking and etc. It is desirable to have a “versatile” spiking model to explore the temporal structure of spike trains and how a neural network might process information using both spike timing and frequency. For this purpose, a model that can replicate more than 20 important neuro-computational features was developed by Izhikevich using bifurcation theory and normal

form reduction [Izhikevich, 2003]. The formalism can be described by Eq. 2.5:

$$\begin{aligned}\frac{du}{dt} &= 0.04u^2 + 5u + 140 - \theta + I \\ \frac{d\theta}{dt} &= a(bu - \theta)\end{aligned}\tag{2.5}$$

with an after-spike resetting:

$$\text{if } u \geq 30 \text{ mV, then } \begin{cases} u \leftarrow c \\ \theta \leftarrow \theta + d \end{cases}\tag{2.6}$$

where variable u represents the membrane potential and θ represents a membrane recovery variable that simulates the potassium activation current and sodium inactivation current. The model can obtain a variety of firing patterns of all known types of cortical neurons with differentially tuned parameters a, b, c, d which are dimensionless.

Hodgkin-and-Huxley Formalism

Theoreticians favor the classic IaF or Izhikevich simple neuron models with few parameters that are amenable to analytical analysis. In contrast, electrophysiologists typically prefer biophysical models that are implemented with the notion of opening and closing ion channels. It is not only because this notion shapes our current understanding of how action potentials are generated but also because the model parameters are biophysically meaningful and measurable directly from experimental procedures. The classic formalism of modeling ion channel is the famous Hodgkin-and-Huxley (HH) equations [Hodgkin and Huxley, 1952]. The HH-formalism extended the RC circuit of a passive membrane (Fig. 2.1) to an equivalent circuit (Fig. 2.3) in which three types of ion currents flow in and out of the membrane: sodium current (Na^+), potassium current (K^+) and a leak current (L) which represents a phenomenological current that summarizes all other channels that might give their minor ionic contributions. Eq. 2.7 describes how the membrane potential u changes in response to the three currents multiplied by their respective voltage-dependent resistors which are $g_{\text{Na}}(u)$, $g_{\text{K}}(u)$ and $g_{\text{L}}(u)$. The potential differences between the membrane potential and respective ion battery potential are denoted as E_{Na} , E_{K} and E_{L} .

$$C \frac{du}{dt} = -g_{\text{Na}}(u)(u - E_{\text{Na}}) - g_{\text{K}}(u)(u - E_{\text{K}}) - g_{\text{L}}(u)(u - E_{\text{L}}) + I_{\text{ext}}\tag{2.7}$$

The opening and closing dynamics of ionic resistors are modeled by a gate variable x (m, n and h in HH equations) with a rate function as Eq. 2.8:

$$\frac{dx}{dt} = \alpha_x(u)(1 - x) - \beta_x(u)x\tag{2.8}$$

where x is a dimensionless value between zero and one, denoting the probability of the corresponding gate is open. $\alpha_x(u)$ and $\beta_x(u)$ are dynamic rate “constants”, depending on the membrane potential u .

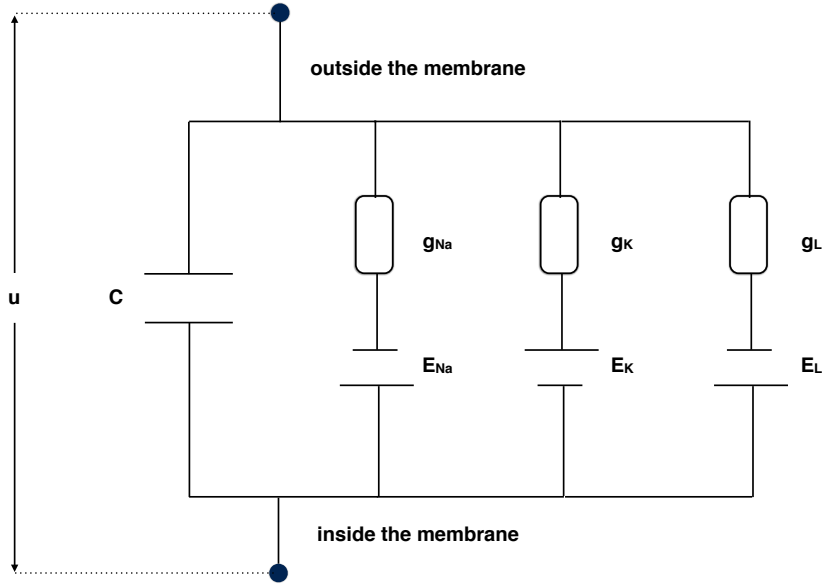


Figure 2.3: **The conceptual model of HH equations.** See text for details.

In the process of parameter fitting, Hodgkin and Huxley found that the K^+ activation curve was best fitted by 4 activating gates n with the form n^4 and the Na^+ was best fitted by 3 activating gates m and 1 inactivating gate h with the form m^3h . Fig. 2.4 illustrates the numerical solutions of HH equations listed in Eq. 2.9. In contrary to the artificial spike generated in an IaF model, the action potential simulated by HH equations is a smooth curve that possesses realistic shape and duration with no strictly-defined threshold defined.

$$\begin{aligned}
 C \frac{du}{dt} &= -\bar{g}_{Na} m^3 h (u - E_{Na}) - \bar{g}_K n^4 (u - E_K) - \bar{g}_L (u - E_L) + I_{ext} \\
 \frac{dm}{dt} &= \alpha_m(u)(1 - m) - \beta_m(u)m \\
 \frac{dn}{dt} &= \alpha_n(u)(1 - n) - \beta_n(u)n \\
 \frac{dh}{dt} &= \alpha_h(u)(1 - h) - \beta_h(u)h
 \end{aligned} \tag{2.9}$$

The HH formalism provides for every electrophysiologist a framework to mathematically express the dynamics of individual ion channel. The key step in this framework is to figure out each rate “constant” x . Eq. 2.8 can be expressed in a different manner as in Eq. 2.10:

$$\frac{dx}{dt} = \frac{1}{\tau_x} (x^\infty - x) \tag{2.10}$$

whose analytical solution $x(t)$ with an initial value $x = x_0$ is Eq. 2.11:

$$x(t) = x^\infty + \exp(t/\tau_x)(x_0 - x^\infty) \tag{2.11}$$

and the voltage-dependent rate “constants” α_x and β_x can be expressed by the time constant τ_x and the finite conductance x^∞ which are also sensitive to the voltage, by Eq. 2.12:

$$\begin{aligned}
 \alpha_x &= x^\infty / \tau_x \\
 \beta_x &= (1 - x^\infty) / \tau_x
 \end{aligned} \tag{2.12}$$

Equipped with HH equations, modeling ion channels is for an electrophysiologist equivalent to determining experimentally the time constant and finite conductance of a specific one. In the simulation of an ion channel, a common strategy is to fit the finite conductances using Boltzmann equation with the form of Eq. 2.13 and directly use the tabulated experimentally-measured time constants. The lower panels of Fig. 2.4 plot the analytical expressions of x_∞ and τ_x for n, m, h with original HH parameters.

$$x^\infty(u) = \frac{1}{1 + \exp[(-1)^\theta(u - u_{1/2})/u_s]} \quad (2.13)$$

where θ determines whether it is activation ($\theta = 1$) or inactivation ($\theta = 2$).

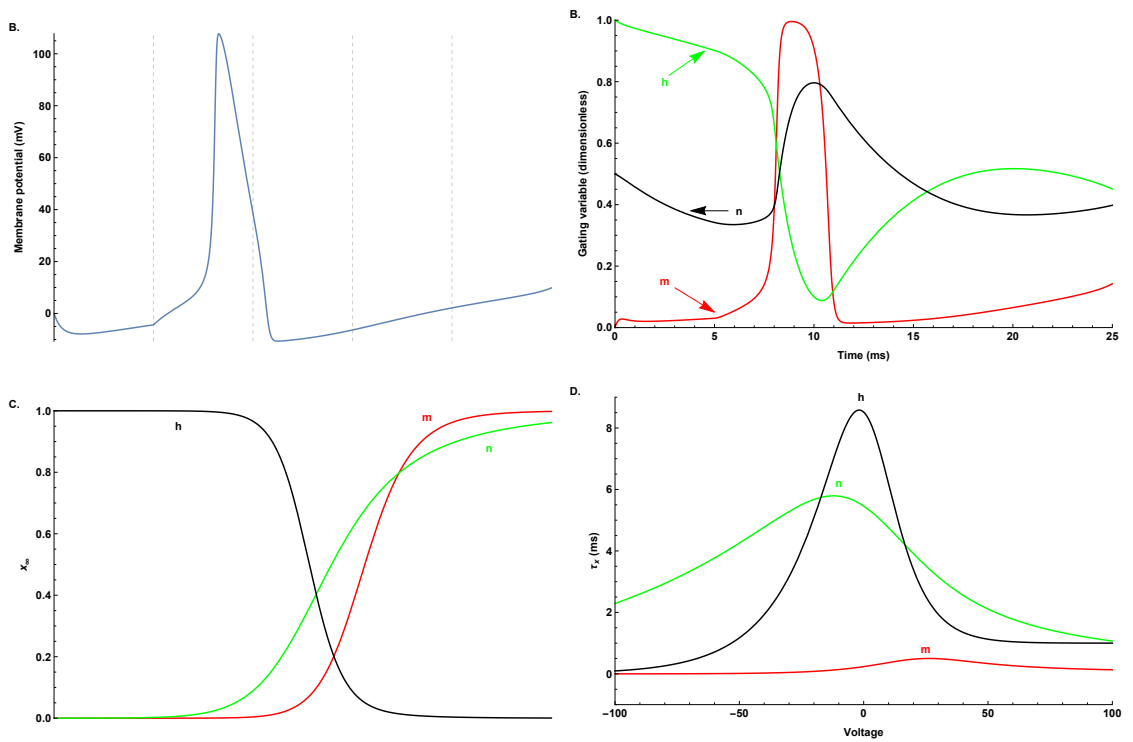


Figure 2.4: **Simulation of the original Hodgkin-Huxley model.**

A & B. The voltage and dynamics of gating variables of a single action potential.

C & D. x_∞ and τ_x plotted with HH parameters.

The simulation was performed by solving Eq. 2.9 with *NSolve* in Mathematica. The parameters and the dynamics of rate constants are directly taken from [Doi et al., 2010].

In summary, the remarkable contribution of Hodgkin and Huxley formalism is that it told us for each possible ion channel that might exist in a biological neuron, we could write down a set of coupled differential equations to describe its voltage dynamics and then simulate its behaviors in an integrated neuronal system. This classic modeling formalism is not just a reference, but is still widely in use today.

2.1.2 Compartmental Models

The RC circuit and HH framework provide the rudimentary methods to map a conceptual neuron model to its computational representation. However, the aforescribed point neuron method can only capture the neuronal process with continuous variables *in time* and a biological neuron does not live in an abstract point-space, but rather in an extremely complex 3D construction with delicate morphology and geometry. Such intricate spatial arrangement anchors every aspect of the neuronal integration and a spatial parameter has to be introduced in the model to capture the spread of electrical signals from one point to another in the branched dendritic architecture (the modeling of axonal structure is omitted in this thesis). For this purpose, the cable theory, first applied to the transatlantic telegraph cable, was then used to study the electrical conducting core of dendrites. In addition to the *transversal* current that flows across the membrane (Fig. 2.1), the cable theory incorporates the *longitudinal* current into the model of the ionic current flow in the neuronal conductor, where the space parameter is usually denoted as x with a unit of μm .

In the cable theory, the current flow through each discretized node inside a neuronal space is illustrated in Fig. 2.5. According to the Kirchhoff's current law (KCL), the algebraic sum of the external, longitudinal and transversal currents at each node shall be zero:

$$I_{ext}(t, x) + \frac{u(t, x + dx) - u(t, x)}{R_L} - I_T(t, x) - \frac{u(t, x) - u(t, x - dx)}{R_L} = 0 \quad (2.14)$$

where the transversal current represents the sum of all the ionic currents “trans-across” the membrane:

$$I_T(t, x) = C \frac{u(t, x)}{R_L} + \sum I_{ion}(t, x) \quad (2.15)$$

Further derivation and simplification lead to the textbook form of cable equation [Rall, 1977]. When it comes to the simulation of cable equation, the numerical details are often taken care of by domain-specific simulation tools such as NEURON [Carnevale and Hines, 2006].

2.2 Models of Synaptic Kinetics

Conductance-based current equation

The synaptic current $I_{syn}(t)$ can be described by the product of a time-dependent channel conductance $g_{syn}(t)$ and an electrical drive originated from the difference between momentary membrane potential $u(t)$ and synaptic reversal potential E_{syn} :

$$I_{syn}(t) = g_{syn}(t)(u(t) - E_{syn}) \quad (2.16)$$

Instantaneous Rise and Exponential Decay

The simplest choice for a time-varying conductance is an exponential decay as in Eq. 2.17:

$$g_{syn}(t) = \bar{g}_{syn} \exp[-(t - t_0)/\tau_d] \mathcal{H}(t - t_0) \quad (2.17)$$

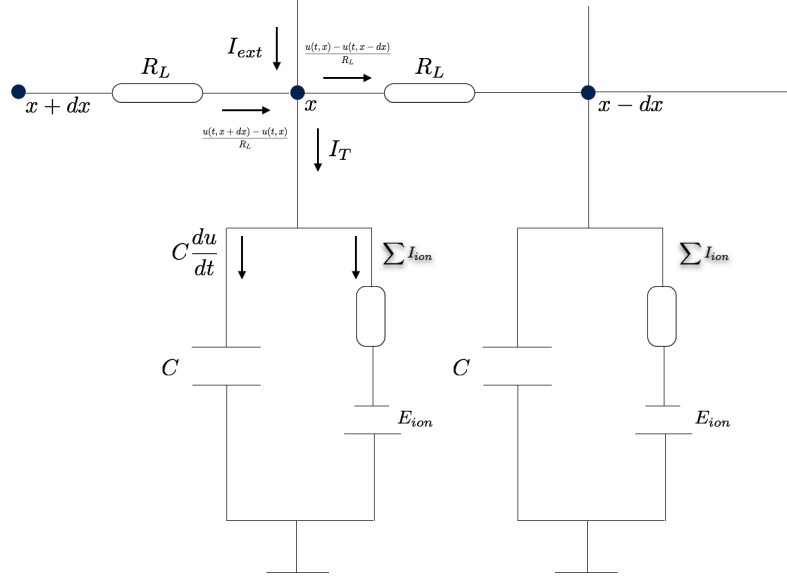


Figure 2.5: **The circuit for a neuronal cable.** See text for details.

with τ_d as the *decay* time constant and \bar{g}_{syn} as finite synaptic conductance. The arrival time of the presynaptic action potential is denoted by t_0 and $\mathcal{H}(t)$ is the Heaviside step function. The conductance $g_{syn}(t)$ peaks instantaneously at t_0 .

Alpha Function

However, for real synapses, the rising phase of synaptic conductance is not instantaneous but has a finite duration, which could have strong effects on network dynamics. The Alpha function can describe such a conductive change with a non-instantaneous rise as in Eq. 2.18:

$$g_{syn}(t) = \bar{g}_{syn}((t - t_0)/\tau) \exp[1 - ((t - t_0)/\tau)] \mathcal{H}(t - t_0) \quad (2.18)$$

with a time constant τ and $g_{syn}(t)$ peaks when $t - t_0 = \tau$.

Separating Rising and Decay Phases

One drawback of the Alpha function is that it has only a single time constant τ , and thus the time courses of the rise and decay phase of $g_{syn}(t)$ cannot be modeled independently. Often a postsynaptic current is made up of at least two different components, a fast rising phase with a much slower decay phase. Therefore, a more general description of synaptic conductance can be written using the double-exponential function as Eq. 2.19, which allows two time constants τ_{rise} and τ_{decay} to be set independently .

$$\begin{aligned} g_{syn}(t) &= \bar{g}_{syn} N f(t) \\ t_{peak} &= t_0 + \frac{\tau_{rise} \tau_{decay}}{\tau_{decay} - \tau_{rise}} \log\left(\frac{\tau_{decay}}{\tau_{rise}}\right) \\ f(t) &= \exp\left(-\frac{t - t_0}{\tau_d}\right) - \exp\left(-\frac{t - t_0}{\tau_r}\right) \\ N &= f(t_{peak}) \end{aligned} \quad (2.19)$$

where the conductance peaks at t_{peak} and N is a normalization factor to ensure that the peak conductance equals to \bar{g}_{syn} .

Voltage Dependence

The NMDAR-mediated conductance depends on the postsynaptic membrane potential u due to a blockade of positively charged magnesium. It is almost completely closed at the resting membrane potential, and the fraction of the channel that is not blocked can be modeled as Eq. 2.20:

$$B(u) = \frac{1}{1 + \exp(-au)[Mg]/b} \quad (2.20)$$

where $[Mg]$ is the extracellular magnesium concentration, usually 1 mM. a and b are the model parameters that need to be fit to the specific experimental data. Thus, the net synaptic current of such voltage-dependent NMDAR channel is given by Eq. 2.21:

$$I_{nmda}(t) = g_{nmda}(t)B(u)(u - E_{nmda}) \quad (2.21)$$

The resulting synaptic integration is nonlinear, which has wide implications for the dendritic plateau potentials in the striatal neuron (Chapter 5) and the dendritic supralinear summation in the neocortical neuron (Chapter 6). The nonlinear feature produced by Eq. 2.21 is illustrated in Fig. 2.6.

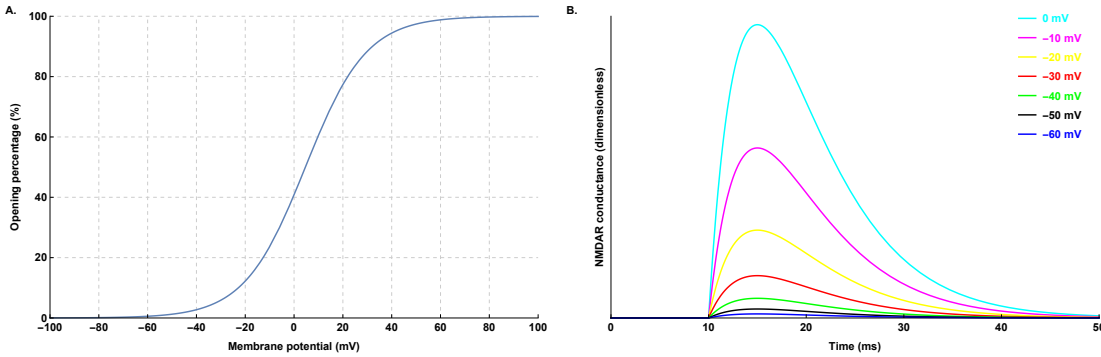


Figure 2.6: **Nonlinear feature of NMDAR conductance.**

A. The fraction curve plotted using Eq. 2.20, where the parameters $a = 0.08$ and $b = 0.69$ are taken from [Grunditz et al., 2008].

B. The NMDAR conductances under a range of voltage levels are simulated by Eq. 2.21.

Markov Models

The aforementioned models are simplified phenomenological models of synapses, they don't tell us much about the underlying mechanism of synaptic transmission. Besides, another major drawback of those models is that there is no criteria for the natural saturation of the conductance. Ideally, a model of synaptic transmission shall incorporate all the three major activities of transmitter: release, diffuse and binding.

Detailed models for the release and diffusion are desirable, but they are usually very expensive computationally. Moreover, the transmitter dynamics is several magnitudes faster than the receptor dynamics. For this reason, it often suffices, when it comes to modeling the post-synaptic effect of synaptic transmission, to assume that the concentration change of neurotransmitter occurs as a pulse [Destexhe et al., 1994a], and the Markov formalism of synaptic model then focuses exclusively on the process of receptor binding [Destexhe et al., 1994b].

The binding process follows a first-order kinetics:



where R and T are respectively the closed receptor and unbound neurotransmitter. k_f and k_b are forward and backward rate constants, and o represents the fraction of opening receptors. The kinetics and corresponding postsynaptic current are described by Eq. 2.23:

$$\begin{aligned} o'(t) &= k_f[T](1 - o(t)) - k_b o(t) \\ I_{syn}(t) &= \bar{g}_{syn} o(t) [u_{syn}(t) - E_{syn}] \end{aligned} \quad (2.23)$$

where $[T]$ is the concentration of neurotransmitter.

Fig. 2.7 illustrates the simulation results of Eq. 2.23: the transmitter concentration dynamics (black), the opening ratio of the channel (red) and the evoked postsynaptic membrane potential (green). In this thesis, a detailed 10-state Markov model was taken to simulate the dynamics of NMDAR channels, which was validated by the opening responses with both brief and sustained applications of glutamate [Kampa et al., 2004].

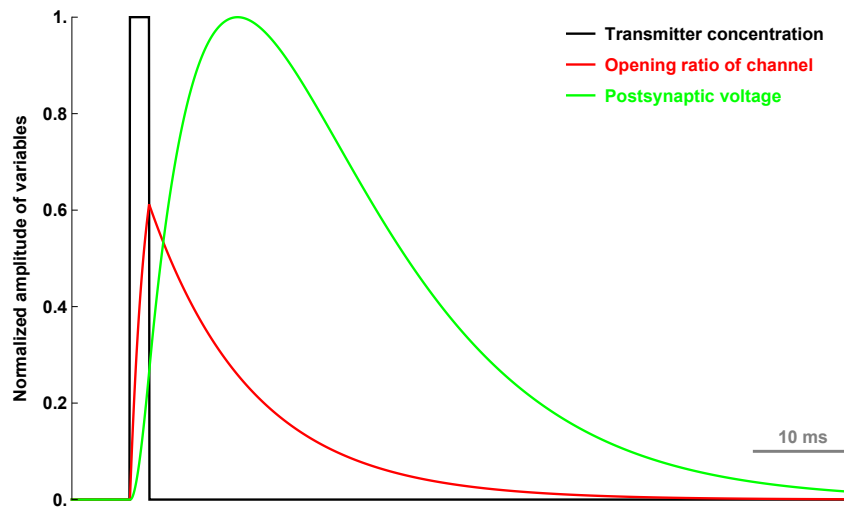


Figure 2.7: The normalized variable dynamics of a simplified Markov model for synaptic transmission. See text for details.

2.3 Models of Bidirectional Synaptic Plasticity

Bidirectional long-term changes in synaptic strength have been reported and described for many neural systems and it is currently believed that synaptic plasticity is essential for the organization and function of neural circuits and provides an activity-dependent mechanism that underlies learning and memory. Rate-based computational models of synaptic plasticity have been intensively studied during the 1980s and 1990s. Numerous attempts have been made to build models that explore the rules of long-term synaptic modification, respectively long-term potentiation (LTP) and long-term depression (LTD). One of the most successful formulations of rate models has been the BCM model which explained an abundance of experimental evidences obtained in preparations of hippocampus and visual cortex [Bienenstock et al., 1982]. Other forms of plasticity such as meta-plasticity [Abraham, 2008] or homeostatic synaptic scaling [Turrigiano, 2008] play also important roles in adjusting synaptic strength, regulating spiking rate and organizing neural circuits. Recently, experimental works from many laboratories across the world have confirmed that the precise timing of spikes in the pre- and postsynaptic neurons is another critical determinant of long-term synaptic plasticity in various brain areas, since the “first” publication [Markram et al., 1997]. The mathematical modeling of this *new* form of synaptic modification, termed as spike-timing-dependent plasticity (STDP), has been hot in the past decade [Caporale and Dan, 2008]. In the following text of the section, I review 3 types of major frameworks modeling bidirectional synaptic plasticity.

2.3.1 Timing Model

One of the simplest models is based on a framework in which the amount of synaptic modification is determined *solely* by the time interval between each pair of pre- and postsynaptic spikes using a phenomenological STDP curve which is extracted directly from the experiments. A typical spike timing model of this kind can be best exemplified by the Song model [Song et al., 2000]. Synaptic modification is induced in the model using a so-called STDP learning window function $F(\Delta t)$ as in Eq. 2.24, which is illustrated in Fig. 2.8:

$$F(\Delta t) = \begin{cases} A_+ \exp(\Delta t / \tau_+), & \Delta t < 0 \\ -A_- \exp(\Delta t / \tau_-), & \Delta t \geq 0 \end{cases} \quad (2.24)$$

where Δt is the time difference between each single pair of spikes. A_+ and A_- determine the maximum amount of synaptic modification per pair for potentiation and depression. The presynaptic spikes in this framework are usually input by some statistical models and the plasticity function is then coupled and simulated together with a neuron model which provides the postsynaptic spikes. The Song model demonstrated that the dependence of synaptic plasticity on spike timing can induce competition between synapses in evoking postsynaptic action potentials and thus lead to competitive Hebbian learning without requiring additional global mechanisms. Moreover, this STDP rule stabilizes the firing rate of the postsynaptic neuron while equilibrating the distribution of synaptic strengths. Furthermore, one of the consequences of the induced learning is to strengthen correlated presynap-

tic neural groups with short latencies in firing the postsynaptic neuron and weaken those with long latencies. Fig. 2.9 illustrates that the effect of correlation-based synaptic modification accompanied by STDP learning is a quicker and stronger postsynaptic response. In summary, the timing model provides a novel and straightforward framework to study the effect of synaptic plasticity that is attributable to the pre- and post-synaptic timings. Because of its simplicity, it is compatible with both current-based [Babadi and Abbott, 2010] and conductance-based [Billings and van Rossum, 2009] neuron models. In addition, it can be easily implemented in a neural network model to explore, for instance, cortical development and remapping through STDP [Song and Abbott, 2001].

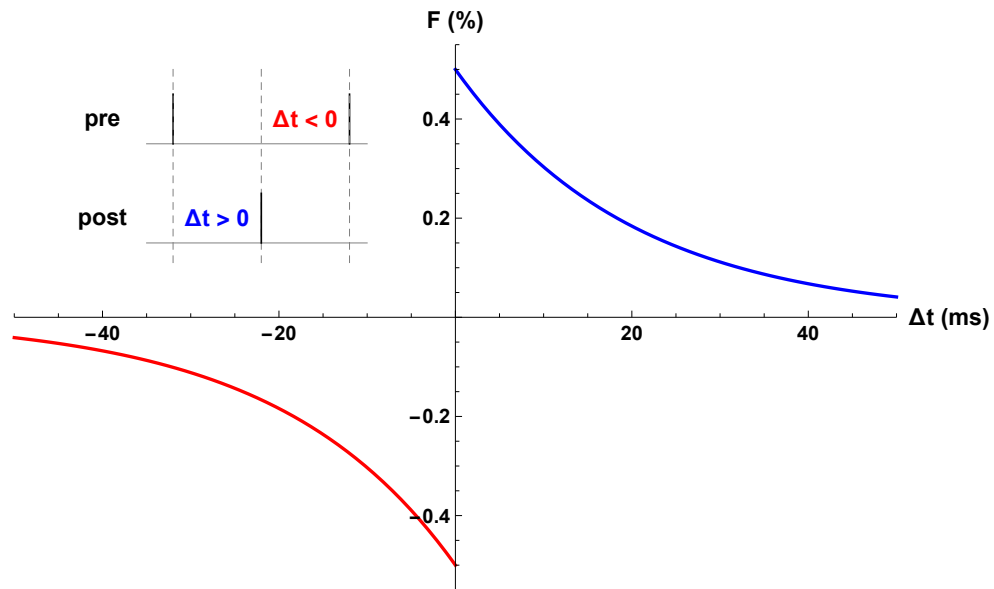


Figure 2.8: **The STDP modification function.**

F represents a percentage of the conductive change at one synapse given each Δt which is the time difference between pre- and postsynaptic spikes, adapted from [Song et al., 2000].

2.3.2 Voltage Model

The timing model described above takes *explicitly* the dependence of synaptic modification upon the difference in timing between pre- and postsynaptic spikes into account by a straightforward STDP learning function with one phase for potentiation and another phase for depression. However, many other aspects of the bidirectional plasticity can not be taken into account in such a framework, most importantly, the dependence of postsynaptic voltage before action potential [Sjöström et al., 2001]. Indeed, long-term synaptic changes is voltage-dependent [Artola et al., 1990] and the level of postsynaptic membrane potential provides a dynamic threshold for bidirectional plasticity [Ngezahayo et al., 2000], independent of spike timing. To account for a large body of experimental observation on bidirectional plasticity induced by various protocols, the postsynaptic voltage is a crucial variable to be incorporated into a mathematical model in addition to the spike timing. A typical voltage

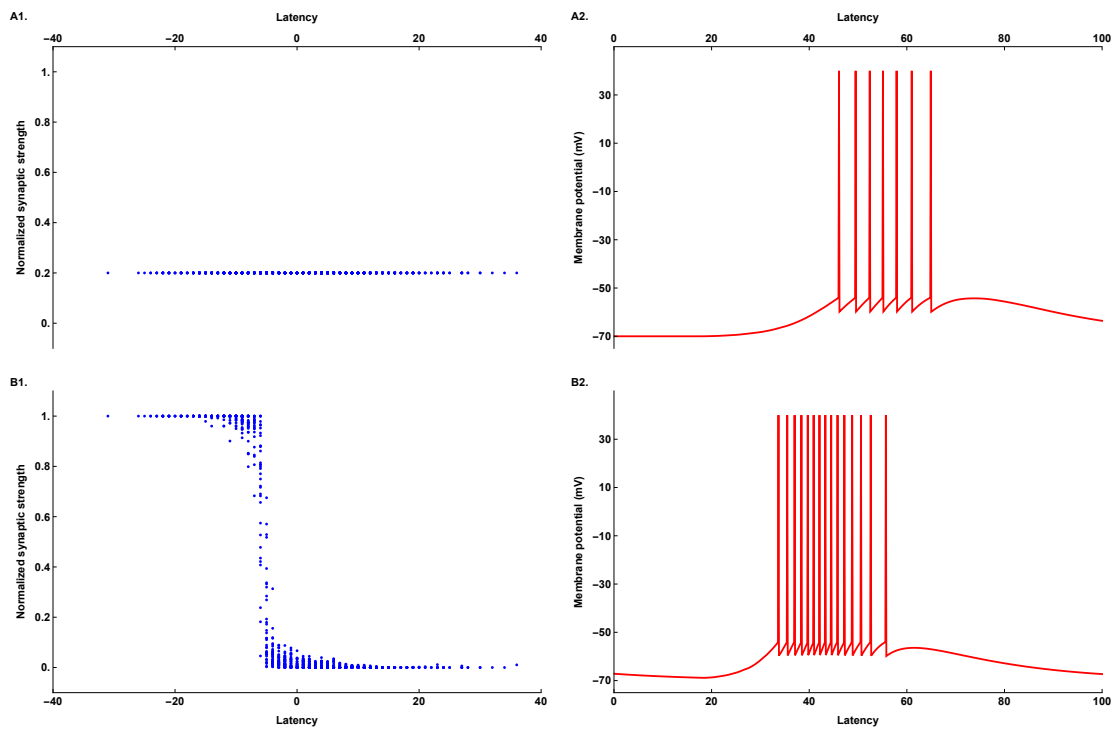


Figure 2.9: The effect of remodeling correlated synaptic groups through STDP.

A1. The initial peak synaptic conductance as a function of assigned latency in firing presynaptic spikes during a burst.

A2. The initial postsynaptic response to presynaptic inputs before STDP learning.

B1. The steady-state peak synaptic conductance as in A1 after STDP learning.

B2. The response of postsynaptic neuron with modified synaptic conductance in B1.

model can be then best exemplified by the Clopath model [Clopath and Gerstner, 2010].

One of the key modeling concept of this voltage model that it makes a distinction between the membrane potential u and two auxiliary voltage variables $\bar{u}_+(t)$ & $\bar{u}_-(t)$ which represent temporal averages of the membrane potential traces with two different time constants and two different thresholds [Cormier et al., 2001]. In addition, the model uses a variable $r(t)$ to track the presynaptic spike trace. When a presynaptic spike arrives and $\bar{u}_-(t)$ is greater than a threshold θ_- , LTD is triggered (Fig. 2.10A). When the membrane potential $u(t)$ is greater than another threshold θ_+ and $\bar{u}_-(t)$ is also greater than a threshold θ_+ , LTP occurs if presynaptic spike already leaves a trace, e.g. $r(t) > 0$ (Fig. 2.10B). The total synaptic change is a combined effect of the potentiation term w^+ and the depression term w^- as in Eq. 2.25:

$$w' = w'^+ - w'^- \quad (2.25)$$

where w'^+ and w'^- depend on the dynamics of the voltage variables and the variable of presynaptic spike trace, as formulated by Eq. 2.26:

$$\begin{cases} \bar{u}'_-(t) = [-\bar{u}_-(t) + u(t)]/\tau_- \\ \bar{u}'_+(t) = [-\bar{u}_+(t) + u(t)]/\tau_+ \\ r'(t) = [-r(t) + x(t)]/\tau_r \\ w'^+ = A^{LTP} r(t) [u(t) - \theta_+]_+ [\bar{u}_+(t) - \theta_+]_+, \text{ if } w < w_{max} \\ w'^- = A^{LTD} x(t) [\bar{u}_-(t) - \theta_-]_+, \text{ if } w > 0 \end{cases} \quad (2.26)$$

where $x(t)$ represents the binary presynaptic events with either 0 or 1 and the notation $[\Omega]_+$ equals Ω if Ω is positive and equals 0 otherwise. A full set of parameters are listed in Table. 2.1. The Clopath model replicates the voltage dependence of synaptic modification as in Fig. 2.11A. In addition, it also reproduces the observations found in the STDP experiments with the pairing protocol (Fig. 2.11B) and the frequency protocol (Fig. 2.11C). Compared to the Song model, the Clopath model represents a more general framework for bidirectional synaptic plasticity, as not only does it provide a reasonable account about STDP but also it demonstrates that with a proper plasticity learning rule, unidirectional and bidirectional strong connections can be formed with differentially conditioned spatio-temporal input correlations in a recurrent network of spiking neurons [Clopath et al., 2010].

Table 2.1: Parameters of Clopath model

A^{LTP}	A^{LTD}	θ_+	τ_+	θ_-	τ_-	τ_r
(1/mV ²)	(1/mV)	(mV)	(ms)	(mV)	(ms)	(ms)
0.00008	0.00014	-45.3	7	-70.6	10	15

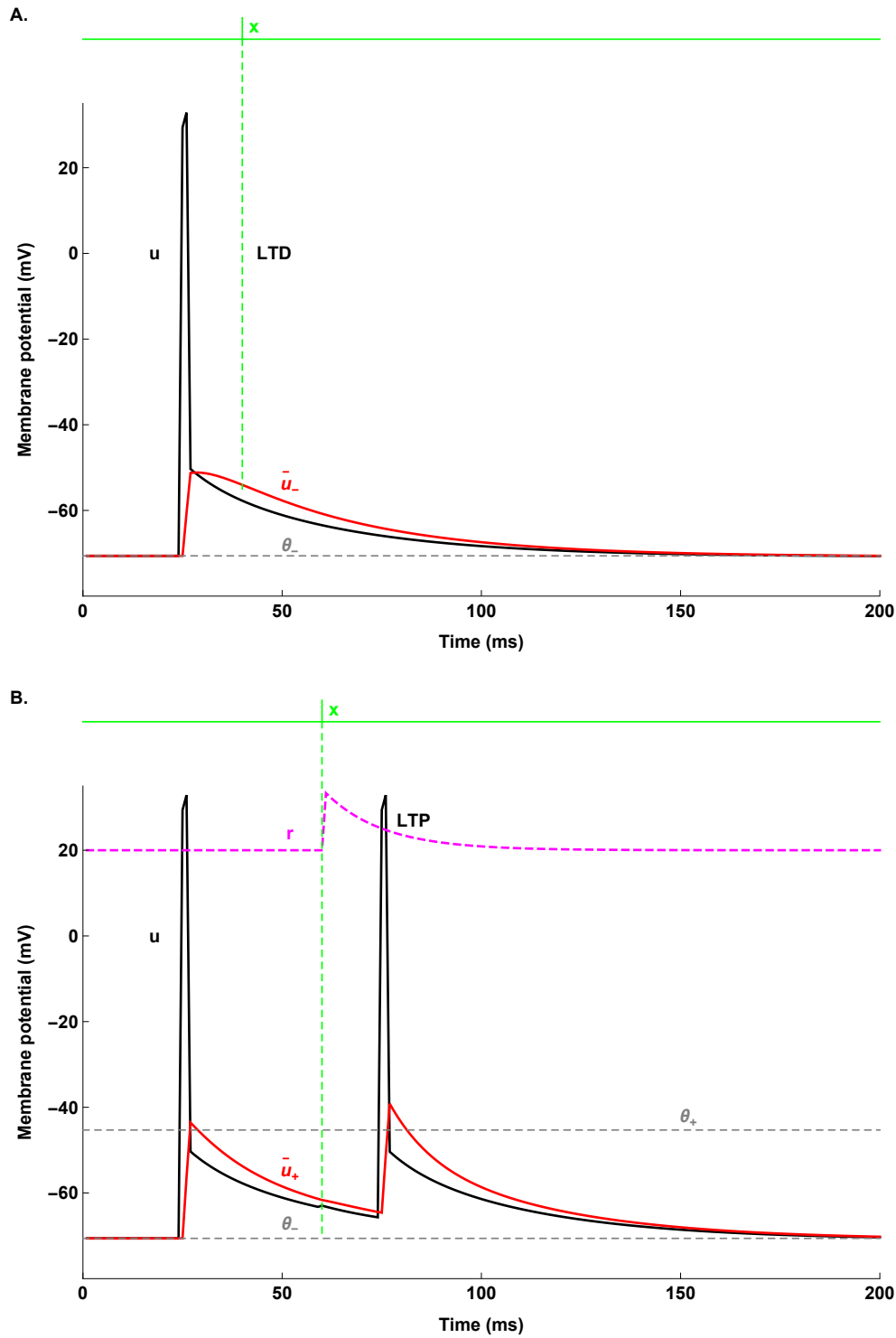


Figure 2.10: The key modeling concept of Clopath model.

A. LTD occurs at the time of presynaptic spike arrival when the postsynaptic neuron is depolarized.

B. LTP occurs at a combination of multiple conditions: 1. the depolarization is big, e.g. above θ_+ ; 2. the voltage trace $\bar{u}_+(t)$ is above θ_- ; 3. there exists a presynaptic spike, e.g. $r(t) > 0$.

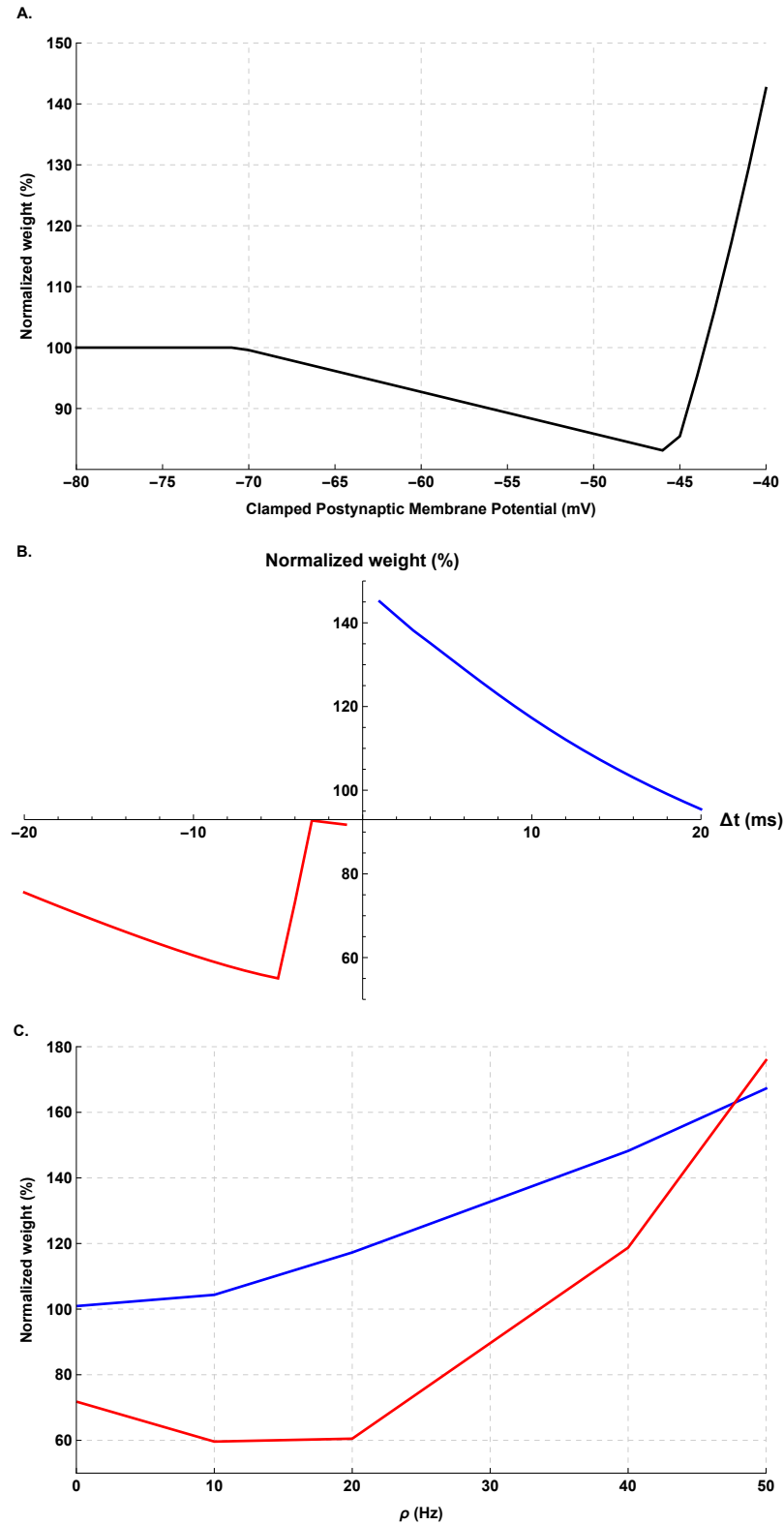


Figure 2.11: Simulated voltage and timing experiments by Clopath model.

A. The voltage-dependent induction curve, using weak presynaptic stimulation of clamped membrane potential with 50 spikes at 1 Hz at the synapse.

B. Spike-timing-dependent learning window as in Fig. 2.8, using 60 pre-post pairs at 20Hz.

C. Synaptic weight change as a function of pairing frequency using a Δt of 10 ms for pre-post pairing (blue) and -10 ms for post-pre pairing (red).

2.3.3 Signaling Transduction Model

Spiking timing gives rise to bidirectional change of synaptic strength in the Song model and a combination of postsynaptic voltage and filtered spiking traces brings about bidirectional modification of synaptic weight in the Clopath model. However, they are both phenomenological types of plasticity model, and therefore none of the frameworks provide any insight into the molecular basis for synaptic modification involving, for example, the changes in the number of specific receptors. Moreover, synaptic modifications are highly regulated by the interplay between networks of biochemical processes and electrical activities, molecular model of synaptic plasticity provides a more realistic description in the integration of biochemical and electrical signals in a multi-scale model [Mattioni and Le Novere, 2013] to investigate the brain's bioelectric properties.

The insertion and removal of AMPAR channels [Malinow and Malenka, 2002] into and out of the postsynaptic membrane alongside the regulation of the phosphorylation of their subunits have been shown to be the key events among the diverse mechanisms in modulating synaptic efficacy. CaMKII plays an important role in driving AMPAR channels into synapses, thereby promoting long-term potentiation [Hayashi et al., 2000]. Its accumulation in the individual spines was shown to be selective and necessary to induce synaptic strengthening [Zhang et al., 2008]. Another LTP player PKA phosphorylates AMPARs and controls directly the synaptic trafficking of the channels into synapses, thereby also in favor of increasing the synaptic strength [Esteban et al., 2003]. In contrast, long-term depression is associated with activity of PP1 which leads to a reduction of the surface expression of AMPAR subunits [Morishita et al., 2001]. Many signaling transduction models have been proposed to identify the role of individual molecules in biochemical networks to gain an understanding of the complex interactions of between molecules [Kotaleski and Blackwell, 2010], but the size of those models is often formidable.

In such context, a typical *simplified* signaling transduction model can be best exemplified, for example, by the Castellani model [Castellani et al., 2009], which involves only a small number of variables. The model describes a simple 2-step chain of enzymatic reactions with 2 phosphorylation processes of AMPAR by CaMKII and PKA, and 2 dephosphorylation processes by PP1, as illustrated in Fig. 2.12. The conceptual modeling diagram was translated into a rule-based language [Faeder et al., 2009] and simulated to display the behavior of bidirectional synaptic change with an optimized software package called RuleBender [Smith et al., 2012] (Fig. 2.13). The model demonstrated that CaMKII, which is thought to function as a molecular switch of the signaling cascade in the induction of synaptic plasticity, can bidirectionally regulates the number of double-phosphorylated AMPAR channels (Fig. 2.14A). In addition, it displays a switching behavior of the effective conductance of AMPAR channels with CaMKII acting as a dynamic threshold (Fig. 2.14B). Furthermore, as the calcium entry constantly fluctuates in an *in vivo* situation, the model shows that only when the level of such fluctuation reaches certain amplitude, the channel will transit from the nonphosphorylated equilibrium to the double-phosphorylated state (Fig. 2.14C).

The model itself is not complete, because it would certainly require some other linkage models to connect CaMKII to the calcium signaling and the direct effector of calcium such calmodulin [Keller et al., 2008]. It reflects a promising progress towards a self-contained molecular plasticity model and provides the minimal substrate to study the dynamic nature of bidirectional plasticity at the molecular level that is certainly beyond the phenomenological modeling of timing and spiking [Cooper, 2010].

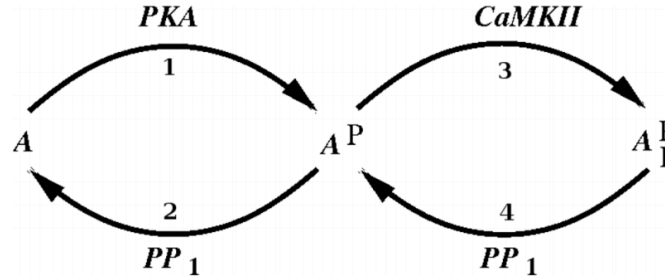


Figure 2.12: Kinetic description of a transduction model of AMPAR phosphorylation.

```

begin reaction rules
  AMPAR(e,Ser845~U,Ser831~U) -> AMPAR(e,Ser845~P,Ser831~U) kcat*PKA/(k1m+AMPAR0)
  AMPAR(e,Ser845~P,Ser831~U) -> AMPAR(e,Ser845~U,Ser831~U) kcat*k2m*PP1/(k2m*k2m+k2m*AMPARp+k2m*AMPARpp)
  AMPAR(e,Ser845~P,Ser831~U) -> AMPAR(e,Ser845~P,Ser831~P) kcat*CaMKII/(k1m+AMPARp)
  AMPAR(e,Ser845~P,Ser831~P) -> AMPAR(e,Ser845~U,Ser831~U) kcat*k2m*PP1/(k2m*k2m+k2m*AMPARp+k2m*AMPARpp)
end reaction rules

```

Figure 2.13: Source code of the Castellani model in BioNetGen.

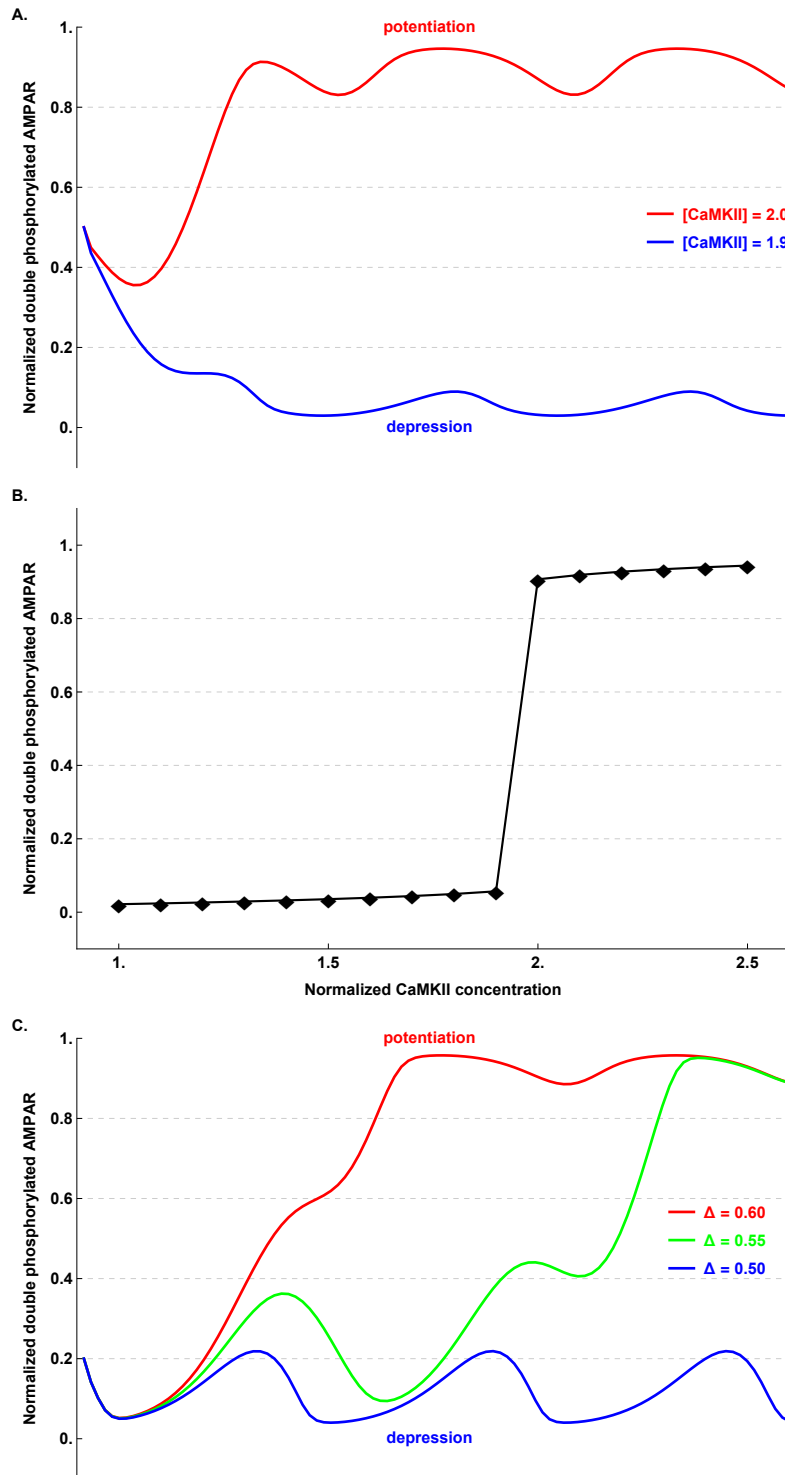


Figure 2.14: Part of simulation results from Castellani model.

A. The concentration of CaMKII determines the direction of synaptic plasticity.

B. The phosphorylated state of AMPAR channel is bistable, regulated by CaMKII.

C. The fluctuation of CaMKII is modeled as $\text{CaMKII}(t) = \text{CaMKII}^0 + \Delta(1 - \cos(\Omega t))$. Δ represents the amplitude of fluctuation and Ωt is set to 0.02π . It affects plasticity when the average concentration though remains identical.

2.4 Models of Dendritic Spines

2.4.1 Biochemical Background

The discovery of dendritic spines by Ramón y Cajal has spurred intense study of their potential functions over the past hundred years. The spines protrude from the dendrites, each consisting a head that is connected to the dendritic shaft by a thin neck (Fig. 2.15A). They are very small, typically with a length less than 3 μm and a diameter not greater than 1.5 μm . As a consequence, a spine head is of tiny volume and isolated from the larger dendrite by the spine neck, providing a restricted space for biochemical reactions (see details below). The distribution of spines on the dendrites of a neuron changes constantly depending on neuronal activity. Moreover, the morphological structure of individual spine is very plastic, reconstructable within a few seconds. Attributable to such dynamic structural plasticity, the spine plays a critical role in the regulation of synaptic strength and has been long thought to be the elementary units of memory.

Almost every spine forms a single synaptic contact, either excitatory or inhibitory, with a presynaptic axon terminal. Each spine head typically contains a complex protein network termed the “postsynaptic density” (PSD). Most proteins in the PSD network are implicated in governing the communication between neurons and the regulation of synaptic strength. Of those proteins, the glutamate receptor of the AMPA-type (AMPA) [Lu et al., 2009] is of particular importance in the processing of synaptic signals, as it gives rise to rapid depolarization that triggers the downstream activity of other proteins in the network and thus the onset and maintenance of synaptic plasticity. Glutamate uncaging experiments have shown that the PSD of a potentiated spine becomes enlarged as more AMPARs are inserted through trafficking process. Another important glutamate receptor is the NMDA-type (NMDAR), which is involved in the bidirectional regulation of synaptic plasticity attributable to its high calcium permeability. Besides the biochemical channels, the morphological changes in the dendritic spines have been long implicated to be associated with long-term synaptic changes [Yuste and Bonhoeffer, 2001]. It is particularly worth noting that the geometrical properties (e.g., the length and the diameter) of spine neck control the NMDAR-mediated synaptic calcium influx [Bloodgood et al., 2009] and interestingly small spines are found to display a larger calcium increase in the spine head as a result of a bottlenecked calcium efflux through the neck [Noguchi et al., 2005].

Taken together, the spine head can be biochemically viewed as a fierce nano-reactor to operate all the reactions inside a tiny space and the spine neck isolates the head from its neighboring synaptic contacts to ensure that the biochemical signaling cascades activated in one spine do not disturb chemical processing in the others [Wiegert and Oertner, 2011]. Adding to the strong experimental evidence, computer simulations also suggested that morphological parameters of spine neck could result in a 10-fold difference in the calcium concentration inside a spine head [Gold and Bear, 1994].

2.4.2 Electrical Compartmentalization

The computational models of spines have been ahead of the experimental measurements and used as an exploration tool to understand their functional importance [Yuste, 2013]. The electrical compartment of a spine head can be modeled as an electrical circuit which consists of a head capacitance C_{head} , a head conductance g_{head} and a synaptic conductance g_{syn} as illustrated in Fig.2.15B. The synaptic conductance is often contributed by the dynamics of both AMPAR and NMDAR channels. The head conductance g_{head} corresponds to a summed conductive change of various postsynaptic active channels, such as calcium channels [Bloodgood and Sabatini, 2007], sodium channels [Araya et al., 2007] and potassium channels [Higley and Sabatini, 2008]. The head resistance $1/g_{\text{head}}$ is often so large that it can be assumed to be infinite because of a very small spine membrane area. A spine neck, which carries a neck resistance R_{neck} , then attaches the spine head to the dendritic shaft. Based on this circuit diagram of the electrical compartments of a spine, theoretical studies have suggested that the local depolarization of spine head V_{head} must be different from the dendritic potential evoked on the shaft V_{shaft} attributable to the effect of R_{neck} , which can be described by Eq. 2.27:

$$\begin{aligned} V_{\text{head}} &= I_{\text{head}}(R_{\text{dend}} + R_{\text{neck}}) \\ V_{\text{shaft}} &= I_{\text{head}}R_{\text{dend}} \end{aligned} \quad (2.27)$$

where I_{head} represents the total current evoked from channels in the spine head.

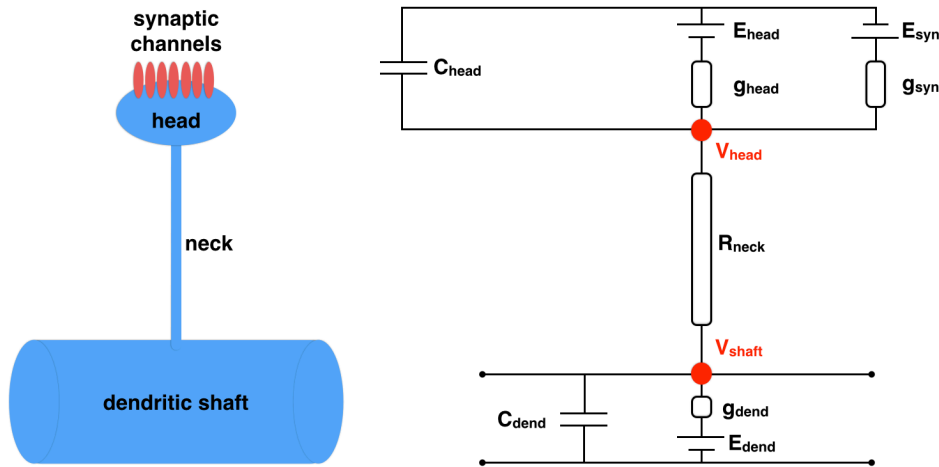


Figure 2.15: Electrical circuits of a single dendritic spine.

- A. The diagram of a connection between a spine head and dendritic shaft by a spine neck.
- B. Modeling an individual spine as a series of electrical compartments.

Recent experimental studies have demonstrated that spine neck is capable of regulating local depolarization inside the spine head [Tønnesen et al., 2014] and the estimated value of spine neck resistance based on cable theory could be incorrect [Svoboda et al., 1996]. Detailed biophysical modeling and simulation can be used to study the consequences of the change

of neck resistance and dissect the relative contribution of the individual glutamatergic receptors and voltage-dependent calcium channels to the depolarization [Grunditz et al., 2008]. A model spine equipped with AMPAR, NMDAR and R-type calcium channels, and connected with a thin neck to a passive CA1 pyramidal neuron is simulated using NEURON [Hines and Carnevale, 2001]. This model is taken from ModelDB (a public database for computational neuroscience [Hines et al., 2004]) and the parameters are adapted to reproduce the experimentally measured fluorescence transients. In the following paragraphs, I replicate the major predictions of this model to illustrate the interplay between biochemical receptors in the spine head and the neuroanatomical structure of spine neck in affecting the essential electrical properties possessed by a spine.

Given two different spine neck length values with one neck 10 times longer than the other, the long-necked spine produces a larger *local* depolarization in the spine head compartment (Fig. 2.16B, blue) due to a larger neck resistance value and this 10mV higher local potential results in almost 10 times higher local calcium activity (Fig. 2.18, blue). However, despite a larger local voltage generation, the long-necked spine depolarizes the neuron with a slight reduction of somatic EPSP (Fig. 2.16A, blue). The underlying mechanism of such short-necked spine generating smaller depolarization in the head but larger global potential in the soma, can in part be illuminated by the equations developed by [Koch and Zador, 1993]. As the postsynaptic effect of neurotransmitter binding during the synaptic transmission can be thought as injecting a current directly into the spine head and this current would then propagate through spine neck to the parent dendritic shaft. In the course of this propagation, almost none of the injected current will leak out through the neck and the head because of a very small head membrane area which makes the head resistance infinite. Hence, almost all the current would arrive upon the parent dendrite without attenuation. Since AMPAR channel is modeled as a double exponential function with a rise and a decay time constants, the injected current contributed by AMPAR can be represented by Eq. 2.28:

$$i_{ampa}(t) = g_{ampa}(t)(E_{syn} - V_{local}(t)), \quad E_{syn} = 0mV \quad (2.28)$$

where the unitary change of $g_{ampa}(t)$ is always identical by each triggered event. Thus, the amplitude of current inversely depends on the dynamics, in particular the peak amplitude of local depolarization $V_{local}(t)$ as its rapid rise decreases the driving force of ion flow which could be termed mathematically as the difference between V_{local} and synaptic reversal potential E_{syn} .

Fig. 2.16B illustrates that the short-necked spine induces a local depolarization up to -20mV, which is double in the amplitude of the potential evoked by the long-neck's -10 mV. By subtracting E_{syn} , this leads to a doubled AMPAR-injected current as depicted by the solid green line (long-necked) and the dashed green line (short-necked) in Fig. 2.17A. This larger current then results in a larger depolarization in the parent dendritic shaft (Fig. 2.17B).

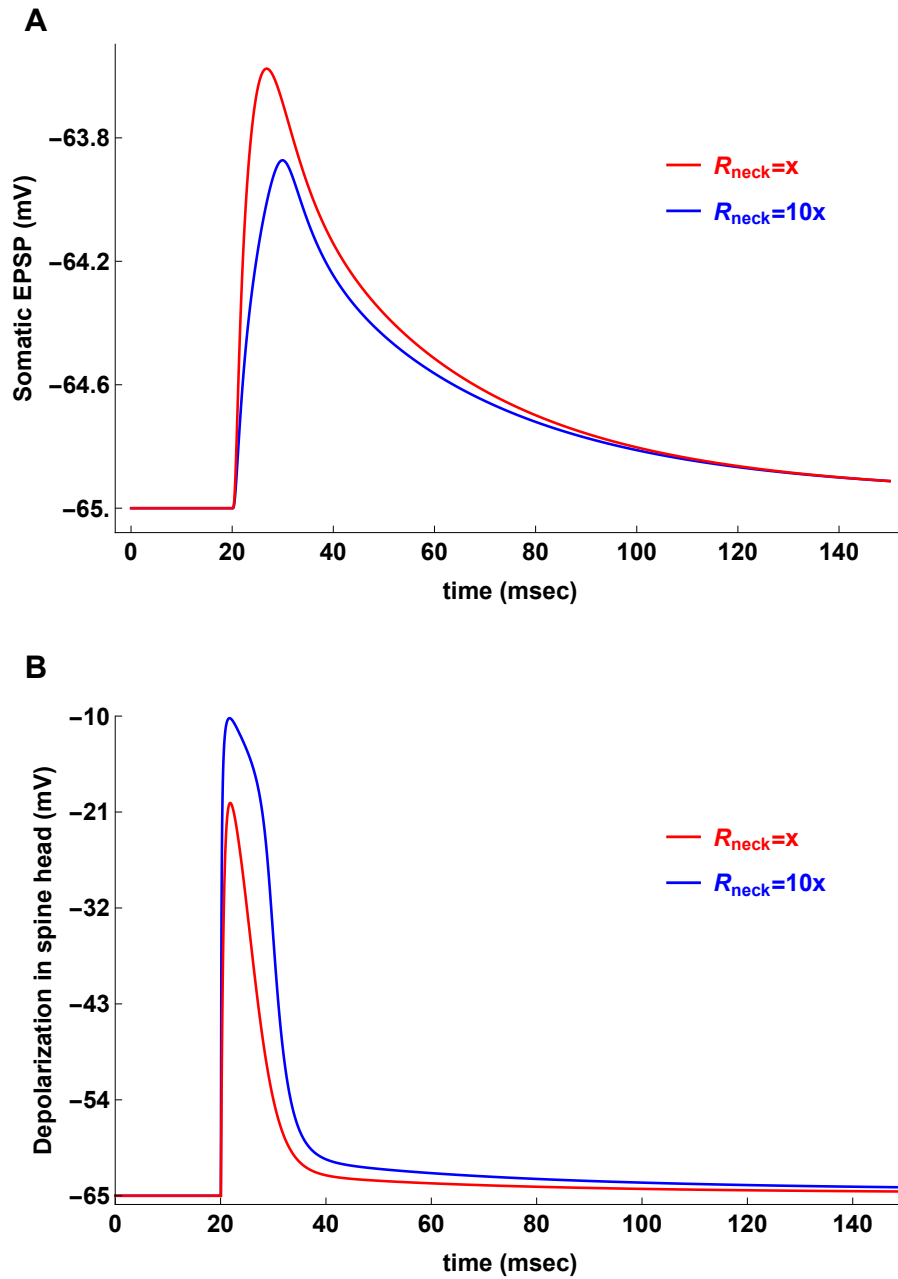


Figure 2.16: The local and global depolarization by differential spine neck resistances.
 A. The long-necked spine (blue) evokes *smaller* somatic EPSP than the short-necked (red).
 B. The long-necked spine (blue) evokes *larger* local EPSP in the spine head than the short-necked (red).

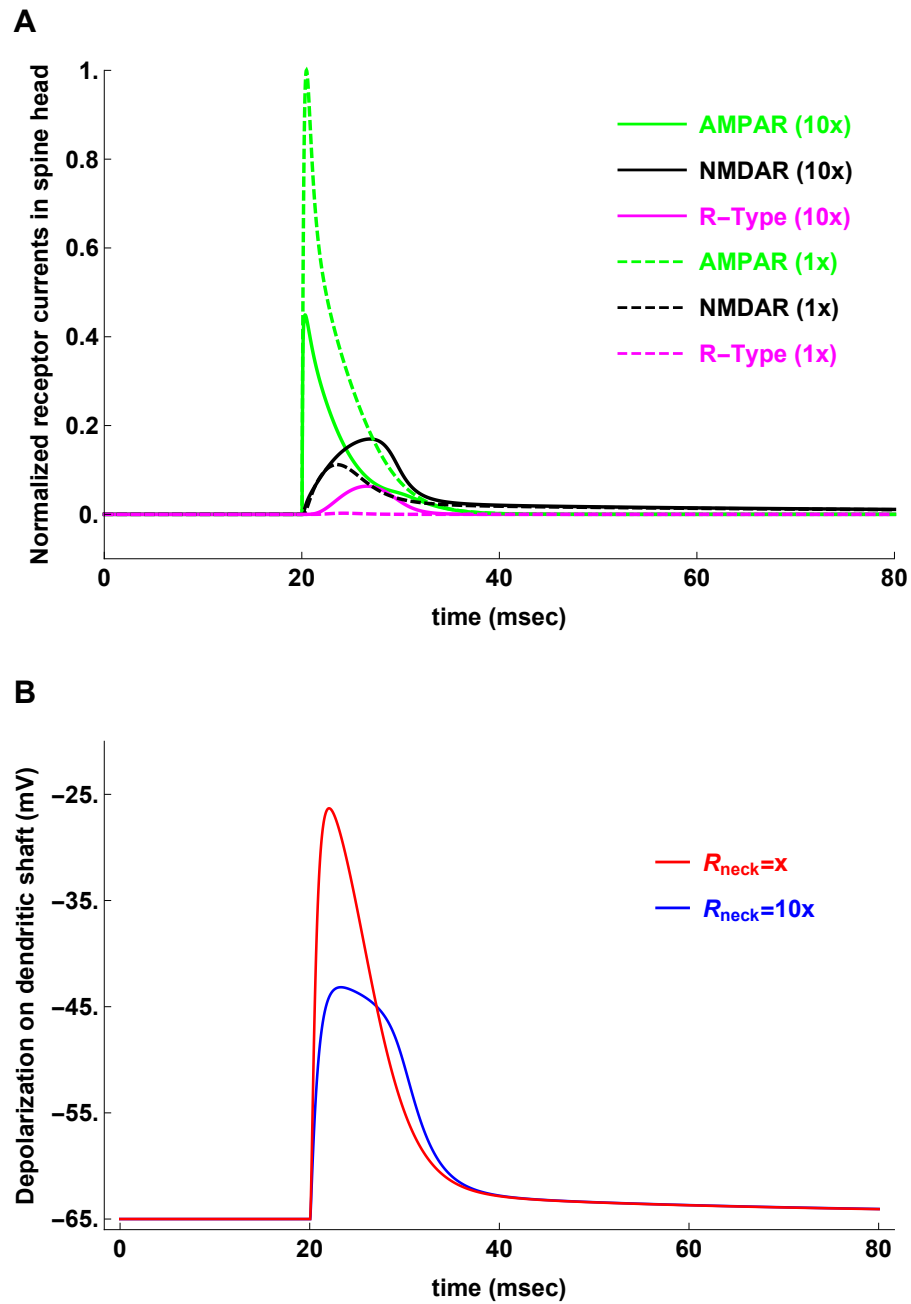


Figure 2.17: The synaptic currents in the spine head and the resulting depolarization on the dendritic shaft. **A.** The short-necked spine generates much larger AMPAR current than the long-necked (green), but much smaller NMDAR (black) and R-type currents (magenta). **B.** The larger net current evoked by the short-necked spine results in a larger depolarization in the dendritic shaft.

2.4.3 Implications for Synaptic Plasticity

Fig. 2.17A shows that AMPAR channels contribute the most among three channels to the evoked synaptic current, with NMDARs the second and R-type calcium channels the third. Here one could relate this observation to a working model of STDP and argue that a mechanistic explanation for narrow t-LTP window is incomplete [Holbro et al., 2010]. Due to the fact that the voltage in the spine head is the central variable governing synaptic plasticity, a strong contribution from AMPAR channels is required to provide sufficient postsynaptic depolarization [Fuenzalida et al., 2010] and gate calcium transients in the spine head, which are both critical for the very narrow time window in spike-timing-dependent potentiation. Emerging evidences [Hao and Oertner, 2012] have put spine in the center of coincidence detection as active conductances like AMPAR and NMDAR channels in the spine head combined with the electrical resistance of the spine neck synergically regulating the depolarization of the spine head (Fig. 2.16) and the NMDAR-mediated calcium-dependent synaptic plasticity (Fig. 2.18).

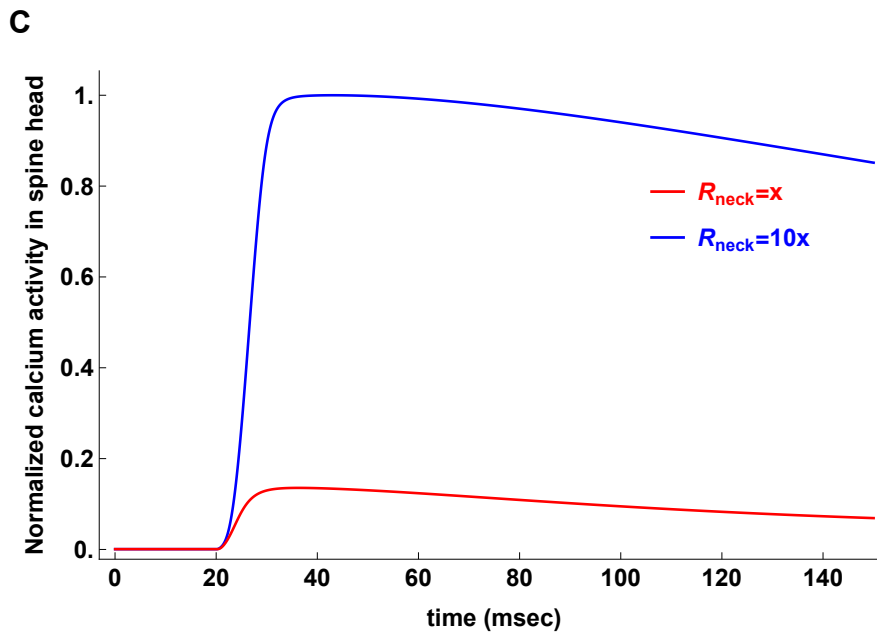


Figure 2.18: **The calcium elevation by differential spine neck resistances.** The long-necked spine (blue) produces nearly 10 times higher calcium elevation in amplitude than the short-necked spine (red).

A diagrammatic picture of how a spine could act as a coincidence detector and how its crew interact to regulate synaptic plasticity can be illustrated in Fig. 2.19: 1) using a single-cell genetic approach, most AMPARs in CA1 pyramidal neurons contains calcium-impermeable subunits that gate the calcium-permeable and voltage-sensitive NMDARs primarily through local depolarization [Lu et al., 2009]. The modeling result shows that AMPAR block significantly reduces NMDAR current amplitude (Fig. 2.20A); 2) blockade of NMDARs doesn't affect the somatic EPSP but significantly depress evoked calcium currents (Fig. 2.20B); 3) spine neck mediates the process of local depolarization with its variable morphology and resultant input resistance, and determines NMDAR-dependent calcium signaling in both the spine head and the parent dendrite [Noguchi et al., 2005].

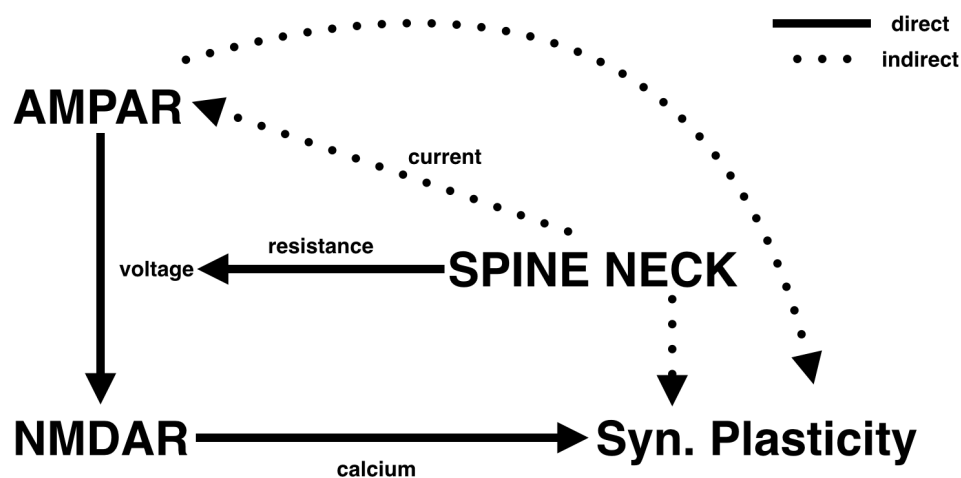


Figure 2.19: A synergistic model of spine as the major site regulating synaptic plasticity. See details in the text.

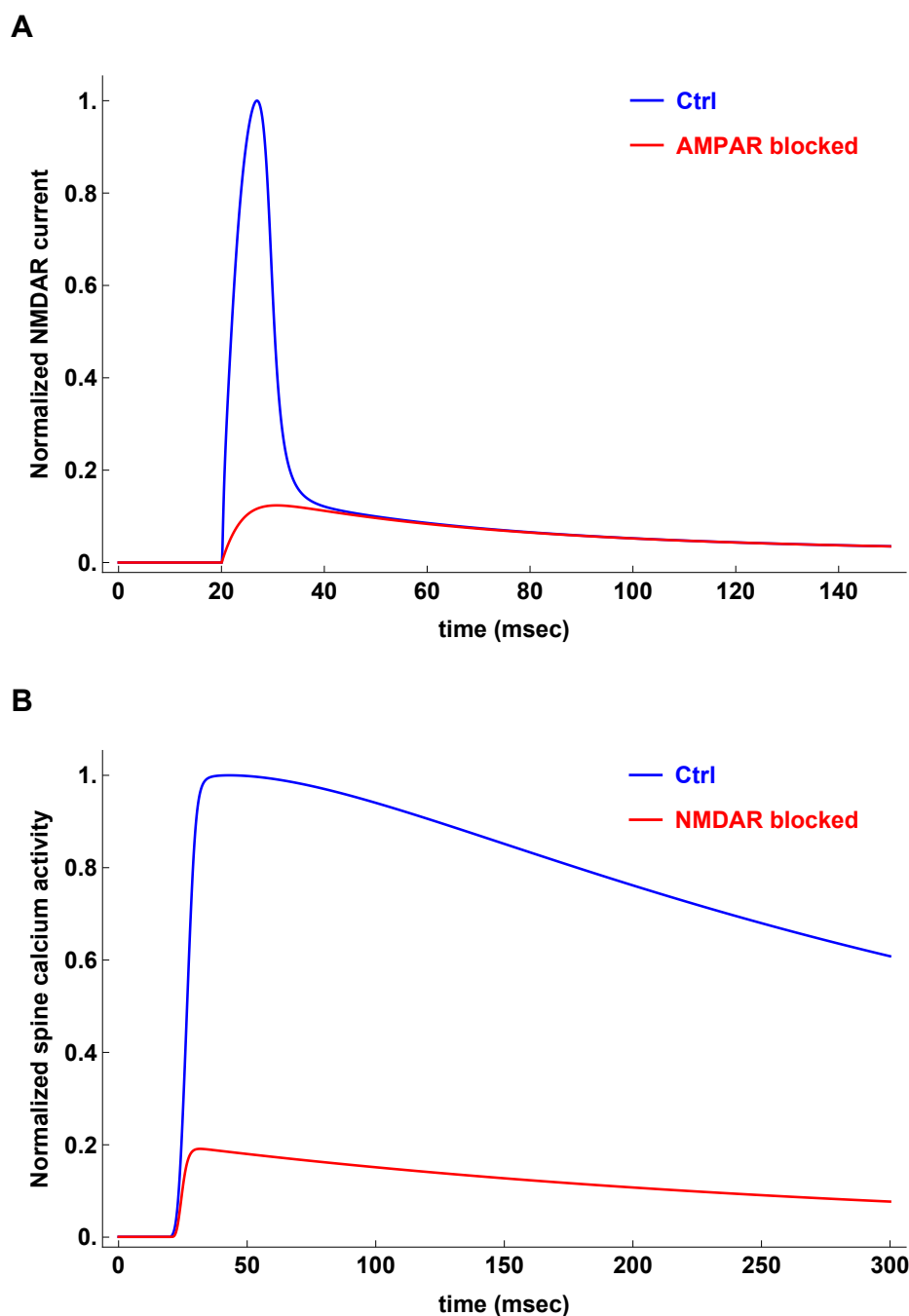


Figure 2.20: Effects of AMPAR channels in regulating the activity of NMDAR channels and calcium. **A.** The activity of NMDAR channels is significantly reduced when AMPAR channels are blocked in the spine head. **B.** The calcium elevation is reduced to only 20% of the control level with AMPAR blockade in the spine head.

Chapter 3

Extrapolating the Predictions of STDP Models to Disease States

In this chapter, I present a framework to address a general problem that occurs very frequently in neuroscience: Often a scientist is interested in inferring the underlying microscopic mechanisms of phenomena at a macroscopic or even behavioral level. This can be done using systematic simulation studies, but very often the structure and parameterization of these models are unknown, or only poorly constrained. Systems Biology and Neuroscience initiatives to “rebuild the brain in silicon” pursue this approach, but the involved complexity is often hard to control, and simulations may call for supercomputers. An alternative approach is to embrace the uncertainty and then deal with it in a systematic way. This is the domain of reasoning with and under uncertainty. Artificial Intelligence has developed methods for this, which are in practical use, for example, in medical expert systems.

In the first section, I lay out the background domain knowledge and the particular motivation that connect our approach to a medical specific problem. In the second, I propose to employ the formalism of Bayesian networks and the inference method of Belief Propagation applied to Bayesian networks, which are parameterized using simulations of biophysical models. As a use case I select a very challenging problem, namely to infer i) the still disputed phenomenological mechanisms of STDP and ii) the nature of certain pathological brain states in terms of the multivariate statistics of neuronal population activity from “observables” that are - at least in principle - accessible at the macroscopic and behavioral level. I formulate the Bayesian network, describe two phenomenological STDP models and draw connections between simulation and knowledge inference. The next following two sections illustrate simulation results and demonstrate how one could exploit them for reasoning within the proposed Bayesian network. In the final section, I discuss the findings and what we can learn about the potential disruptive roles of STDP during epileptic seizures using this approach.

3.1 Background and Motivation

Recent years have seen an enormous interest in data and model sharing in neuroscience, which now also extends towards sharing formal models in machine-readable formats, such as NeuroML (neuroml.org), NineML (nineml.org), or yet to be developed model descriptions [Ansorg and Schwabe, 2010]. These efforts are ongoing and meet many challenges in practice, for example, convincing researchers to share their data, where major funding agencies and publishers certainly have to establish more rigid measures in the future. While standards for model exchange in systems biology and cellular computational neuroscience have been established [Le Novère, 2006], the sharing of network models in neuroscience is currently hindered by the lack of widely accepted standards for describing these models. However, even if both data and model sharing would be in place and supported by proper platforms like web-portals, here I ask: *in which way would such platforms support research in neuro-theory and modeling?*

Data and model sharing is desperately needed as the data provides the yardstick for any model, and accurate quantitative models are needed for proper predictions as required in, for example, personalized medicine. Having both data and models available in machine-readable formats is also beneficial for computer-aided or fully automatic model generation from data using statistical and machine learning approaches. However, despite the inherent complexity of neuronal systems, I still believe that their understanding in terms of theories embodying simple principles is possible. Researchers in neuro-theory, who work out such principles, will make use of such platforms as a source of inspiration to validate their theories which are usually developed without much informatics support and are largely informed by the available scientific literature. I hypothesize that even the development of theories, which go beyond plain model fitting, can be performed in a computer-aided or fully automatic manner [Langley et al., 1987] as demonstrated recently by so-called “robot scientists” [Sparkes et al., 2010].

I envision annotations of scientific publications using formal statements of the empirical findings (see Fig. 3.1). This is similar to the semantic web, which is still only a vision, because it depends on the authors of web pages to annotate their content. For the majority of content on the web, this may not even be worth the effort. However, from scientists, one shall expect the motivation and skills to formulate such annotations. Once such annotations are available, including references to proper domain ontologies, they could enter inference engines for automated knowledge discovery, which is a well-studied topic in classical artificial intelligence.

As the specific simulation problem, I investigate how memories are affected by the combination of synaptic plasticity and paroxysmal brain activity observed during seizures. This is a challenge for multiple reasons. First, despite decades of investigations on the mechanisms of synaptic plasticity and memory, we still have only a partial understanding of how the former underlies the network phenomena of encoding, maintenance, recall, and loss of memories.

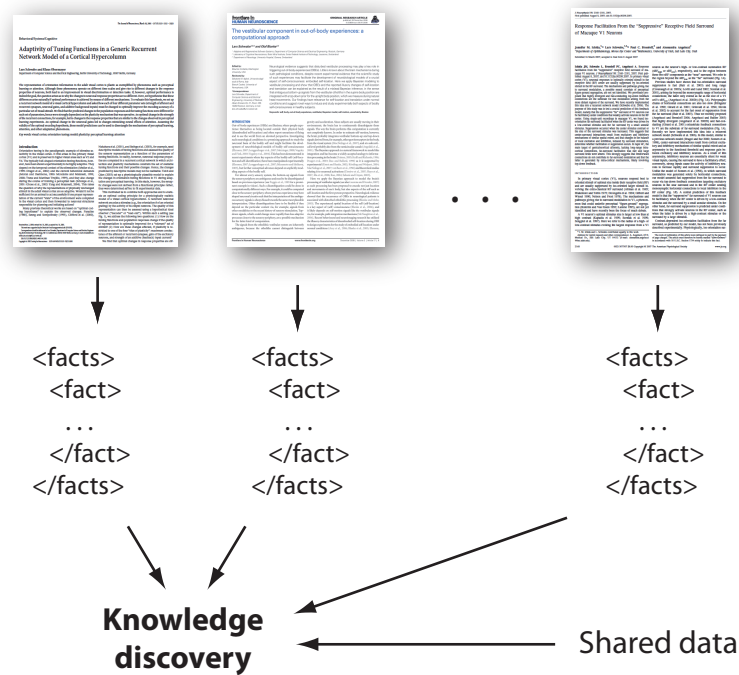


Figure 3.1: An illustration of how to exploit semantic annotations of publications.

Scientific publications will be annotated using formal statements of the empirical findings, similar to the semantic web and with reference to domain ontologies. Then, new knowledge could be inferred based on these qualitative findings, which are already interpreted by the experimentalists. Shared data can be used to validate existing and inferred theories.

Second, after more than a decade of theoretical investigations of spike-timing form of synaptic plasticity (STDP), the modeling of STDP remains controversial, i.e. there is not even a census yet regarding phenomenological STDP models. Third, long-term memory retention via STDP has been studied only recently [Billings and van Rossum, 2009]. Consequently, to the best of my knowledge, the possibly perturbing role of STDP during paroxysmal brain activity as observed during epileptic seizures has not been studied.

3.2 Bayesian Network and STDP models

3.2.1 From Data-Model Comparison to Knowledge Representation

The integration of data and models has a long tradition in neuroscience, and the Bayesian approach is emerging as the *de facto* standard for that [O'Reilly et al., 2012]. Here, prior assumptions and a generative model for the data are combined with new observations in order to arrive at the posterior distribution over candidate models. It is widely used when the signal to noise ratio is low such as in, for example, functional brain imaging. Fig. 3.2a shows a graphical model for Bayesian model comparison and selection, where different models M can be parameterized with a parameter vector θ . Once prior distributions $P(\theta|M)$ are specified, observed data D can be used in order to compare different models M_1 and M_2 using the posterior odds $P(M_1|D)/P(M_2|D)$. This is certainly the method of choice once the raw data is available, even though such a comparison is technically demanding because defining the prior distributions $P(\theta|M)$ and estimating the Bayes factor is non-trivial.

Here I focus on comparing models when only qualitative observations are available. I suggest to set up Bayesian networks for a particular domain and then perform inference given new experimental evidence. Fig. 3.2b shows the Bayesian network I set up for this study, in which all the nodes are binary. Paroxysmal brain activity such as seizures can be identified clearly using local field potentials and electroencephalography, but until today it is not clear if the individual neurons are synchronizing their discharges, or if the high-frequency population spikes are only a property at the level of neuronal populations without synchronicity of individual spikes. Therefore, I define two modes of paroxysmal activity, which correspond to two extreme scenarios in the population of neurons, namely changes in the mean firing rate and changes in the synchronicity with an unchanged mean firing rate, i.e. $Act \in \{\text{rate}, \text{sync}\}$. Another unknown is the nature of STDP, where I consider the “additive” and “mixed” rules, i.e. $StdpMech \in \{\text{add}, \text{mix}\}$. As observables, I first consider changes in the postsynaptic firing rate of a neuron, which is driven by the paroxysmal activity via plastic synapses. The firing rate of this neuron could be transiently increased and then decay during the intra-ictal period, or be elevated throughout entire intra-ictal period, i.e. $RateIntra \in \{\text{transient}, \text{elevated}\}$. Interestingly, recent experimental evidence suggests heterogeneous changes [Truccolo et al., 2011]; I return to this in the Discussion. Second, I consider activity in this neuron during the post-ictal period, where the firing rate can be lowered but recovers to the pre-ictal level, or be unchanged relative to the pre-ictal period, i.e. $RatePost \in \{\text{recovering}, \text{unchanged}\}$. Third, I consider mem-

ory retention after a seizure, where I distinguish between mild and severe memory loss, i.e. $MemoryLoss \in \{\text{mild}, \text{severe}\}$.

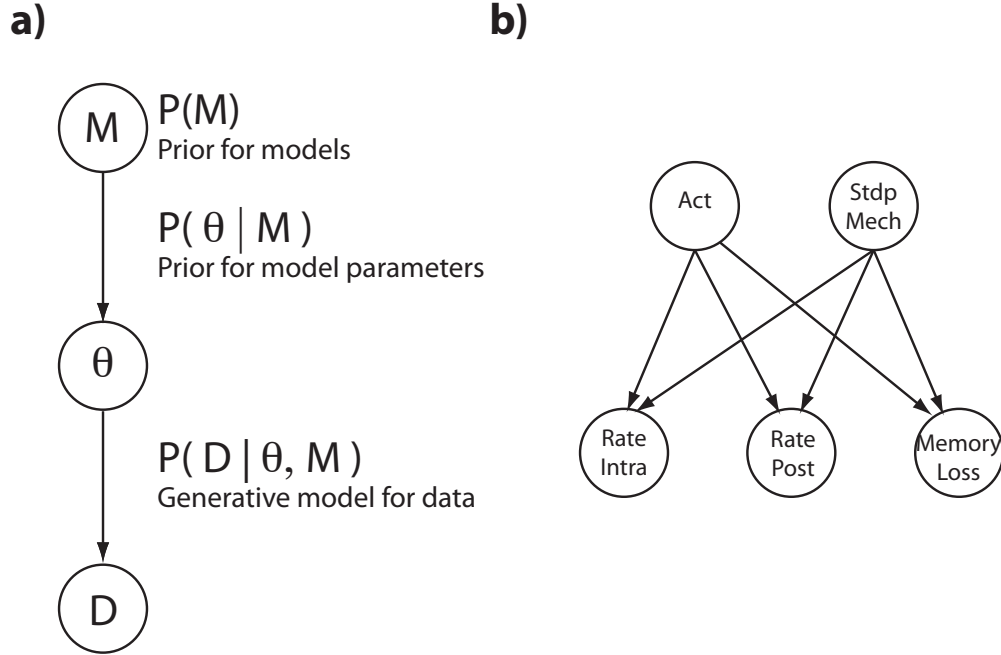


Figure 3.2: **The Bayesian approach to inference in neuroscience.**

A. The graphical model for Bayesian model comparison and selection.

B. The Bayesian network as an example for knowledge representation, which requires qualitative simulation observations (lower three nodes) to make inference about unknown model properties (upper two nodes).

3.2.2 Leaky Integrate-and-Fire Neuron and Synapse Model

I simulate a conductance-based leaky integrate-and-fire neuron with membrane potential dynamics given by Eq. 3.1 (see also Fig. 3.3a):

$$\tau_m \frac{dV_m}{dt} = (V_{rest} - V_m) + \frac{G_{exc}(t)}{G_L} (E_{exc} - V_m) + \frac{G_{inh}(t)}{G_L} (E_{inh} - V_m) \quad (3.1)$$

where $\tau_m = 20$ ms is the membrane time constant and $G_L = 10$ nS is the membrane leak-conductance. $E_{exc} = 0$ mV and $E_{inh} = -70$ mV are the excitatory and inhibitory reversal potentials, respectively. The neuron fires an action potential when the membrane potential V_m reaches the threshold value -54 mV, and then V_m is reset to -60 mV. The model neuron has 1000 excitatory and 200 inhibitory synapses. Synaptic strengths of individual synapses are also conductance-based. The total strengths $G_{exc}(t)$ and $G_{inh}(t)$ in Eq. 3.1 represent the summed contribution from excitatory and inhibitory synapses. On arrival of a presynaptic spike at the i -th excitatory synapse, the overall excitatory synaptic strength is increased instantaneously by g_{exc}^i , i.e. $G_{exc}(t) \leftarrow G_{exc}(t) + g_{exc}^i$ and then decays with a

time constant $\tau_{syn} = 20$ ms. The same applies to inhibitory synapses, where the synaptic strength $g_{inh}^i = 500$ pS is kept fix (no learning occurs at inhibitory synapses). All simulations were performed using Matlab with a forward Euler integration of 0.1 ms resolution.

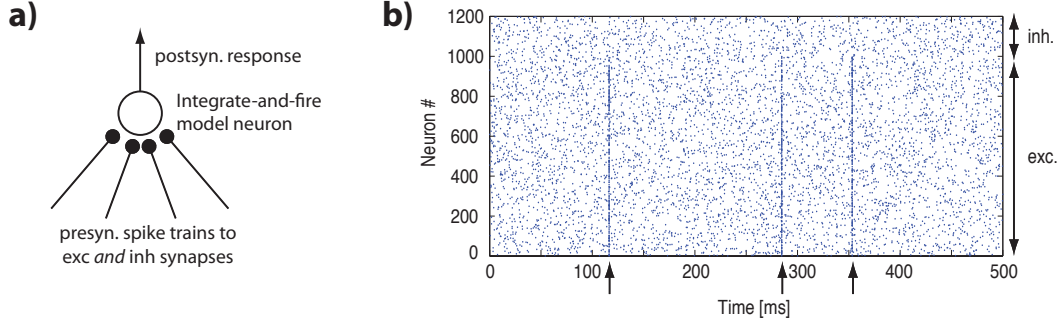


Figure 3.3: **Model setup and examples of synchronicity events.**

A. Conductance-based single compartment leaky integrate-and-fire model neuron.

The presynaptic activity for 1000 excitatory and 200 inhibitory neurons is sampled using statistical models and the learning occurs only at excitatory, not inhibitory synapses.

B. Example raster-plot of presynaptic activity with three synchronicity events (see arrows), where for each synchronicity 200 excitatory neurons are randomly selected. Dots indicate presynaptic spiking times for excitatory (1 ... 1000) and inhibitory (1001 ... 1200) neurons.

3.2.3 Spike-Timing Dependent Plasticity Models

The modification of synaptic strength of individual synapses depends on the relative timing of paired spikes [Markram et al., 1997]. As a consequence, the strengths of modeled excitatory synapses, $g_{exc}^i = g_{exc}^i + \Delta g$, are subject to learning via STDP learning rules which encompass both synaptic potentiation *and* depression. More specifically, I use “additive” and “mixed” learning rules [Kepecs et al., 2002]. The change of synaptic strength Δg under additive rule is independent of the current strength but constrained by a maximum boundary ($\bar{g}_{max} = 150$ pS), which can be described by Eq. 3.2:

$$\Delta g = \begin{cases} \bar{g}_{max} \cdot A_+ \cdot \exp(-\Delta t / \tau_+) & \text{if } \Delta t < 0 \\ -\bar{g}_{max} \cdot A_- \cdot \exp(\Delta t / \tau_-) & \text{if } \Delta t > 0 \end{cases} \quad (3.2)$$

where $\Delta t = t_{post} - t_{pre}$ is the time difference between pre and postsynaptic spikes on each individual synapse. $A_+ = 0.005$ and $A_- = \alpha A_+$ are scaling factors with $\alpha = 1.05$. The mixed rule incorporates a dependence of the magnitude of synaptic depression on the initial synaptic strength [Bi and Poo, 1998]. Such a dependence can be modeled by Eq. 3.3 with $\tilde{A}_- = 0.0114$ where through all $\tau_+ = \tau_- = 20$ ms.

$$\Delta g = \begin{cases} \bar{g}_{max} \cdot A_+ \cdot \exp(-\Delta t / \tau_+) & \text{if } \Delta t < 0 \\ -g_{exc}^i \cdot \tilde{A}_- \cdot \exp(\Delta t / \tau_-) & \text{if } \Delta t > 0 \end{cases} \quad (3.3)$$

3.2.4 Modeling presynaptic Population Activity

All the presynaptic spike trains are generated via Poisson processes with the rate for both excitatory and inhibitory inputs set to 10 sp/s, during the initial phase of learning. In order to mimic paroxysmal brain activity of an epileptic seizure, two different transient modification schemes are employed. First, the rate is increased from 10 sp/s to 12 sp/s. Second, the synchronicity is increased while the rate remains unaltered. This is achieved as follows. One synchronized “spike train” is sampled to determine a synchronicity event with Poisson rate of 10 Hz. Triggered by such an event, 5 % of *randomly* selected presynaptic excitatory neurons synchronize their discharges. Compared to the first scenario, the average activity could be regarded unchanged, but synchronous discharges of a subset of presynaptic neurons at each synchronicity event strongly drive the postsynaptic neuron to fire action potentials. Fig. 3.3b shows a raster-plot for the second scenario with 20 % synchronicity.

3.2.5 Quantification of Memory Loss and Retention

The change in the firing rate of postsynaptic model neuron is an observable which can be easily measured. Nevertheless, the “memory loss” is not straightforward to quantify using single neuron models. It is widely accepted that the pattern of synaptic strengths is one important form of memory storage. Here I calculate the correlation between strength vectors of all excitatory synaptic connections at two different times as the interpretation of memory retention by using the Pearson correlation coefficient [Lee Rodgers and Nicewander, 1988]. A reference time t_0 is set before the simulated paroxysmal activity at which the distribution of synaptic weights reaches its equilibrium (see Fig. 3.4a). The strength vector at t_0 is denoted as w_0 . Afterwards I let the model neuron continue to experience presynaptic activity and learn to adapt its synaptic strengths according to the STDP rules. Then, the correlation coefficient $r(t_0, t)$ between two strength vectors w_0 and w_t , is calculated by Eq.3.4 where it is assumed that $t_0 < t$:

$$r(t_0, t) = \frac{\sum_{i=1}^n (w_t^i - \bar{w}_t)(w_0^i - \bar{w}_0)}{\sqrt{\sum_{i=1}^n (w_t^i - \bar{w}_t)^2 \sum_{i=1}^n (w_0^i - \bar{w}_0)^2}} \quad (3.4)$$

where w^i represents the synaptic strength of i -th synapse and \bar{w} is the average of the strength vector at a specific time. The coefficient $r(t_0, t)$ quantifies how much memory is retained. High values correspond to good memory retention whereas low values to poor. Note that even though the synaptic pattern may have reached equilibrium, individual synapses are still undergoing changes and this is most prominent for “additive” STDP rule (see Fig. 3.4b for an example). The ongoing changes of synaptic strengths are the main cause of memory fading, and this course of inevitable memory fading is the baseline for our quantification of additional memory loss due to the paroxysmal activity. The baselines are shown for two STDP rules in Fig. 3.4c in terms of the coefficient $r(t_0, t)$, where no paroxysmal activity is simulated.

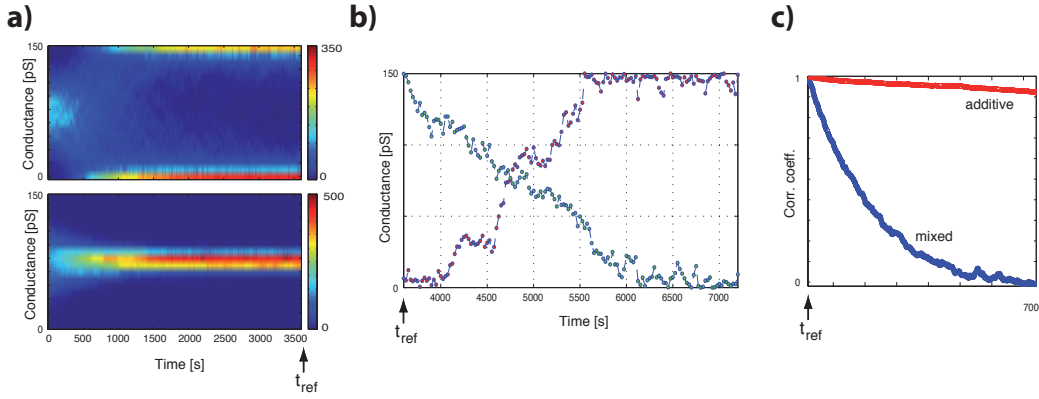


Figure 3.4: **Dynamics of synaptic strengths.**

A. Evolving distribution (in terms of absolute numbers) of excitatory synaptic strengths g_{exc}^i for “additive” (upper panel) and “mixed” (lower panel) STDP rules.

B. Example synaptic strength traces of two selected excitatory synapses under “additive” STDP rule, where individual synapses are undergoing changes. For example, a weak synapse gets stronger and a strong synapse gets weaker. Note that such dynamics take place after the distribution reaches equilibrium.

C. Baseline dynamics of memory retention in terms of $r(t_0, t)$ for both STDP rules where no paroxysmal activity is employed (t_{ref} here is equivalent to t_0 in the text).

3.3 Results

I perform a systematic simulation study of how transient paroxysmal activity may affect memories via STDP. I explicitly consider alternatives for the currently unknown STDP mechanisms and the nature of the paroxysmal activity. For different choices of these unknowns, the simulations make different predictions and I demonstrate how Bayesian networks, which are a prominent method for representing knowledge with uncertainty in expert systems, could be used in order to combine the simulation results with prior assumptions and new empirical evidence. The structure of the Bayesian network shown in Fig. 3.2b needs to be accompanied with the definition of conditional probability tables (CPTs), which embody the expert knowledge. This is where the simulation and analysis of the models enter. Thus, let me first interpret the simulation results, and then in the next section, I show how these results can be translated into a CPT and perform inference.

Fig. 3.5 shows the results for all combinations of $Act \in \{\text{rate}, \text{sync}\}$ and $StdpMech \in \{\text{add}, \text{mix}\}$. The top four panels show predicted postsynaptic firing rate before (pre-ictal), during (intra-ictal) and after (post-ictal) a simulated seizure and the four lower panels show the memory retention during intra-ictal period in terms of the correlation coefficient (Fig. 3.5, thick red lines) in comparison with the memory retention predicted when no seizure is simulated (dashed blue lines). Interestingly, the firing rate remains elevated in three out of four scenarios. Only under “additive” STDP, an increase of presynaptic mean firing rate results in a transient increase of postsynaptic rate, which decays afterwards be-

cause the STDP rule weakens many strong synapses (see also Fig. 3.4b). The postsynaptic rate for the “additive” STDP with increased synchronicity remains elevated, because many previously weak synapses are strengthened. The firing rates for the “mixed” STDP (Fig. 3.5, right column) during pre-ictal and post-ictal periods are low (≈ 1 sp/s) and an increase in presynaptic firing rate is directly reflected in the postsynaptic response.

[Billings and van Rossum, 2009] has reported that “mixed” STDP leads to very poor memory retention. Here I demonstrate that the memory loss due to perturbing presynaptic activity is even more severe for the “mixed” than the “additive” rule. In contrast, the memory fading for the “additive” STDP during intra-ictal period is obviously bigger caused by perturbing presynaptic activity than non-perturbing one, but much less pronounced than for the “mixed” STDP. It is particularly worth noting that synchronicity perturbation is more disruptive than rate perturbation, due to the fact that many previously weak synapses are strengthened, reshaping the distribution of synaptic strengths.

3.4 Inference with proposed Bayesian Network

The simulation results above have given valuable insights into the consequences of STDP for regulating neuronal responses and how paroxysmal activity may cause harm beyond the actual seizure, namely changing the network connectivity and hence disrupting long-term memory. Based on these results, a human expert could resort to the scientific literature or laboratory in order to reason about the actual mechanisms. However, as I have considered only a small set of possible alternatives, it is likely that mechanisms I have not included are operating as well during a seizure, for example, an increase in both firing rate *and* synchronicity. In addition, the experimental literature shows that the changes in firing rates before, during, and after a seizure are diverse [Truccolo et al., 2011]. Thus, simply reading off the most likely combination of the unobserved model properties by having a human expert comparing the simulation results with the experimental literature is not even beneficial in our very simple example.

Therefore, I have to first translate the simulation readouts from Fig. 3.5 into a CPT of the Bayesian network shown in Fig. 3.2b. This CPT is shown in Fig. 3.6a, where for all four combinations of the latent variables *Act* and *StdpMech*, the probability of the values at the evidence nodes *RateIntra*, *RatePost*, and *MemLoss* is given. Even though some results are crisp in the sense that they are only observed for a certain combination values of the latent variables, such as *RateIntr* = transient for rate increases under “additive” STDP, I decide to express this via probabilities 0.9 vs. 0.1 instead of 1.0 vs. 0.0. The prior probabilities for each of the latent variables are set to 0.5. Now I determine how new evidence changes the prior beliefs by setting evidence nodes to certain values and apply Pearl’s belief propagation algorithm to update the marginal probabilities over the latent variables. I perform this crucial inference step by using the Bayes Net Toolbox for Matlab [BNT, 2007]. The updated posteriors for all combination of evidence are shown in Fig. 3.6b. Obviously, when the three observations correspond exactly to the simulation results, the corresponding

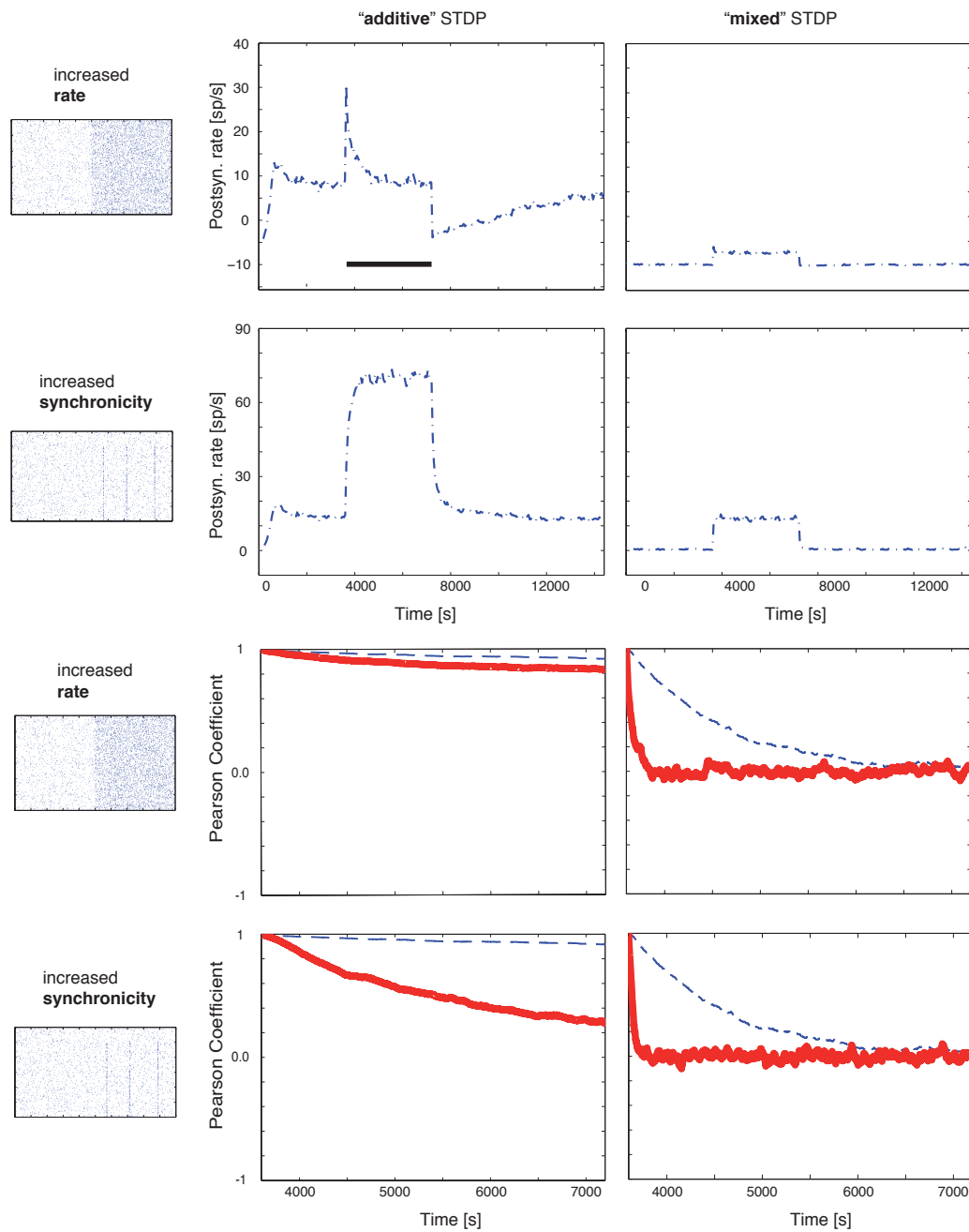


Figure 3.5: Simulation results for all four combinations of paroxysmal activities and STDP rules. The four upper panels depict the postsynaptic firing rates under various combinations and the four lower panels draw the memory retention with the dashed blue lines indicating the normal conditions without the perturbation of input spike trains and the solid red lines with perturbation.

latent variables have high posterior probabilities. For example, for observed transient decay of postsynaptic activity during the seizure ($RateIntra = \text{transient}$), a “recovering” post-ictal firing rate ($RatePost = \text{recovering}$) and “mild” memory loss ($MemLoss = \text{mild}$) are predictable only by “additive” STDP. However, it is conceivable that experimental evidence may yield results not compatible with any of the four combinations of latent variables such as $RateIntra = \text{elevated}$, $RatePost = \text{recovering}$, and $MemLoss = \text{severe}$, which leads to almost equal posterior probabilities for Act (second row, fourth column).

I argue that such a systematic comparison of different mechanisms, even without a full data-driven Bayesian model comparison, will yield valuable insights into the actually employed mechanisms. Most importantly, however, I believe that this approach of comparing alternative mechanisms is ideally suited as a basis for further refinement of the models and the domain knowledge expressed in terms of a Bayesian network.

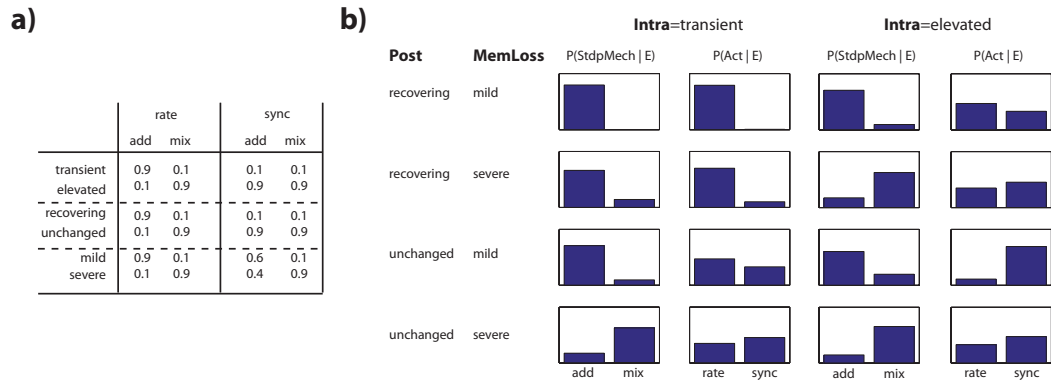


Figure 3.6: **Conditional probabilities for the Bayesian network and inferred posteriors.** **A.** CPTs set up based on the simulation results. **B.** Inferred posterior distributions over the latent variables for all combinations of observable evidence at the three evidence nodes (leaf nodes in Fig. 3.2b).

3.5 Discussion and Future Vision

I propose that data and model sharing in neuroscience shall be accompanied with the sharing of knowledge via annotating scientific publications with formal statements of the qualitative empirical findings, similar to the semantic web. In this work, one particular knowledge representation is demonstrated where inferences generated from qualitative observations could easily be translated to machine-readably annotations. I have shown how to translate simulation results into a Bayesian network and how to perform such inferences using qualitative observations from the literature even without access to the raw quantitative data. Certainly, the annotation of scientific publications using semantic knowledge is desirable. But this, of course, leaves open the problem of how to get these annotations in the first place. Ideally, for new publications, the authors themselves formulate the findings and hypotheses in a machine-readable format. A prerequisite for that is the availability of proper ontologies and markup languages. Efforts for standardized ontologies in neuro- and brain science are under way, and research in semantic web technologies has produced methods and tools for formalizing knowledge. However, for already published works such annotations need to be made *post hoc*. I envision a web site with curated annotations, which would then be applicable for both new and older publications, where standards are enforced as part of the curation procedure.

The particular example I considered here is challenging, because as of now, it is not known in which way paroxysmal brain activity may affect memory via STDP. Directly measuring this will remain beyond the technical possibilities for the foreseeable future. Thus, making use of a variety of experimental observations both from animal and human studies will be most promising. The experimental literature shows a diverse picture: for example, the intra-ictal activity of some granule cells in the rat hippocampus was observed to be elevated while others remained unchanged [Bower and Buckmaster, 2008]. In addition, the firing of some cells became more regular approx. 1 min before seizure onset, and some other cells showed a firing rate reduction for the seizure. Recent observations from human spike activity during seizures revealed that the single neuron activity is indeed “highly heterogeneous, not hyper-synchronous” and showed clear termination of activity after a seizure [Truccolo et al., 2011]. Within the class of the mutually exclusive alternatives I considered, the latter findings are most compatible with an “additive” STDP rule, and an increased firing rate of the presynaptic neurons. Taken the poor performance of the “mixed” STDP in terms of memory retention, however, one could even rule it out as a candidate mechanism.

Future work will have to: i) derive formal statements of these experimental findings using, for example, temporal logic expressions; ii) extend the space of models to more alternatives for the presynaptic spike activity to allow for increased rates, increased synchronicity and changes in the regularity of firing; iii) introduce more observables such as the Fano factor for the postsynaptic response; iv) link all descriptions to neuro-ontologies.

Chapter 4

Adapting the Ensemble of Synaptic Weights via STDP by Changing the Action Potential Shape

The models of synaptic plasticity explored in the previous chapter are phenomenological models that treat the occurrence of both pre- and postsynaptic spikes as all-or-none events. However, even though the biophysics of action potentials are well characterized, they may differ significantly between individual cells. Most recent studies have not taken the detailed dynamics of action potentials into account when exploring the consequences of plasticity rules for the ensemble of “synaptic weights”, or even the connections in (recurrent) networks. Moreover, the experimental literature has not yet characterized the potential effects of the action potential dynamics (the “shape” of an action potential in the time vs. voltage plane) on synaptic plasticity (see Sec 4.1 for details).

In this chapter, I develop a new model within the Song framework that incorporates an AP-dependent STDP window. I then explore the impact of AP duration on i) synaptic plasticity in terms of how the ensemble of synaptic “weights” of a single postsynaptic neuron is affected by the AP duration and ii) neuronal dynamics in terms of how the average firing rate of the model neuron is regulated by the adapting ensemble. This model is rooted in a biophysically more realistic model [Clopath and Gerstner, 2010], but it retains the simplicity of the Song framework, which eases simulation studies and may allow for theoretical investigations. In Sec 4.2, I present the modeling results from [Clopath and Gerstner, 2010] and [Shouval et al., 2002] that motivate my simplified dSTDP model formulated in the ensuing section. The main simulation observations are illustrated in Sec 4.3, and I summarize the chapter and derive experimentally-testable model predictions in Sec 4.4.

4.1 Background and Motivation

Synaptic plasticity is sensitive to the timing of pre- and postsynaptic firings. Ever since the first experiments demonstrating that Hebbian synapse exists [Kelso et al., 1986] and first recordings revealing that the coincidence of postsynaptic action potentials (APs) and excitatory postsynaptic potentials (EPSPs) was sufficient to induce long-term changes in synaptic efficacy [Markram et al., 1997], many experimentalists and theoreticians believed that “timing is everything”. For the past decade, these findings led to a generally accepted phenomenon known as spike timing-dependent plasticity (STDP) [Caporale and Dan, 2008], even though its generality has been questioned [Lisman and Spruston, 2010] as STDP-induced modification is contingent upon many other factors [Lisman and Spruston, 2005]. Despite ongoing debates over spike timing as the most critical parameter within the multi-factor plasticity rule of STDP [Feldman, 2012], the key principle of the Hebbian learning is still thought to be the spike-pair causality [Sejnowski, 2003].

APs, or the back-propagating signals triggered by APs, are believed to play the most crucial role in STDP. However, theoretical studies usually treated spikes as all-or-none events, with the duration and magnitude of which not being taken into consideration. Thus, it is no surprise that the functional role of AP duration or magnitude on STDP has never been investigated, neither experimentally nor theoretically. It is worth noting that AP duration differs between cell types. GABAergic interneurons often [McCormick et al., 1985], but not always [Kawaguchi and Kubota, 1993] or exclusively [Gray and McCormick, 1996], have shorter AP durations than pyramidal neurons. In addition, AP duration is widely used to identify dopamine (DA) neurons and it was shown that the projection targets of DA neurons correlate with their AP durations, for instance, nucleus accumbens-projecting neurons may have a duration of 5 ms, which is almost twice as long as for amygdala-projecting ones [Margolis et al., 2008]. Even within the same neuron type, what’s more worth noting is that AP duration, which is generally accepted as a stereotypic property, can be modulated via BK channels [Deng et al., 2013]. All the evidences above led us to the hypothesis that such differences are not accidental but may play a role in information processing, learning, memory and even in certain disease models. Besides, since AP broadening may exert a significant impact on various types of calcium channels that can lead to an increase of calcium entry and thus favor a strengthening of synaptic conductance [Wheeler et al., 1996], AP duration may have an impact on synaptic plasticity that is not negligible. From the biological perspective, elucidating this impact will shade light on the mechanisms underlying how synaptic plasticity shapes cortical networks of excitatory and inhibitory neurons, and how various pathways of DA and non-DA neurons differ, e.g., given identical protocols.

In addition to the biological standpoint, some mathematical models have also attested that the change of the duration of action potential could have remarkable consequences on the elevation of calcium concentration and synaptic modification. For example, a biophysical model proposed by [Shouval et al., 2002] demonstrated that a post-stimulus with a wider postsynaptic spike results in a much larger increase of calcium concentration (Fig. 4.1B).

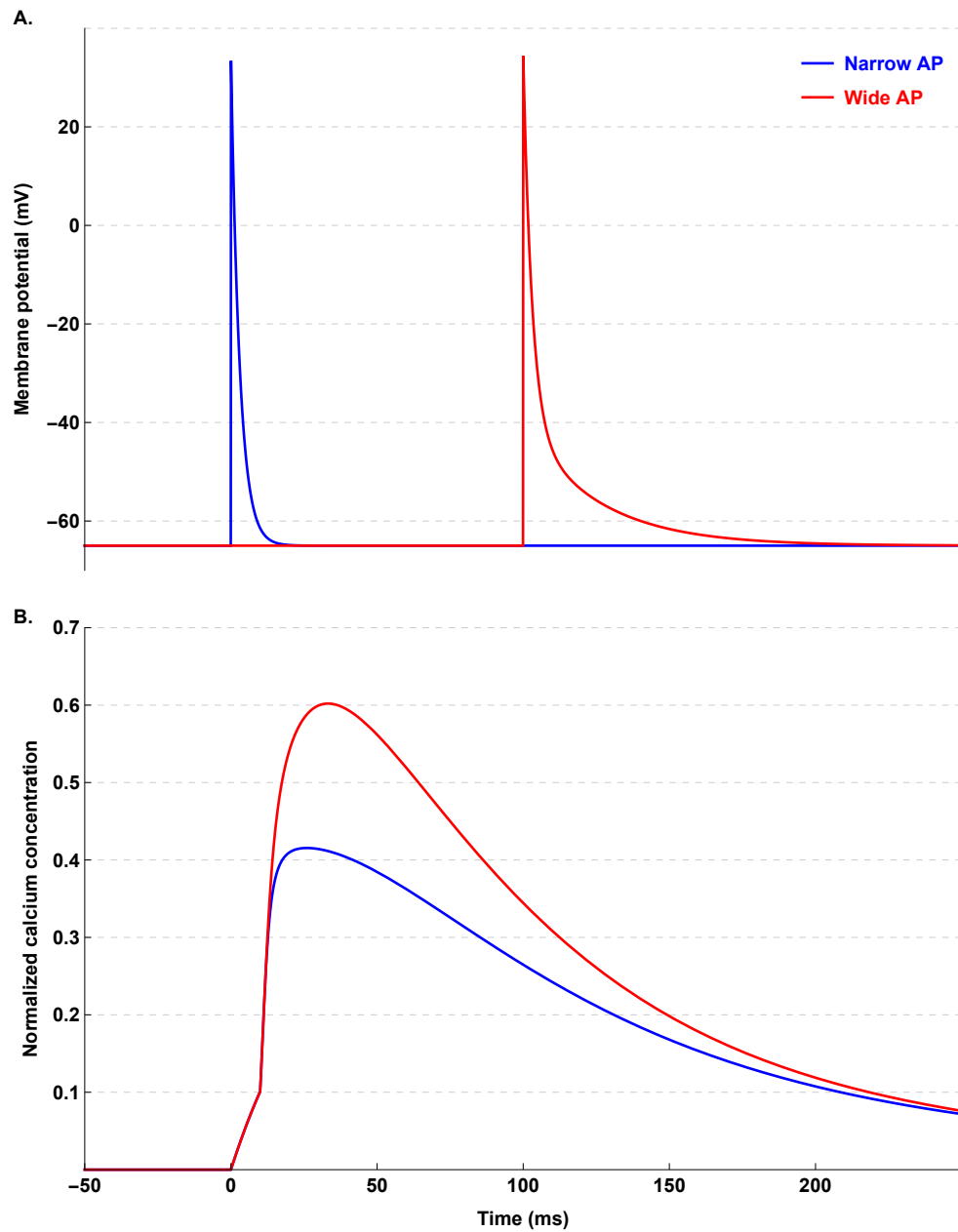


Figure 4.1: The shape of postsynaptic spike contributes to calcium elevation.

A. Examples of two action potentials with different shapes (lengths).

B. The calcium elevations induced by the action potentials of different lengths as in A.

For another example, a recently proposed phenomenological model accounts for a variety of experimental findings of STDP [Clopath et al., 2010]. This model is voltage dependent and does *not* treat spikes as all-or-none phenomena, from which the predicted synaptic modifications depend not only on the plasticity model but also on the neuron model. I first replicated the simulation results from [Clopath et al., 2010] and then experimented with the model by varying AP duration. Two typical STDP experimental protocols were simulated: an inter-spike interval (ISI) protocol and an inter-spike frequency (ISF) protocol, respectively with a set of AP durations. Fig. 4.2A shows the STDP curves obtained from the ISI protocols with 20 pairs per second and different inter-spike intervals Δt . I observe that the longer the AP duration the more the predicted STDP window is stretched. In particular, a synapse is potentiated for long APs even when presynaptic spikes arrive within, which resembles the curves reported in [Nevian and Sakmann, 2006]. The peak potentiation is higher for long AP durations, because at pre-post pairings they keep the membrane potential at higher voltage, which in the model translates into more potentiation. Moreover, I find that AP duration affects as well the predicted synaptic modifications under the ISF protocol. Potentiation is predicted to increase with higher frequencies of pre-post pairs, $\Delta t = 10$ ms, for longer but not for short APs (Fig. 4.2B & C). Altogether I confirm that AP duration of 2.0 ms produced the model predictions, that are in agreement with previous experiments [Sjöström et al., 2001].

These modeling results emphasize the importance of the postsynaptic AP duration in synaptic plasticity from a modeling & theoretical point of view. The important predictions I then include below into my new model are: i) presynaptic spikes strengthen a synapse when they arrive before and during an AP, but they weaken a synapse when arriving afterwards; ii) the magnitudes of these modifications depend on AP duration. In support of these model predictions, one of the original STDP papers did show some data points, illustrating positive synaptic weight changes given negative Δt [Bi and Poo, 1998].

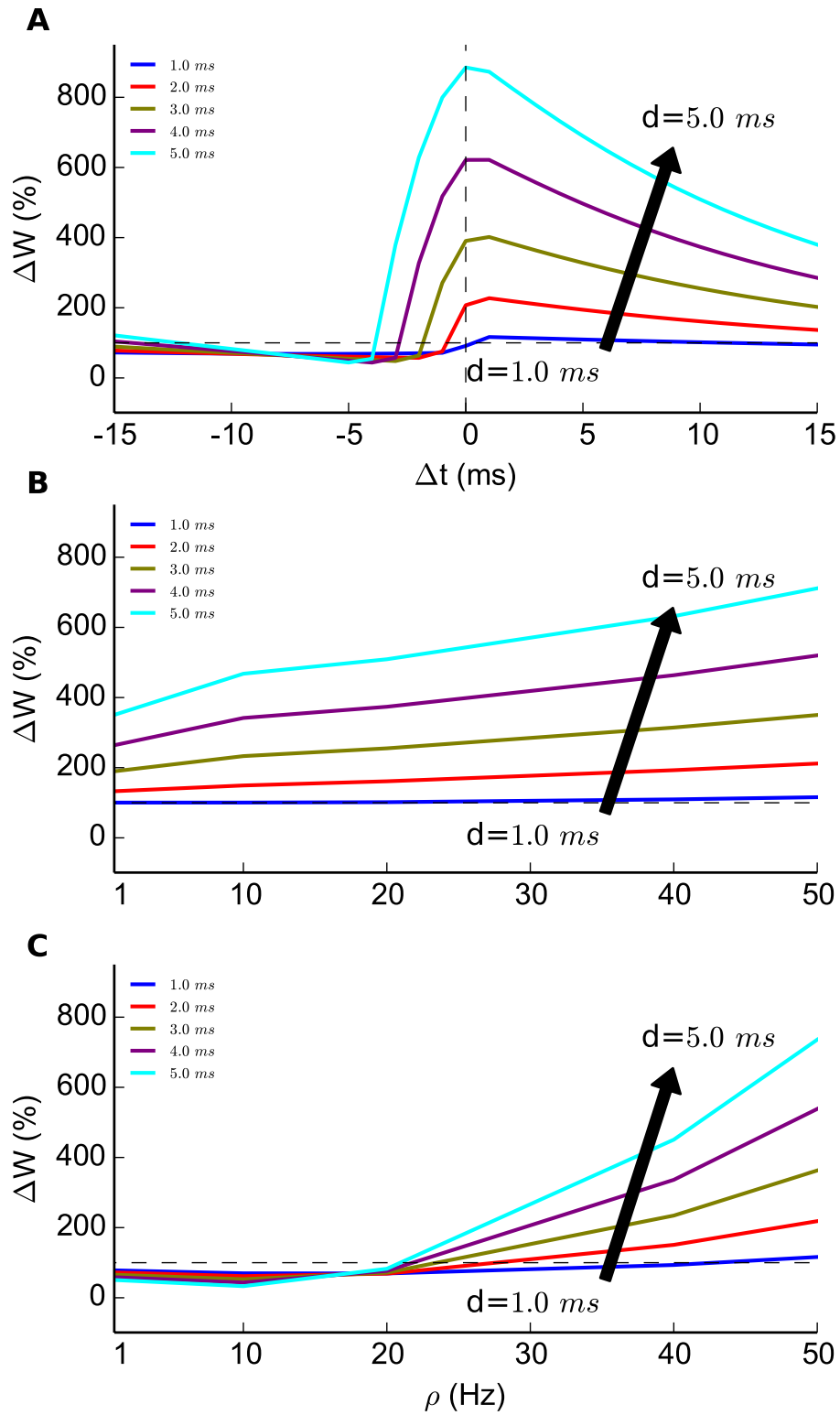


Figure 4.2: Synaptic modification by a voltage-dependent STDP model.

A. STDP windows generated by stimulating Clopath model [Clopath et al., 2010] with 75 pairs (20 pairs per second) of pre- and postsynaptic spikes with 5 different pairing intervals Δt (1.0 to 5.0 ms). B & C. The relative peak modification of synaptic weight simulated by different pairing frequency ρ with $\Delta t = +10$ ms (pre-post) and $\Delta t = -10$ ms (post-pre).

4.2 Formulation of dSTDP model

One could focus on one out of two aspects when modeling synaptic plasticity, namely the detailed biophysical/biochemical dynamics or the emergent functional properties of learning rules. In this study, my emphasis is on the latter and I define a phenomenological model to study how AP duration may shape the pattern of synaptic weights. In the model, the individual synapses do *not* interact directly with each other, but their synaptic strengths become interdependent via the spiking of the postsynaptic neuron. For instance, [Song et al., 2000] have demonstrated in their study how competition could arise in this way. This already shows that even apparently simplistic phenomenological models can lead to surprising non-linear emergent effects at the level of a single neuron that shall be understood before the biophysical/biochemical dynamics at a single synapses are investigated. The new model is based on three assumptions: First, a synapse is potentiated when a presynaptic spike arrives before *and* during a postsynaptic AP; Second, a synapse with a presynaptic spike arriving after the postsynaptic AP is depressed with a magnitude depending on AP duration in order to control the overall LTP/LTD ratio; Third, the effect of AP duration is uniformly distributed through the length, modeled via a plateau in the STDP window. I construct the model in such a way that it could be simulated in both additive [Song et al., 2000] and mixed modes (additive update for potentiation and multiplicative update for depression, see details in [Kepecs et al., 2002]). For AP duration is explicitly included within the model, I name it dSTDP.

More specifically, given a presynaptic spike at i -th excitatory synapse and a postsynaptic spike elicited by an interval Δt , the corresponding change of the synaptic weight w_{exc}^i is illustrated in Fig. 4.3A and defined as:

$$\Delta w_{exc}^i = \begin{cases} w_{max} \cdot A_+ \cdot \exp(-\Delta t / \tau_+) & \text{if } \Delta t > 0 \\ w_{max} \cdot A_+ & \text{if } -d_{AP} \leq \Delta t \leq 0 \\ w_{LTD} \cdot A_+ \exp((\Delta t + d_{AP}) / \tau_-) & \text{if } \Delta t < -d_{AP} \end{cases} \quad (4.1)$$

where $w_{LTD} = -w_{max} \cdot \beta(\alpha, d_{AP})$ and $w_{LTD} = -w^i \cdot \beta(\tilde{\alpha}, d_{AP})$ in are used respectively in the additive and mixed modes. The AP duration dependent term $\beta(\alpha, d) = \alpha \cdot e^{\frac{2d}{\tau_+}}$ is introduced to keep the ratio of positive integral to negative integral equal to constant α (Fig. 4.3B). This procedure is intended to eliminate significant changes in the ratio of LTP/LTD areas induced by AP duration, which could be a potential confounding factor [Song et al., 2000]. An all-to-all pairing scheme is implemented to update synaptic modifications [Izhikevich and Desai, 2003].

As described in the previous chapter, a phenomenological STDP model has to be simulated in tandem with a neuron model that serves to receive presynaptic spikes and generate postsynaptic APs. The model neuron receives N_{exc} excitatory and N_{inh} inhibitory poisson spike trains similar as the way implemented in [Song et al., 2000] and [Van Rossum et al., 2000]. A standard single-compartment conductance-based leaky integrate-and-fire neuron with a

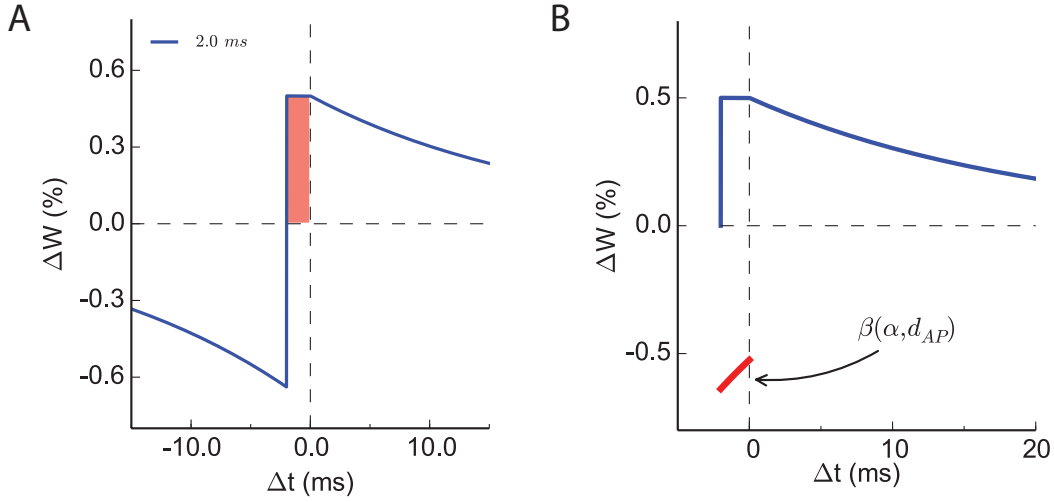


Figure 4.3: **dSTDP window function.** **A.** The relative modification of synaptic weight Δw varies as a function of inter-spike interval Δt ($d_{AP} = 2.0$ ms). **B.** The update for depression is modeled with an AP-duration-dependent term $\beta(\alpha, d) = \alpha \cdot e^{\frac{2d}{\tau_+}}$.

spike-triggered adaptation current [Delgado et al., 2010] is used to simulate the dynamics of membrane potential V_m with membrane capacity C_m and leak conductance G_L :

$$C_m \frac{dV_m}{dt} = G_L (V_r - V_m) + G_{exc}(t) (E_{exc} - V_m) + G_{inh}(t) (E_{inh} - V_m) + g_{adpt}(t) (E_{adpt} - V_m) \quad (4.2)$$

The model neuron spikes an AP when the membrane potential reaches the threshold V_{th} . To cooperate with the dSTDP model I introduce d_{AP} as the new parameter, denoting AP duration, such that when the membrane potential reaches the threshold from below at time t_{spike} , I assign $V_m(t) = V_{peak}$ for $t_{spike} \leq t < t_{spike} + d_{AP}$ and then reset $V_m(t) = V_{reset}$ at $t = t + d_{AP}$. This is certainly a gross simplification for modeling the effects of AP duration, but I introduce this simplistic parameterization in order to obtain a first qualitative characterization of its impact on synaptic conductances via synaptic learning. The adaptation conductance $g_{adpt}(t)$ increments by 1 nS after each postsynaptic spike, namely at the time of threshold crossing t_{spike} , and then decays with a time constant τ_{adpt} . It models spike-frequency adaptation due to, for example, calcium-dependent potassium currents. The total synaptic conductances $G_{exc}(t)$ and $G_{inh}(t)$ represent summed contributions from all excitatory and inhibitory synapses. The corresponding total conductance is increased instantaneously by w^i whenever a presynaptic spike arrives at the i -th synapse, and then decays with a time constant τ_{syn} . All inhibitory synapses have an unmodifiable strength w_{inh} , whereas w_{exc}^i is updated by STDP learning. Important parameters for both neuron and plasticity model are listed in Table. 4.1.

Table 4.1: Neuronal, synaptic and plasticity parameters

Parameter	Symbol	Default value
Membrane capacity	C_m	200 pF
Leak conductance	G_L	10 nS
Membrane time constant	τ_m	20 ms
Spiking threshold	V_{th}	-54 mV
Resting membrane potential	V_r	-70 mV
Reset membrane potential	V_{reset}	-60 mV
Adaptive reversal potential	E_{adap}	-70 mV
Adaptation time constant	τ_{adap}	100 ms
Action potential duration	d_{AP}	2.0 ms
Synaptic time constant	τ_{syn}	5 ms
Potential time constant	τ_+	20 ms
Depression time constant	τ_-	20 ms
Inhibitory synaptic strength	w_{inh}	500 pS
Number of excitatory synapses	N_{exc}	1000
Number of inhibitory synapses	N_{inh}	200
Excitatory input rate	r_{exc}	10 Hz
Inhibitory input rate	r_{inh}	10 Hz
Maximum potentiation amplitude	A_+	0.005
Learning ratio in additive mode	α	1.05
Learning ratio in mixed mode	$\tilde{\alpha}$	2

4.3 Results

4.3.1 Comparison of equilibrium weight distributions

I first study one of the functional consequences of STDP: the shape of synaptic weight distribution. The dSTDP model is simulated together with an integrate-and-fire model neuron whose activity is driven by both excitatory and inhibitory poisson spike trains. The equilibrium synaptic weight distributions are first re-examined for short AP duration 0.1 ms (equivalent to the model with a canonical STDP window, e.g. [Song et al., 2000]) in both modes. The additive mode produces a U-shaped bimodal distribution with synaptic weights tamed by an upper-bound (Fig. 4.4A), well matching the results reported in [Song et al., 2000]. The weight-dependent mixed mode generates a centered unimodal distribution (Fig. 4.4B) in which the synaptic weights are very narrowly distributed, consistent with a previous simulation study [Billings and van Rossum, 2009]. As previously contemplated, when simulated without imposing an upper-bound, the additive mode has an inherent instability in that a few synapses get boundlessly stronger due to a destabilizing force, while the others become weaker (Fig. 4.4C). By contrast, the mixed mode has an intrinsic stability and produces the very same distribution, independent of the existence of an upper-bound (Fig. 4.4D), because the effect of the destabilizing force is relatively small as the stabilizing force dominates, which then constrains the weight growth [Van Rossum et al., 2000].

For simulations of dSTDP models I chose an AP duration of 2.0 ms. Interestingly, dSTDP in the additive mode predicts a wide unimodal distribution (Fig. 4.4E), which clearly differs from the U-shaped as in Fig. 4.4A. This difference can be understood as follows: the additional potentiation force introduced by the AP duration counters the extra depression induced by the β -term. As a consequence, independent of the initial synaptic weights, most of the synapses tend to stay in the middle range of the weight spectrum (Fig. 4.5). Note that the distribution remains stable without an upper-bound (Fig. 4.4G), indicating an intrinsic stability property possessed by the model. The dSTDP model simulated in the mixed mode predicts a similar narrow unimodal distribution, but slightly skewed (Fig. 4.4F & H).

4.3.2 AP duration determines the shape of synaptic weight distribution

The results shown in Fig. 4.4 suggest to me that the equilibrium synaptic weight distribution could be largely attributable to the length of AP duration in dSTDP models. I decide to simulate dSTDP model in the additive mode with an upper-bound w_{max} for various AP durations, ranging from 0.1 to 5.0 ms, and observe the resultant distributions which is illustrated in Fig. 4.6E. The weight distribution loses its bimodal shape as AP duration increases and transforms to a complete unimodal for durations that are larger than approximately 1.0 ms, and it becomes narrower for larger ones. Accompanied with the reshaping of weight distribution, the average and the standard deviation of synaptic weights decrease for longer AP durations (Fig. 4.6A & B), which are computed from the histograms shown in Fig. 4.6E and they illustrate one experimentally-testable prediction of dSTDP model: the postsynaptic AP duration is predicted to be inversely correlated with the average synaptic strength as well as its variability.

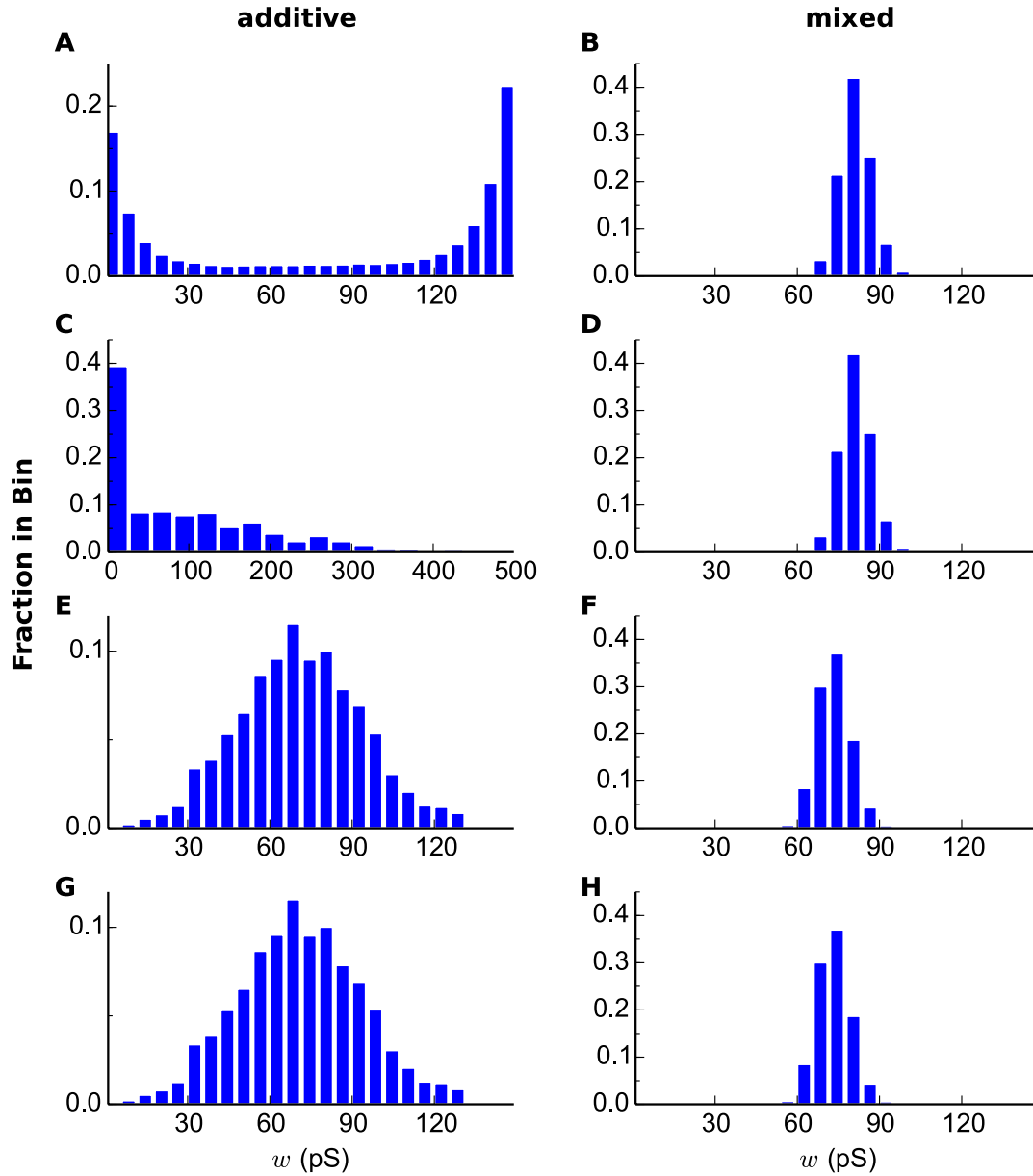


Figure 4.4: Equilibrium synaptic weight distributions for dSTDP models.

(For A,B,C,D: $d_{AP} = 0.1$ ms.)

A: A U-shaped bimodal distribution generated by additive mode, with an upper-bound.

B: A centered unimodal distribution generated by mixed mode, with an upper-bound.

C: Similar to A, without an upper-bound. The distribution doesn't equilibrate as in A and the data is taken at $t = 3000$ sec.

D: Similar to B, without an upper-bound. (For E,F,G,H: $d_{AP} = 2.0$ ms.)

E: The wide unimodal distribution by additive mode, with an upper-bound.

F: The slightly-skewed unimodal distribution by mixed mode, with an upper-bound.

G: Similar to E, without an upper-bound.

H: Similar to F, without an upper-bound.

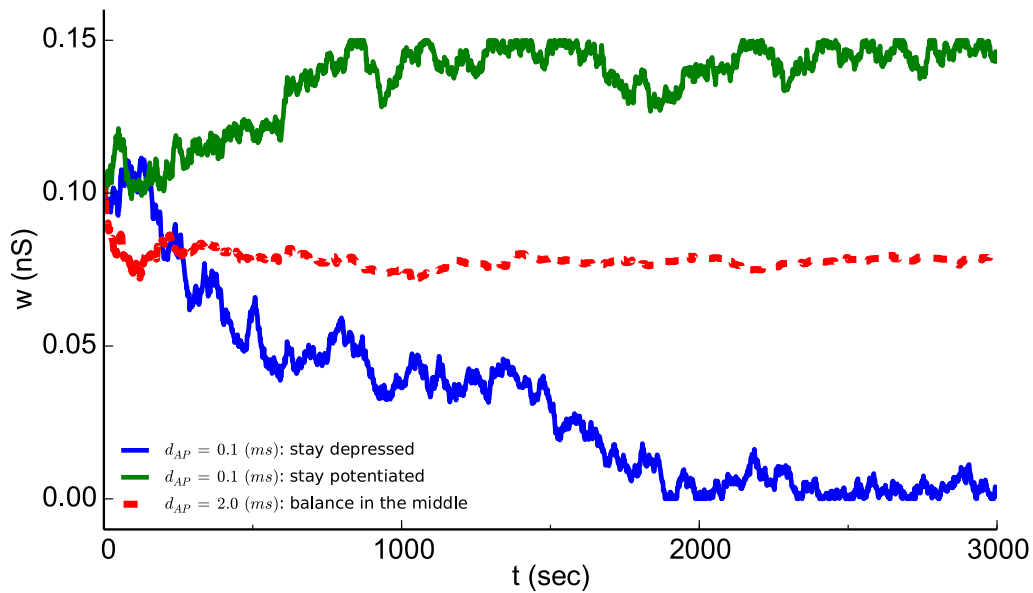


Figure 4.5: The developments of synaptic weights under different AP durations.

By short AP duration, the additive mode drives most of the synapses either to a potentiated state (green) or a depressed state (blue), thereby resulting in a bimodal distribution.

In contrast, most synapses tend to stay in the middle (red) by long AP duration.

Note that even though the distribution reaches an equilibrium state, individual weights keep fluctuating as the simulation goes along. The fluctuation is around one order of magnitude larger than for short AP durations (Fig. 4.6C & D). This reflects the difference between the bimodal and unimodal weight distributions as for instance in the former, strong synapses can become weak and vice versa, which results in large temporal fluctuations. In comparison, the mixed mode exhibits fairly small variations in both statistical properties and hence doesn't result in significant AP duration dependent changes in equilibrium synaptic weight distribution (Fig. 4.7).

4.3.3 Postsynaptic response to signal and noise inputs

Next, I study another functional consequence of STDP: the regulation of postsynaptic spiking rate [Abbott and Nelson, 2000]. In this modeling study, most of the presynaptic inputs were modeled as poisson spike trains, similar as what was conducted also in some previous works in the literature. It is currently not clear if in the real brain such poisson spikes carry relevant information or should rather be considered as a source of background noise, however, recent evidences suggested that correlated synchronous neural activity is informative about the features of stimulus in the early sensory processing [Stanley et al., 2012] as well as about behavioral states [Salinas and Sejnowski, 2001]. Therefore, I decide to explore the role of AP duration in dSTDP for processing inputs that are composed of both synchronous spikes as the signal and poisson spikes as the noise.

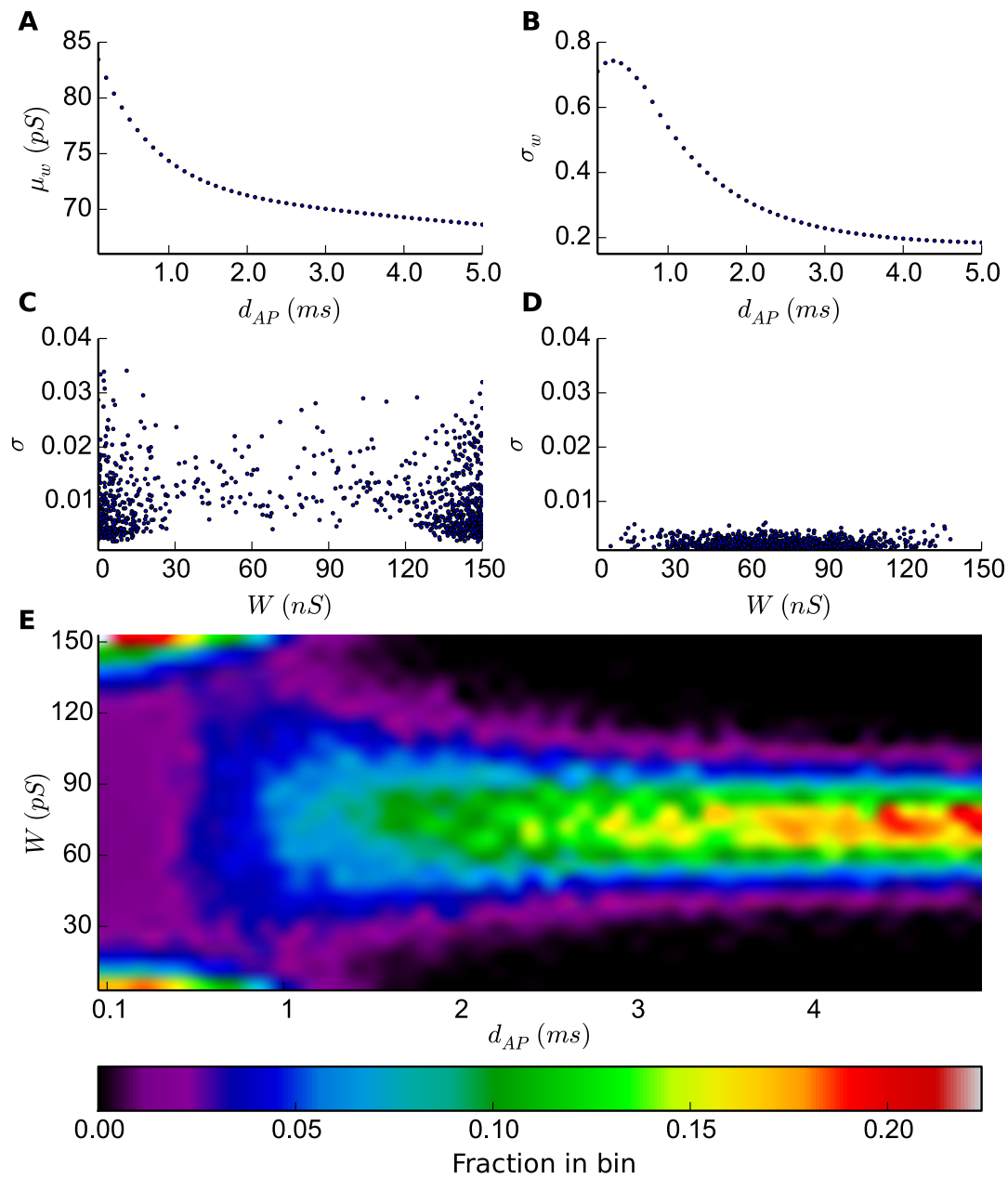


Figure 4.6: AP duration determines the shape of equilibrium synaptic weight distribution (additive mode).

A: The average of excitatory synaptic weights given various AP durations.

B: The standard deviation of excitatory synaptic weights given various AP durations.

C: The standard deviation of each individual synaptic weight for an 1000-sec post-equilibrium simulation run ($d_{AP} = 0.1$ ms).

D: Same as in C, $d_{AP} = 2.0$ ms.

E: The horizontal axis is AP duration, the vertical axis is synaptic weight and color bar indicates the probability density.

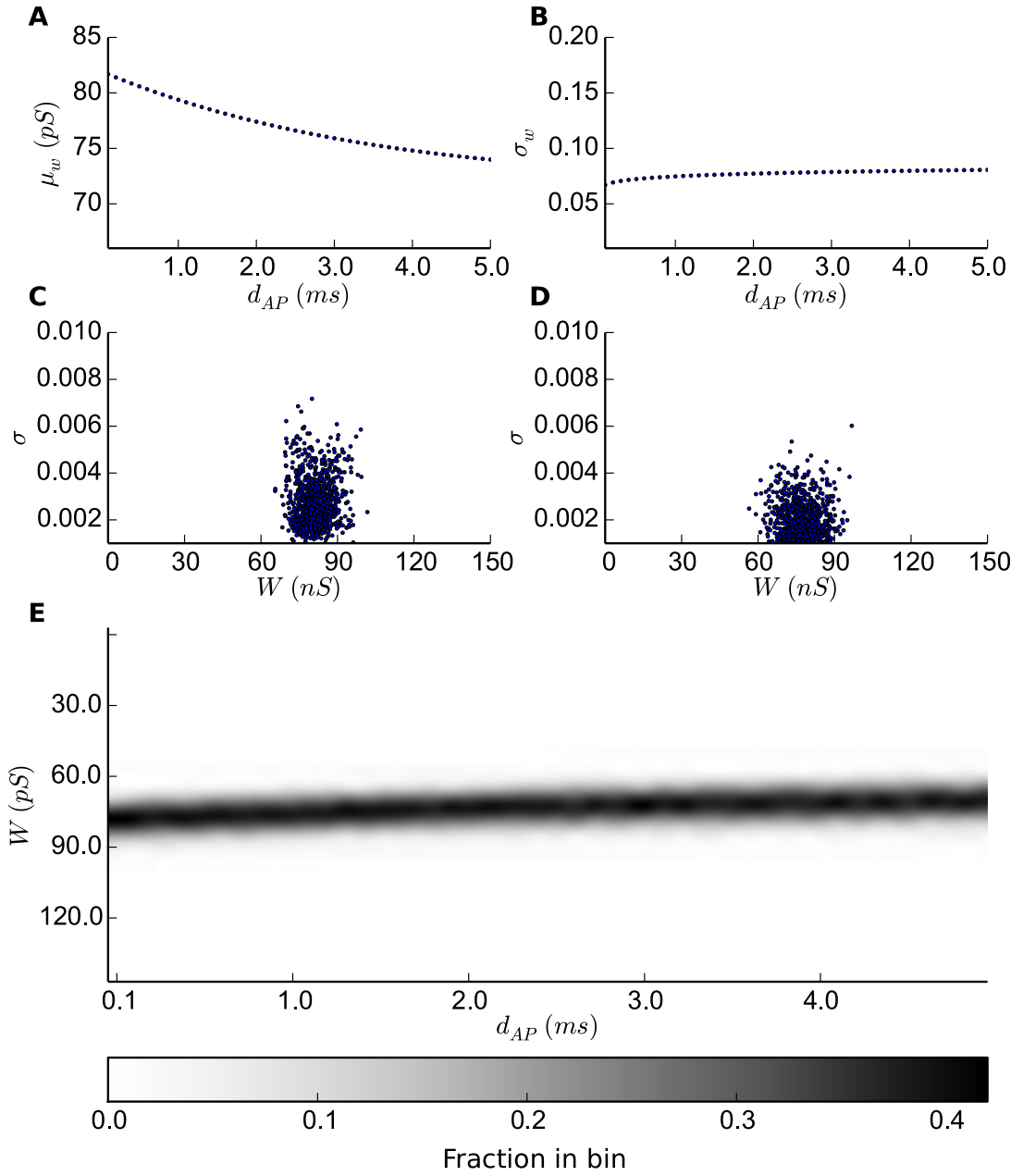


Figure 4.7: AP duration has little effect on shaping synaptic weight distribution in the mixed mode. Similar as what is illustrated in Fig. 4.6, but simulated with mixed mode.

As done above for investigating the synaptic weight distributions, I first explore the effect of AP duration on regulating the postsynaptic response to the noise. The fluctuation analysis suggests that the dynamics of the postsynaptic neuron must also undergo a big change. It has been discovered that given poisson noise, STDP rules have remarkable effects on regulating the long-term average spiking rate of the postsynaptic neuron [Kempster et al., 2001] as the synaptic weight distribution converges to an equilibrated state. I find that dSTDP models also possess such a regulation of the postsynaptic spiking: 1) the rate simulated with the additive mode dSTDP decreases quickly as AP duration extends (normalized ratio in Fig. 4.8A, red); 2) such effect is as prominent with the mixed mode, the rate drops almost by 60% when varying AP duration from 0.1 ms to 2.0 ms (Fig. 4.8A, green), despite the fact that the weight distribution has only a small shift to the *left* (Fig. 4.4F).

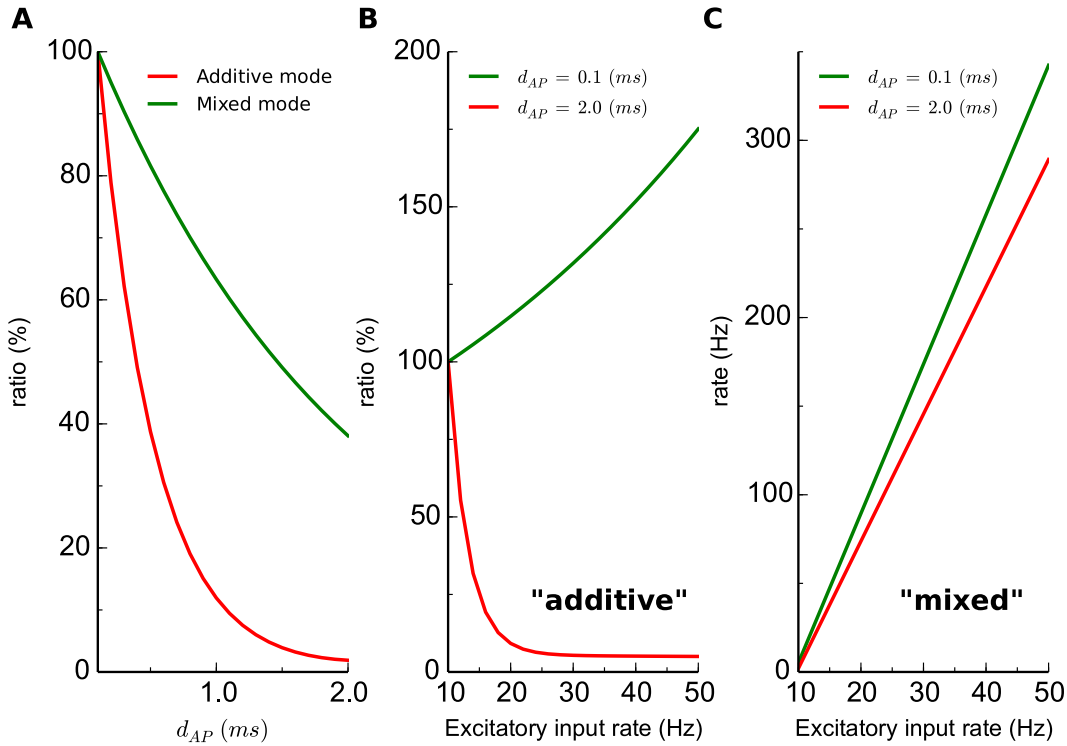


Figure 4.8: Regulation of postsynaptic spiking rate by AP duration (noise).

A. The normalized postsynaptic rates for various AP durations.

B. The normalized postsynaptic rates for various excitatory input rates (additive mode).

C. Similar as B, but the rates are not normalized (mixed mode).

Analyzing a selected simulation run shows that the absolute asymptotic postsynaptic spiking rate for a long AP duration is much lower compared to a short one (0.1 vs 7.5 Hz, see traces in Fig. 4.9). The simulations reveal that AP duration exerts a significant effect on the steady-state spiking rate, making the model neuron much insensitive to the noise (Fig. 4.8A & B). Such regulation is expected as the weight distribution narrows (Fig. 4.6E) and total weight of synapses decreases when AP duration is elevated (Fig. 4.6A).

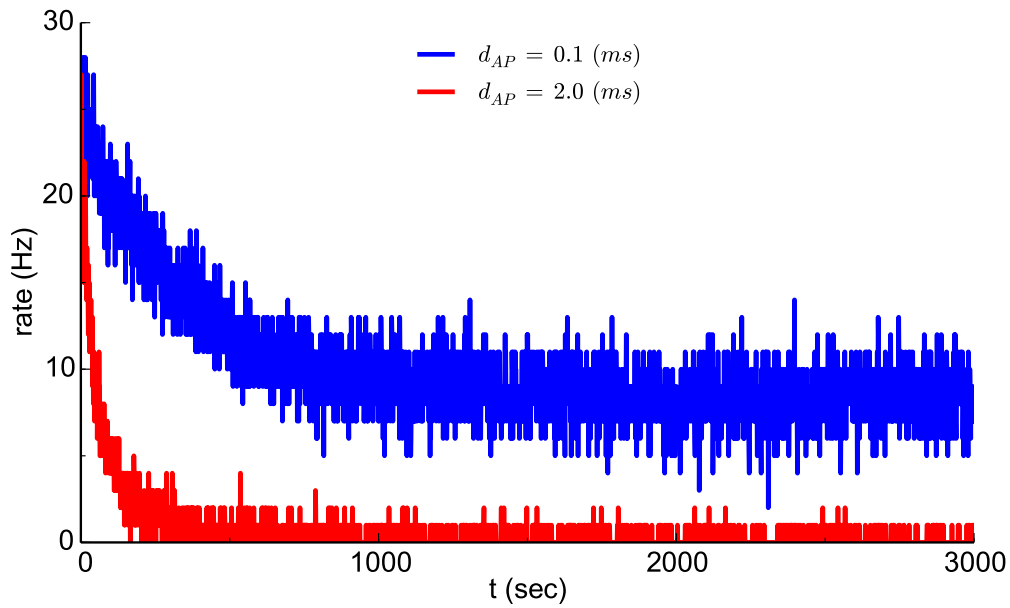


Figure 4.9: **Postsynaptic spiking rate traces.** The rates are calculated by simulating $d_{AP} = 0.1$ ms (blue) and $d_{AP} = 2.0$ ms (red).

A recent model showed an interesting regulation of the postsynaptic spiking, by which the rate has a nonlinear dependence with the level of excitatory noise [Babadi and Abbott, 2010]. Such feature is also present by dSTDP models, which is affected by the length of AP duration. I find that in the additive mode: 1) when AP duration is short, the postsynaptic rate rises from 7.5 Hz to about 13 Hz as the excitatory input rate is elevated from 10 Hz to 50 Hz (Fig. 4.8B, green). This result is consistent with the previous study, as each 5 Hz increase causes an elevation of the output rate roughly by 1 Hz [Song et al., 2000]; 2) when AP duration is long, however, an exponential-decreasing dependence is observed (Fig. 4.8B, red), which can be understood intuitively as the postsynaptic neuron shifts most of the synapses to weaker strengths for higher presynaptic activities (Fig. 4.10). Such "buffering" effect is much weaker in the mixed mode (Fig. 4.8C) and the rate undergoes a more than 60-fold increase from 5 Hz to 300 Hz for just a 5-fold increase of the input rate, but still, the increase is less pronounced for longer AP durations (Fig. 4.8C, red). Then I simulated a scenario where the model neuron is first driven by the noise alone and let weight distribution converges towards an equilibrium. Afterwards, a signal modeled as synchronous events generated in a poisson manner is applied for 200 seconds to drive the neuron model. More specifically, I define a rate r and a fraction f of the presynaptic spikes being synchronized, then within each simulation time bin Δt , the probability of a synchronous event to occur is $r\Delta t$, and on every occurrence of such synchrony, $f \cdot N_{exc}$ presynaptic excitatory spikes are synchronized. After removing the signal the weight distribution re-equilibrated again (Fig. 4.11). Interestingly, I observe that postsynaptic spiking remains equally sensitive to the signal (plateau phase), while the noise is much more effectively filtered (decay phase) by a long AP duration than a short one (Fig. 4.12).

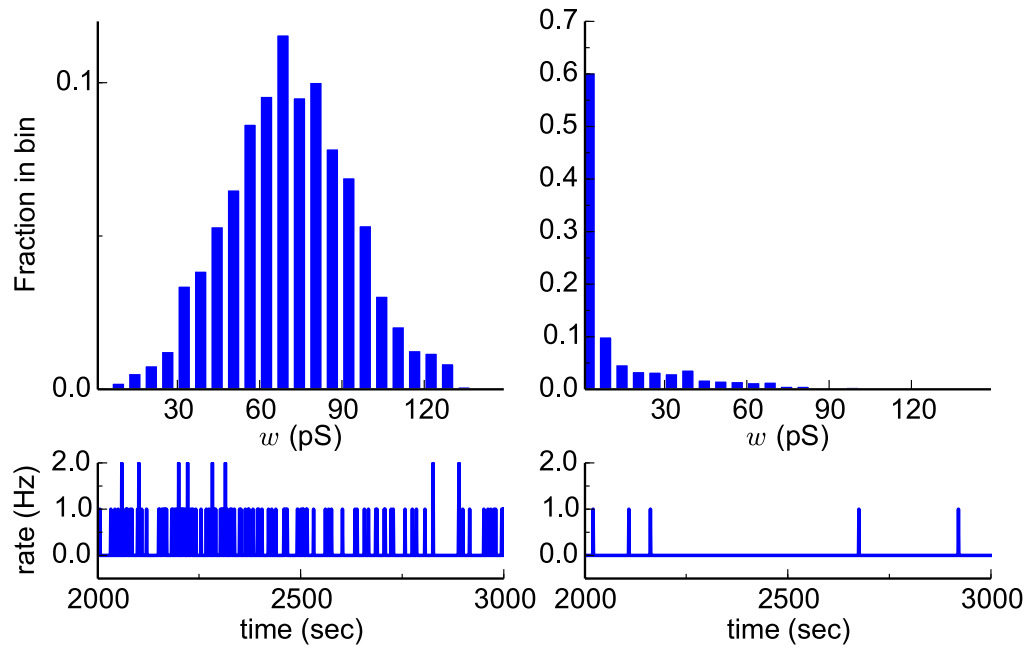


Figure 4.10: **The effect of elevated excitatory noise input on synaptic weight distribution and postsynaptic rate (additive mode).** The synaptic distributions (upper) and postsynaptic firing rates (lower) are depicted for $r_{exc} = 10$ (left panels) and $r_{exc} = 50$ (right panels).

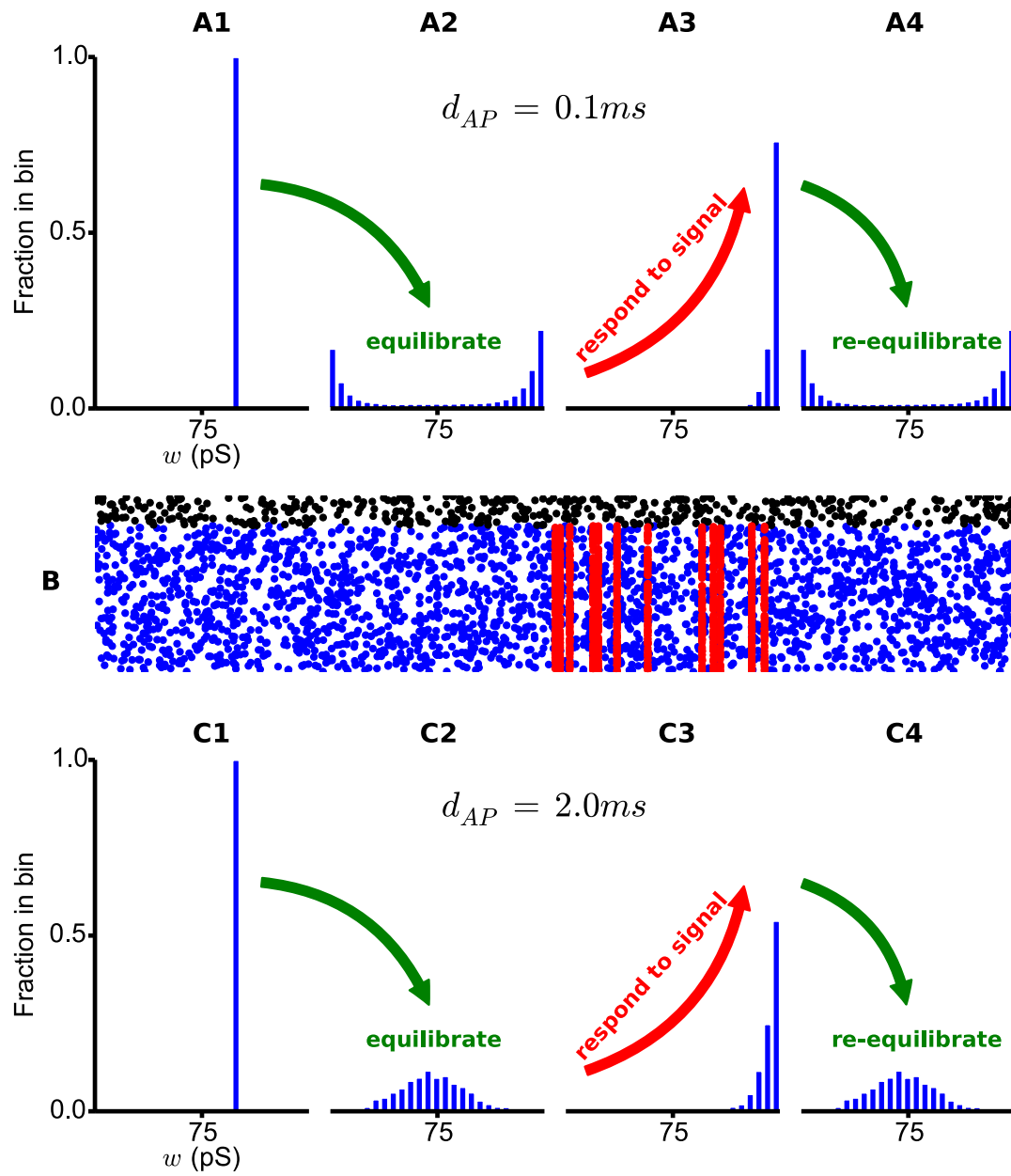


Figure 4.11: The effect of signal input on synaptic distribution (additive mode).

A1: All the excitatory synapses have an initial weight of 100 pS.

A2: The equilibrium synaptic weight distribution converges to a bimodal shape after receiving noise only.

A3: Most of the synapses are strengthened towards w_{max} when afterwards receiving both noise and signal.

A4: The removal of the signal re-equilibrates the distribution back to a bimodal shape.

B: A raster plot represents the presynaptic spike trains, aligned with the different stages that cause the change of synaptic weight distribution.

C: All panels are similar to A, but simulated with AP duration 2.0 ms.

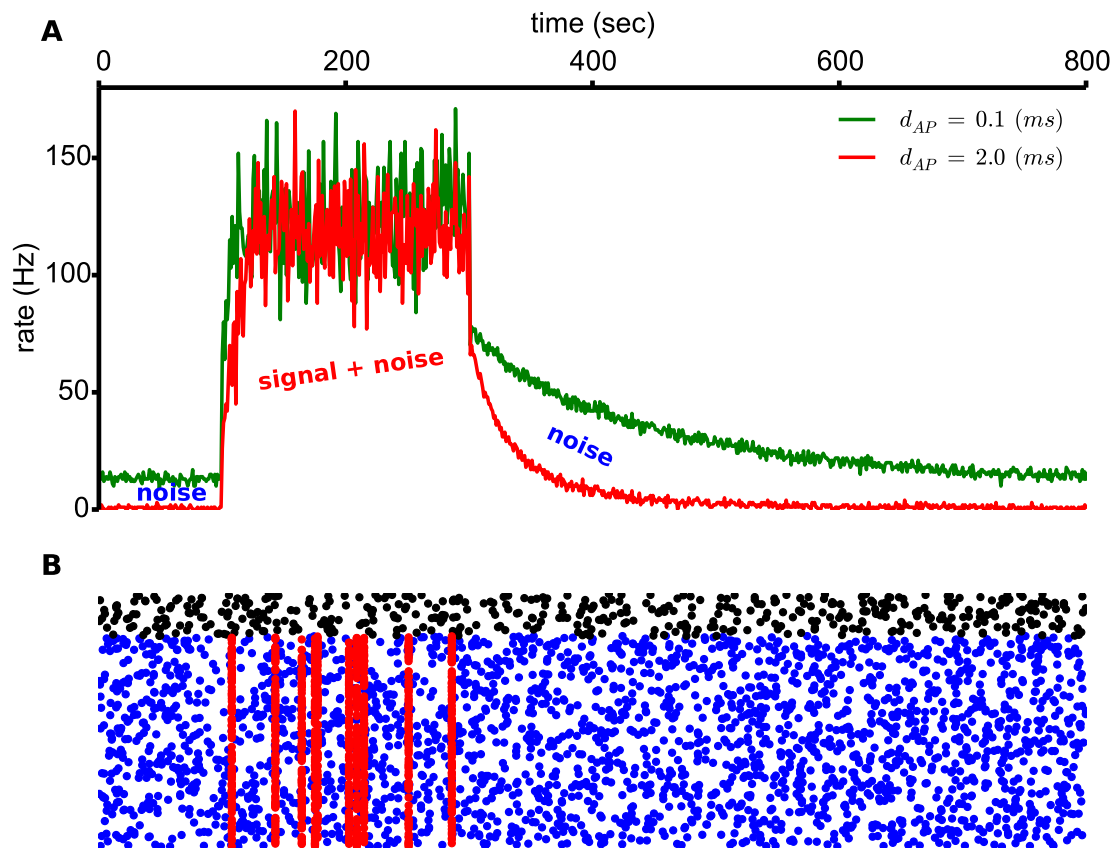


Figure 4.12: Sensitivity of postsynaptic spiking rate to synchronized spikes.

A. The actual postsynaptic rates are shown for two different AP durations, driven by the presynaptic spike activity as illustrated in B.

B. A raster plot of the poisson spike trains (noise) and the synchronized spikes (signal).

The blue dots represent the excitatory inputs (10 Hz) and the black dots indicate the inhibitory ones (10 Hz). The synchronous spikes are represented by the red dots which occur on excitatory synapses only ($r = 10 \text{ Hz}$ and $f = 0.1$).

4.3.4 Simulations of unbounded dSTDP

The hard boundary imposed in the simulations with short AP duration is very artificial, essentially lacking a biological underpinning for its usage in the simulation study. I have shown that without an upper-bound, short AP duration leads in the additive mode to a development in which a number of very strong synapses continue to grow their strengths way beyond w_{max} (Fig. 4.4C). Taking a snapshot at time 1500 sec in the simulations, I observe that on average only 72% of the excitatory synapses have weights smaller than or equal to w_{max} . Nevertheless, long AP duration intrinsically stabilizes the synaptic strength without bounds (Fig. 4.4G). Therefore, I am very keen to know whether varying the AP duration may systematically alter the below-bound ratio of synaptic population, the ratio of the synaptic weights below w_{max} . I find that this below-bound ratio increases as AP duration is extended (Fig. 4.13A), for instance, all synaptic weights are constrained below w_{max} once AP duration is larger than 2.0 ms. Moreover, I also picked out the maximum synaptic weights for various AP durations from simulations (each ran for 3000 sec). The maximum decreases when AP duration is prolonged and no single weight exceeds w_{max} when APs are longer than 2.0 ms (Fig. 4.13B). These results confirm from a different perspective that AP duration has an inherently stabilizing effects which should motivate further studies.

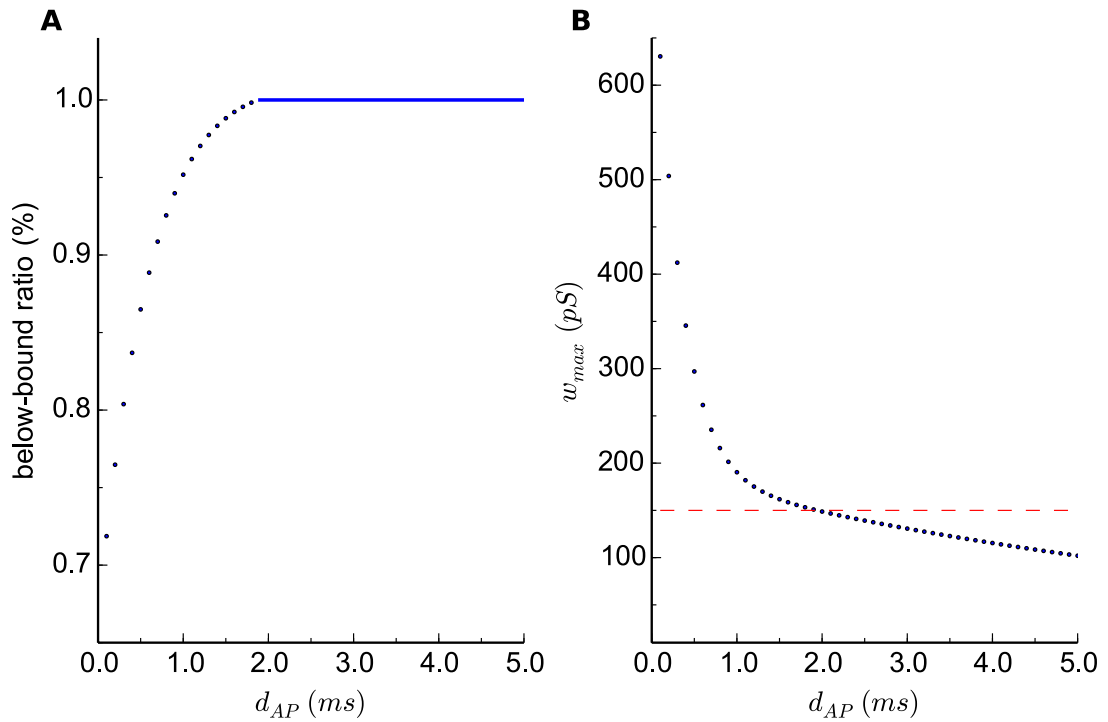


Figure 4.13: dSTDP models unbounded.

A: The ratio of synaptic weights below w_{max} .

B: The maximum synaptic weight obtained throughout each simulation run (3000 sec).

4.4 Discussion

The main contribution of the study described in this chapter is to emphasize that AP duration is an important and so far poorly investigated feature of STDP. Here I particularly refer to the emergent properties of AP duration in a model neuron driven by a number of excitatory and inhibitory poisson noisy spike trains as well as the synchronized on the synapses, *not* its effects in microscopic models of synaptic plasticity [Shouval et al., 2002] or signal transduction pathway models of a postsynaptic spine [Manninen et al., 2010]. In my simulation study I used a recently proposed unified model [Clopath and Gerstner, 2010] as the basis for my novel simplified linear dSTDP model, which includes AP duration directly into a STDP window function.

This dSTDP model in the additive mode makes several unique and testable predictions:

i) the synaptic weight distribution depends on AP duration with a bimodal shape for short ones and a unimodal for the longer (Fig. 4.6E). This prediction can be experimentally tested by e.g., ensemble statistics of spontaneous miniature or evoked EPSPs; ii) the mean and standard deviation of this distribution decrease for elevated APs (Fig. 4.6A & B). It is worth noting that this prediction is in good consistency with the data reported by a few previous experimental works. For instance the duration of bAP typically increases on the dendrites with the distance from soma [Kampa and Stuart, 2006] which may account for a decremental average response observed in the distal compartments [Froemke et al., 2005]. Besides, the results are also in agreement with another simulation work that modeled the effect of AP duration as axonal delay [Knoblauch et al., 2012], this work showed also a decrease in summed synaptic strengths after STDP training; iii) the fluctuations of individual synaptic weights over time depend on AP duration with stronger fluctuations for the short (Fig. 4.6C & D); iv) the model neuron with long APs is able to filter out most of the poisson noise input while remains very sensitive to the modeled signal (Fig. 4.12).

One could question the validity of our simulation study, given that one of my starting points was a phenomenological model itself [Clopath et al., 2010]. However, I used this model as our starting point, because it is a model from which the plasticity outcome is *directly* determined by the duration and magnitude of the postsynaptic AP, whereas the prediction from more complex models may be indirect, for instance, depending on the modeling of calcium concentration [Shouval et al., 2002] or kinetics of NMDA receptors [Urakubo et al., 2008]. Moreover, the dSTDP window I postulate here is consistent with the published experimental data, which is itself rather noisy and does not fully constrain the window function at the transition between potentiation and depression.

One could argue that neither a narrow unimodal [Billings and van Rossum, 2009] nor a bimodal weight distribution are of functional interests, and a stable *Gaussian* distribution should be the goal of modeling studies [Babadi and Abbott, 2010]. This contradicts the experimental observation which reported a unimodal weight distribution with long tail (a few strong connections immersed in a sea of weaker ones' [Song et al., 2005]). Interestingly, I

do obtain such a distribution as plotted in Fig. 4.14 from another version of dSTDP model which does not have the control for the ratio of integrated LTP/LTD windows, or in other words the $\beta(\alpha, d)$ term in the model.

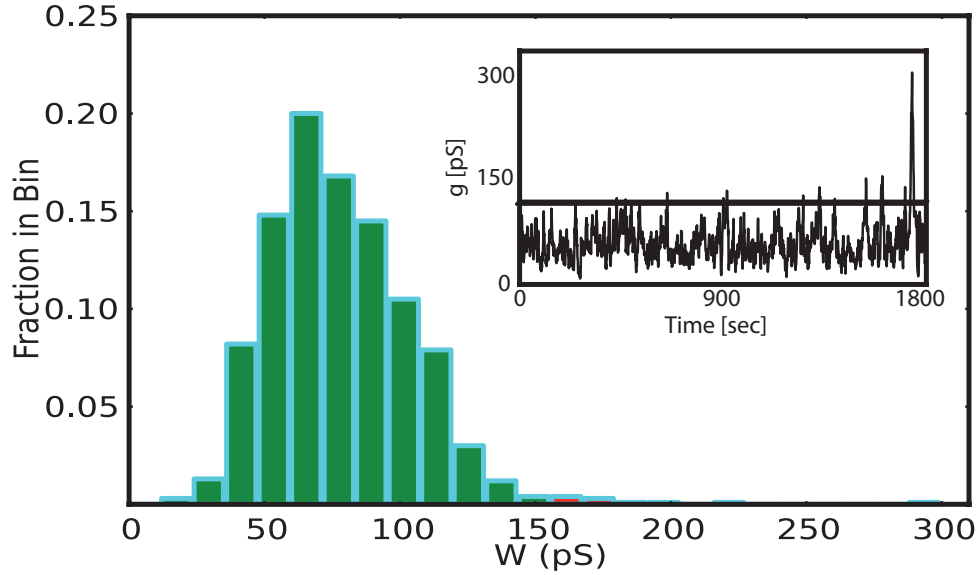


Figure 4.14: **Model prediction of dSTDP without constraint on the ratio of integrated LTP/LTD windows.** A slightly skewed unimodal distribution in the mixed mode with an upper-bound.

Conclusively, studying how AP duration affects the emergent properties of synaptic plasticity in a single neuron or neural networks, is certainly a field of interest for both theoreticians and experimentalists. More than half a century after Hodgkin and Huxley's original publication, the action potential (its shape and duration) should get renewed attention in particular from the field of synaptic plasticity and this simulation work may qualify as yet another candidate model in the spectrum of STDP modeling to be further explored, analytically and experimentally.

Chapter 5

Exploring the Consequences of State Transition in Striatal Principal Neurons by Detailed and Reduced Approaches

Striatal projection neurons (SPNs) integrate diverse cortical and thalamic inputs, and then relay the processed information to output nuclei of the basal ganglia. SPNs *in vivo* fire action potentials only from depolarized “upstates”, which appear for certain spatiotemporal patterns of multiple excitatory synaptic inputs. Such synaptically-driven state transitions from hyperpolarized “downstates” are believed to endow SPNs with the capacity to associate contextual, sensory and motor cues to control the striatal output.

In this chapter, I first introduce in Sec 5.1 the upstate phenomenon and a revised *in vitro* experimental model of how it might be produced [Plotkin et al., 2011]. In Sec 5.2, I present a detailed compartmental neuron model of a SPN with a full set of parameter values. This model is validated by replicating experimental observations of both distal upstate given glutamate uncaging and somatic spiking given current injection. I then use the model to explore how another factor may govern the state transition and its restriction to distal (but not proximal) dendrites: dendritic anatomy. Moreover, I propose a model in which the interplay between proximal and distal dendrites of a SPN can realize associative computation.

Both experimental observation and compartmental modeling support the notion that *active* channels in dendrites are indispensable for single neuron computation of SPNs. However, I show that this is *not* necessarily the case as models with only passive dendrites without active channels can predict key characteristics of the upstate. Rall’s work is the basis for investigating dendritic computations [Segev et al., 1994], particularly neuronal information processing with *passive* dendrites [Rall, 1964]. In Sec 5.3, I first recapitulate the modeling background of passive dendrites and then present a passive neuron model of a SPN with a reduced compartmental approach inspired by one of the original works from Wilfred Rall. Afterwards, I investigate under which conditions of synaptic drive, a *passive* dendrite is able to integrate specific stimuli and realize an association-based information processing.

5.1 State Transitions in Striatal Principal Neurons

As for many other neuron types, people have been studying SPNs for more than several decades, with ever-innovating tools and new technologies. It has been long discovered and known that SPNs *in vivo* operate in two different modes with two distinct levels of subthreshold membrane potential. One is the downstate around -86 mV and the other is around -55 mV, the upstate where action potential generation occurs. It is worth noting that the upstate phenomenon was indeed first found in SPNs [Wilson and Kawaguchi, 1996]. Over the years, the manifestation of downstate has been very well understood but the mechanisms for the upstate generation are still not as clear. Surmeier Lab therefore asked the question: from where the upstate originates in SPNs? His colleagues worked out the first *in-vitro* experiment that produced the upstate by using 2-photon microscopy and uncaging techniques [Plotkin et al., 2011]. They demonstrated that dendritic regenerative plateau potentials which resemble upstates can be reliably evoked by high-frequency uncaging protocols onto about ten adjacent spines in the distal region of a dendritic branch (Fig. 5.1, left panel). The generated plateau potentials can last for tens or even hundreds of milliseconds long and only the distal dendrites but not the proximal ones are capable of evoking such state transitions (Fig. 5.1, right panel).

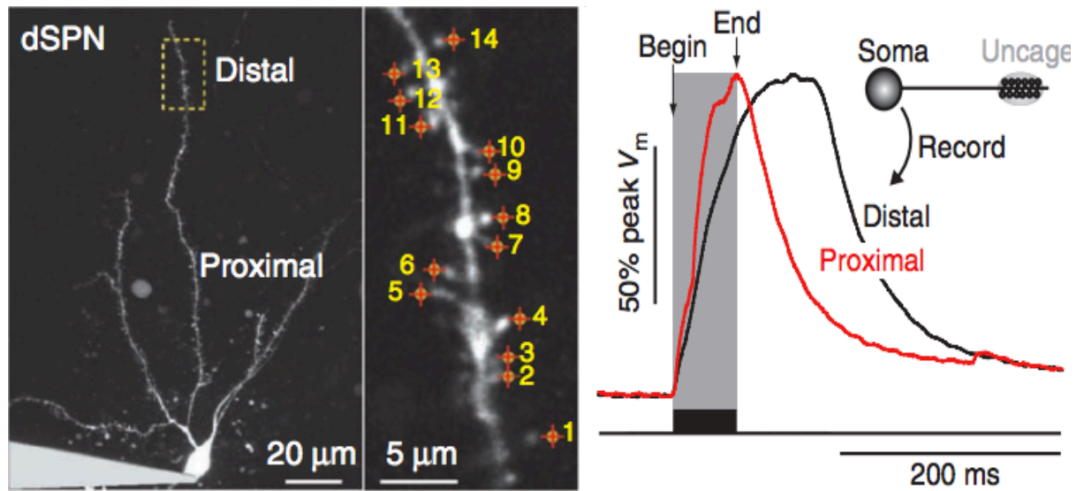


Figure 5.1: The physiological evidence of synaptically-driven state transitions in SPNs. taken from [Plotkin et al., 2011] and see texts for details.

5.2 The Detailed Compartmental Model

5.2.1 Spiny SPN Model

Neuronal Anatomy

The anatomy of this multi-compartmental SPN model is adapted from the one presented in [Wolf et al., 2005] and all the anatomical parameters are specified in the hoc files using the frameworks provided by NEURON. This model possesses one soma and four primary dendritic branches. Each primary branch bifurcates twice, extending to 8 secondary dendrites and 16 tertiary dendrites. Previous studies of SPNs have focused on either single-compartment models [Biddell and Johnson, 2013] or multi-compartmental models with a compensation for the additional membrane area attributable to spines [Wolf et al., 2005]. In contrast, I taper two of the tertiary dendrites and put onto them explicitly 349 dendritic spines each (Fig. 5.5A). The anatomical parameters are listed in Table. 5.1 and the density used to distribute spines along the two branches are plotted in Fig. 5.2, which accord quantitatively with the statistics inferred from [Wilson, 1992]. To ensure a sufficient spatial accuracy of numerical solution, an overall spatial grid for each section is specified using a d-lambda value of 0.15 [Hines and Carnevale, 2001].

Table 5.1: The anatomical parameters of SPN model

	number of sections	length	diameter
soma	1	16	16
primary dendrites	4	20	2.25
secondary dendrites	8	24.23	1.1
tertiary dendrites without spines	14	395.2	0.72
tertiary dendrites with spines	2	180	0:0.85 = 1.1:0.7 0.85:1 = 0.7:0.3

Ion Channels

To implement a diverse range of neuronal functions, SPNs have evolved a broad array of ion channels [Kreitzer, 2009], in particular, the voltage-dependent potassium channels which govern virtually every aspect of neuronal processes as diverse as synaptic integration, membrane potential stabilization and repetitive spiking. For this model, four *calcium-insensitive* voltage-dependent potassium channels are invested in the somatic and dendritic sections, which are modeled on the basis of the published data from Surmeier Lab:

1) *Inward Rectifier*: One of the striatal principal potassium channels is an inwardly-rectifying channel, known as KIR [Mermelstein et al., 1998]. The channel kinetics, however, have not been experimentally characterized by Surmeier Lab and have to be matched using data from *Aplysia* as done in [Wolf et al., 2005]. The signature characteristic of inward rectification is an increase of potassium conductance under hyperpolarization and a decrease of channel conductance under depolarization. This feature plays a crucial role in setting the resting potential as well as the input resistance of the downstate. The channel dominates the neuronal

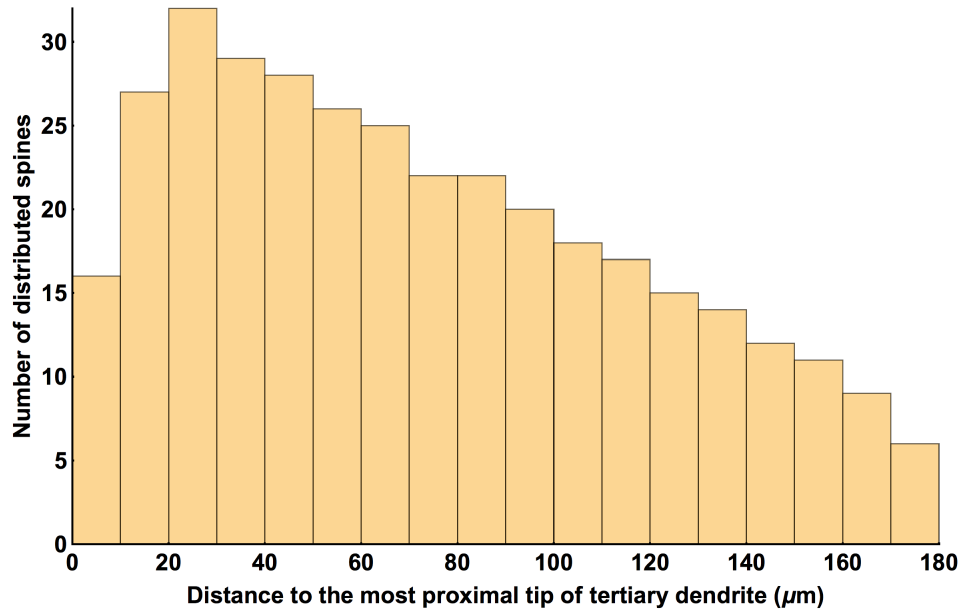


Figure 5.2: The distribution density of spines on the tapered dendritic branches.

conductance profile in the downstate and stabilizes the membrane potential close to E_k . Hence, it is this channel that makes SPNs difficult to be excited at rest. As the membrane potential becomes more positive, the channel rectifies due to the blockade of intracellular magnesium [Matsuda, 1991], thereby gradually reducing the intensity of excitatory stimuli required to produce state transitions;

2) *A-type Fast*: A-type potassium current is evident in striatal spiny neurons and a major *fast* component of this current is contributed by Kv4.2 subunits (termed as Kv4 channels below). The parameters of channel kinetics are directly taken from [Tkatch et al., 2000] (activation from Fig.2 and inactivation from Fig.3). However, the functional role of Kv4 channels in term of regulating dendritic excitability of striatal neurons is not as well-understood. In the dendrites of pyramidal neurons, Kv4 channels have very high density which increases with distance from the soma. This could also be the case for SPNs. Previous experimental and computational studies discovered that the Kv4 channel regulates the propagation of dendritic current in both orthograde and retrograde directions [Hoffman et al., 1997], e.g., its inactivation induced by synaptic activity could result in a remarkable increase in amplitude of back-propagating action potentials [Migliore et al., 1999], which is a feature that is very critical for not only dendritic integration but also the induction of associative synaptic plasticity. Recently, Surmeier Lab published new empirical results that suggested a potential regulatory role of Kv4 channels in the striatal neurons [Day et al., 2008], similar to what has been observed in the pyramidal neurons. Part of the results make an claim that action potential back-propagates into very distal dendritic regions in both D1 and D2 neurons, and this invasion is modulated by Kv4 channels. This finding is consistent with what has been reported in other cell types, stating that the Kv4 channel depresses the amplitude of

bAPs in the distal dendrite (see Fig.4 in [Day et al., 2008]). Another worth-investigating issue I find is that unlike in the pyramidal cells, there is so far no evidence for sodium investment in the distal dendrites of SPNs (see Fig.2 in [Day et al., 2008]). The only possible way to boost calcium signal in the distal dendrite given bAPs may indeed be the mechanism through the inactivation of Kv4 channels caused by clustered synaptic inputs as proposed by [Migliore et al., 1999]. Nevertheless it is not clear whether the Kv4 channel possesses a similar functionality as shown in pyramidal neurons or may be involved in other forms of dendritic information processing that is unique to SPNs. The functional consequences of such attributes are discussed in the last chapter;

3) *A-type Slow*: Kv4 channels, as described above, inactivate very rapidly with a time constant of about 10 milliseconds, making them ineffective in the regulation of *sustained* synaptic activity. In contrast, another A-type potassium channel composed of Kv1.2 subunits, is evolved relatively later in development to compensate for such inefficiency (termed as Kv1 channels below). This channel is often referred to as slow-inactivating potassium channel. The biophysical properties of Kv1 channels enable them to possess a comparably fast activation rate but a much slower deactivation, and therefore ensure their contribution to regulate dendritic excitability during sustained upstate firing [Shen et al., 2004], from which the original modeling parameters are extracted. For example, the channel can induce a use-dependent short-term (2 seconds) increase of membrane excitability attributable to a slow inactivation of the gating variable (Fig. 5.3). Besides, nearly half of the total potassium current is constituted by Kv1 channels at upstate potentials from -60mV to -55mV, making them play critical roles in regulating state transitions and repetitive discharge. Furthermore, in spite of the relatively less contribution (10-20%) at very depolarized membrane potentials, their strategic location in the spike generation zone [Day et al., 2008] still endows the channel with a major impact on modulating spiking frequency and first spike latency;

4) *4-AP Resistant Persistent*: Except Kv1 and Kv4 channels which inactivate, the potassium current recorded from striatal principal neurons indicates that there exists a third component that is rather persistent and 4-aminopyridine (4-AP) resistant (termed as KRP channels below). The kinetic parameters of the channel are taken from [Nisenbaum et al., 1996] (activation kinetics from Fig.6; activation and deactivation time constants from Fig.8; inactivation kinetics and time constants in Fig.9). Because of the relatively slow activation rate, the current of KRP channels makes a distinctive contribution at subthreshold membrane potential by having a very minimal influence on the voltage transition from the hyperpolarized state to the depolarized but enabling SPNs to constrain the amplitude and duration of membrane depolarization, e.g., regulating the maintenance of dendritic regenerative events. Three characteristics of the channel kinetics are: slow activation rate with time constant at about 100 ms near -45 mV; only about 20% of the current is inactivated near the resting potential; and the time constant of inactivation is 3 times slower than that of Kv1 channels.

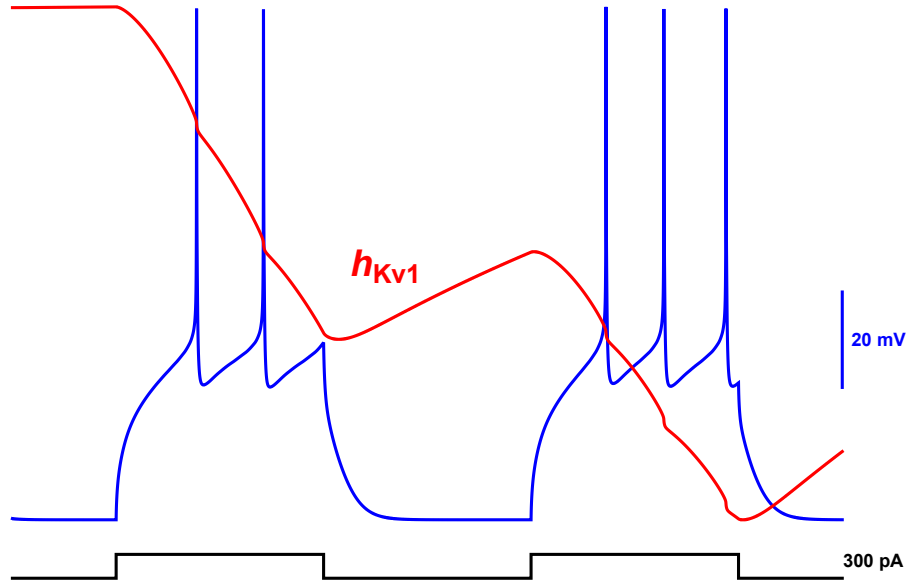


Figure 5.3: **The slow inactivating Kv1 channel facilitates short-term excitability of SPNs.** The blue trace is the membrane potential evoked by the injected current (black curve). The red curve is re-scaled to illustrate the effect of inactivation variable h_{Kv1} on the reduction of first spike latency and interspike interval due to its partial recovery before the second ramp.

Sodium channels of both fast (NaF) and persistent (NaP) types are distributed throughout the model with differential finite conductances. As the gating kinetics of sodium channels are not available in the striatal literature, the parameters are taken from the studies of other brain areas. For the fast type, the kinetic parameters are extracted from principal neurons of rat hippocampus [Martina and Jonas, 1997]. The persistent type is different from the fast type in a number of kinetic aspects. It possesses a lower threshold and fast kinetics for activation (Fig. 5.4A). In addition, the most prominent difference is that its kinetics of inactivation is several thousand times slower (Fig. 5.4B). Besides, the conductance has a lower amplitude which represents only less than 2% of the total sodium conductance. Most of the parameters of the persistent type are taken from principal neurons of rat cortex [Magistretti and Alonso, 1999], except for the kinetics for activation τ [Traub et al., 2003]. In order to generate realistic spiking behavior and avoid doublets of action potentials, it is necessary to set the conductances in the soma to be 10 times the ones in the dendrites.

Calcium channels are of particular interest to the study of dopaminergic modulation of striatal function, and two subtypes have been implicated to modulate the initiation and duration of state transitions [Plotkin et al., 2011]: T-type and R-type. Surmeier Lab has characterized the R-type and the kinetic parameters are all extracted from [Foehring et al., 2000] (activation from Fig.6 and inactivation from Fig.7). The T-type channel is distinguished from the R-type in several aspects: more hyperpolarized voltage threshold for activation, much slower deactivation and voltage-dependent kinetics of inactivation. However, the kinetics of T-type channel has not been characterized in the neostriatal and the model-

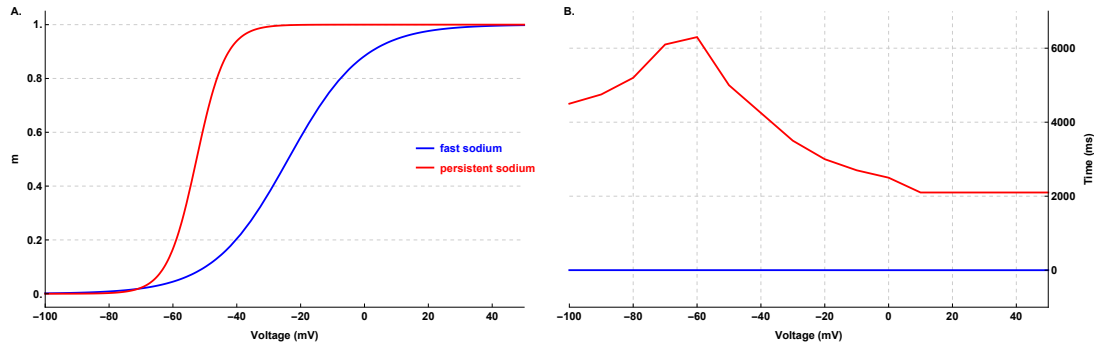


Figure 5.4: The kinetics of sodium channels in the SPN model.

A. The kinetics of voltage-dependent gating variables. B. The inactivation time constants.

ing parameters if necessary must be taken from other cell types, e.g., [Wang et al., 1991]. These two calcium channels are excluded from the somatic and dendritic compartments (not spines) for the reason that the sodium and potassium channels listed in Table 5.2 are sufficient to generate reasonable behaviors in response to the current injection.

Using a modified version of HH formalism [Hodgkin and Huxley, 1952], the channels are individually modeled by following Eq. 5.1, with the gating variables m and h defined using Eq. 5.2 and Eq. 5.3 respectively.

$$I_z = \bar{g}_z m^x (ah^y + (1 - a))(V - E_z) \quad (5.1)$$

$$m' = \frac{m_\infty - m}{\tau_m} \quad \text{with} \quad m_\infty(V) = \frac{1}{1 + \exp(-\frac{V - V_{1/2}}{V_s})} \quad (5.2)$$

$$h' = \frac{h_\infty - h}{\tau_h} \quad \text{with} \quad h_\infty(V) = \frac{1}{1 + \exp(\frac{V - V_{1/2}}{V_s})} \quad (5.3)$$

where m and h are gating variables for activation and inactivation. m_∞ and h_∞ represent steady-state activation and inactivation curves. τ_m and τ_h are time constants for variable m and h at voltage V . The half-activation and inactivation voltage constants are represented by $V_{1/2}$ and V_s is the slope of the Boltzmann fit to m_∞ and h_∞ curves. \bar{g}_z is the maximal conductance of a specific channel z . The ionic channels are all implemented as separate mod files and then loaded to work together with the hoc files using the interfaces provided within NEURON. The parameter values are listed in Table. 5.2.

Table 5.2: Parameter values of ion channels implemented in SPN model

	\bar{g}_z (S/cm ²)	HH form		$V_{1/2}$ (mV)	V_s (mV)	τ (ms)
NaF	1.5, soma	x=3, y=1	m	-23.9	11.8	Tabulated
	0.0195, dendrites	a=1	h	-62.9	10.7	Tabulated
NaP	4e-5, soma	x=1, y=1	m	-52.6	4.6	Tabulated
	1.38e-7, dendrites	a=1	h	-48.8	10.0	Tabulated
Kv4	0.225, soma and proximal	x=2, y=1	m	-10.0	17.7	Tabulated
	0.02, middle and distal	a=1	h	-75.6	10.0	4.67
Kv1	0.0104, soma and proximal	x=2, y=1	m	-27.0	16	Tabulated
	9.51e-4, middle and distal	a=0.996	h	-33.5	21.5	Tabulated
K _{IR}	1.4e-4, all	x=1, y=0	m	-82.0	13	Tabulated
K _{RP}	0.001, all	x=1, y=1	m	-13.5	11.8	Tabulated
		a=0.7	h	-54.7	18.6	Tabulated

Dendritic spines

Spines are modeled using the electrical circuits described in Sec 2.4, by having spine heads connected to spine necks attached to their parent dendritic shafts. The spine necks are passive but spine heads are modeled with fast-activating AMPA and NMDA receptors, and various voltage-sensitive calcium channels, such as T-type and R-type.

5.2.2 Simulation Results

The somatic response to current injection and location independence of evoked EPSPs

I illustrate a part of the SPN model in Fig. 5.5A which shows a soma, one full dendritic branch and spines that receive proximal and distal inputs. Somatic current injection protocols are conducted to verify the model to the reported somatic recordings. One of the signature characteristics of a SPN is an extended depolarizing ramp in response to the current injection before firing the first spike. This behavior is manifest in the model in response to supra-threshold current injection (Fig. 5.5B, red). An injected current of larger amplitude leads to a repetitive firing (Fig. 5.5B, black). In addition, the experiment using glutamate uncaging has shown that the amplitudes of somatic EPSPs evoked by activating glutamate receptors of single spines are independent of their dendritic locations (see Supplementary Fig.3 in [Plotkin et al., 2011]). The model replicates such independence by synaptically activating one proximal and one distal spine, with each possessing an identical glutamate receptor composition. The resulting EPSPs have similar amplitudes when triggered by either distal or proximal stimulation (Fig. 5.6A). The rise times of proximally-triggered somatic EPSPs are faster, as expected.

The upstate replication and potential role of spine neck

SPN state transitions can be evoked experimentally by spatially and temporally coordinated activation of about a dozen distal dendritic spines. The model reproduces this phenomenon

with an activation of 12 spines in rapid succession (500 HZ) on a distal dendrite ($> 120 \mu m$ from soma). The resulting membrane potential trajectory at the soma demonstrates at least 3 features of an experimentally observed distal upstate (Fig. 5.6B, solid red):

- 1) the depolarization peaks tens of milliseconds after the termination of stimulus;
- 2) the depolarization is sustained as a plateau potential;
- 3) the depolarization decays to the baseline voltage rapidly when the plateau potential falls.

Unlike distal dendrites, proximal dendrites are not capable of sustaining regenerative events [Plotkin et al., 2011]. Consistent with this observation, activating 12 proximal spines ($> 60 \mu m$ from soma) in rapid succession (500 Hz) produces a somatic response that reaches the same peak as the distally-evoked response and decays almost immediately after the protocol ends (Fig. 5.6B, solid black). Moreover, the dendritically-evoked upstate requires an engagement of NMDA receptors (NMDARs) and voltage-gated calcium channels (VGCCs). The model confirms the contribution of these channels to EPSPs evoked by rapid activation of 12 distal or proximal spines. Removal of these channels reduces both the amplitude and duration of distally-evoked EPSPs (dashed red), but has little effect on proximally-evoked responses (Fig. 5.6B, dashed black). These results confirm the previous demonstration that not only do NMDARs and VGCCs contribute to dendritic plateau potentials, but they are more efficiently engaged in distal dendrites. Furthermore, the lengths of distal spine necks are parameter-scanned, which is something not tangible in a real experiment. The result illustrates that the neck length can alter the dynamics of evoked state transitions with long necks extending the duration and short necks elevating the amplitude (Fig. 5.6C).

The contribution of thin dendrites for upstate generation

Plateau potentials in the distal SPN dendrites require current flow through NMDARs and VGCCs. It was suggested by [Plotkin et al., 2011] that the ability of distal, but not proximal, SPN dendrites to support regenerative events is a consequence of a distance-dependent increase in the input resistance caused by dendritic tapering. Thus, I examine the role of dendritic tapering in the origin of plateau potentials and distance-dependent responses to synaptic stimulation. I hypothesize that if dendritic shaft tapering enhances distal synaptic responses by increasing input resistance and restricting the current flow away from the site of stimulation, then local dendritic depolarization induced by a single synaptic stimulus should be greater in distal dendritic shafts (see also discussion for details in [Plotkin et al., 2011]). To test this hypothesis, single spines are activated at proximal and distal locations within the tertiary dendritic segment. Although the local peak EPSP amplitude in spine heads is independent of the distance from the soma, the local peak EPSP amplitude in distal dendritic shafts is 2-fold larger than their proximal counterparts (Fig. 5.7A, CTRL). Blocking active channels in spine heads results in no significant difference in peak EPSP amplitudes of spines (Fig. 5.7A, -NMDAR & VGCCs). However, the peak EPSP amplitude of dendritic shafts is greatly attenuated (dist/prox=2 vs. dist/prox=1.2 in Fig. 5.7A).

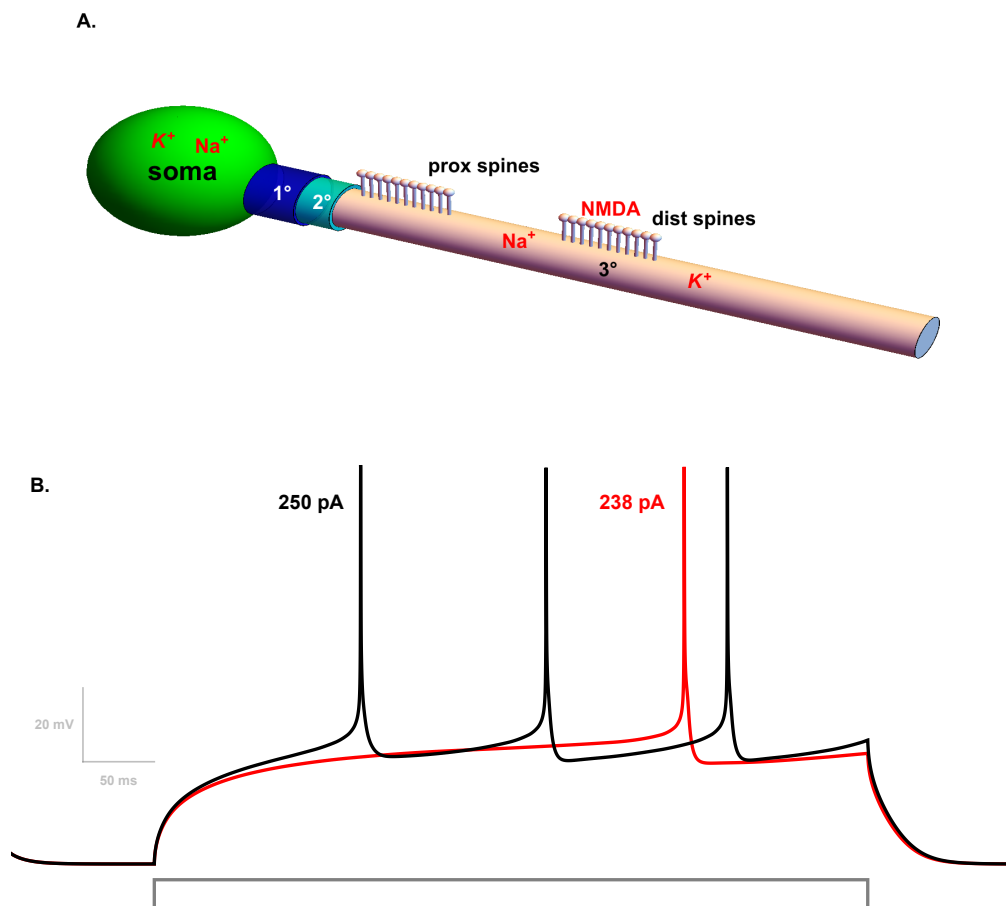


Figure 5.5: Somatic responses of SPN model to injected currents.

A: Schematic representation of SPN geometry with the spines labeled as matchsticks.

B: Somatic membrane potential traces in response to depolarizing current injections.

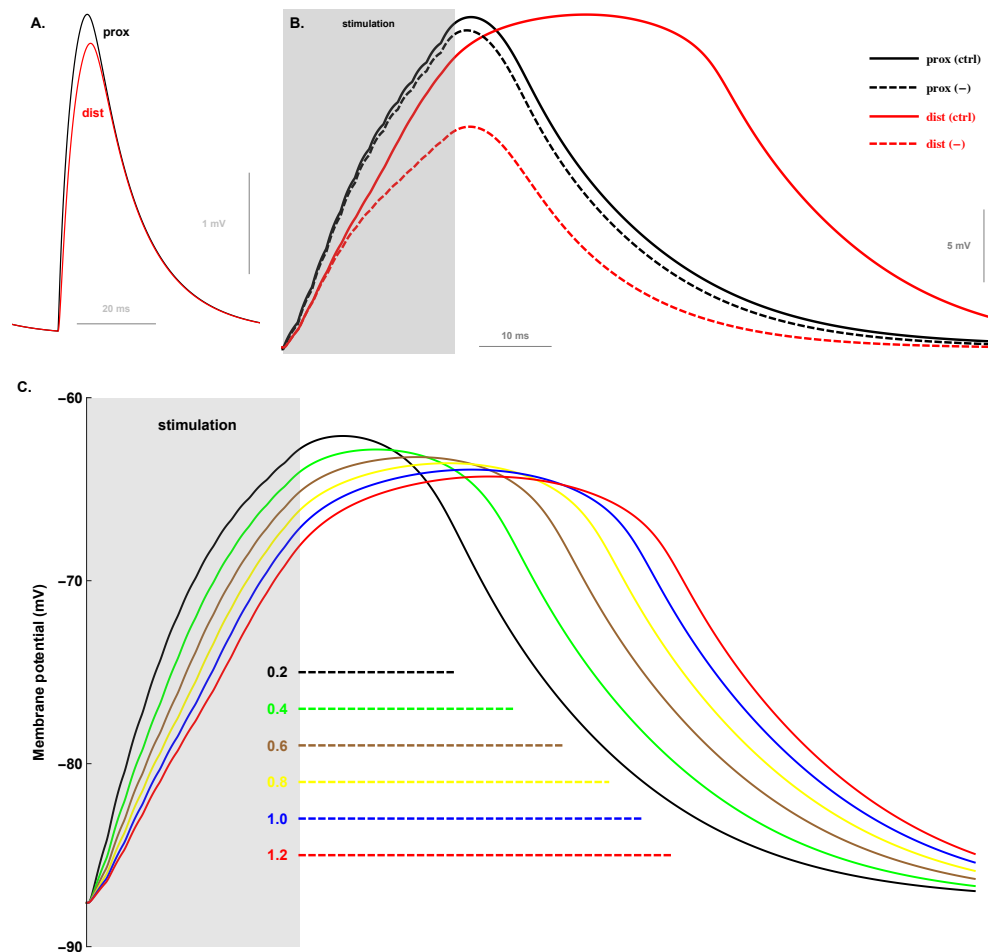


Figure 5.6: The roles of voltage-dependent channels and spine neck in the distal upstate.

A: Somatic EPSPs evoked by stimulating either a proximal (prox) or distal (dist) spine.

B: Somatic voltage traces in response to stimulation of 12 proximal (black, solid) or distal (red, solid) spines. The dashed traces simulate the model without NMDAR and VGCCs.

C: Spine neck modulates the amplitude and duration of evoked distal upstate.

These results can be interpreted with the aid of previously published theoretical analysis [Koch and Zador, 1993]. The total spine input impedance (R_{sp}) is assumed to be the summed impedance (Eq. 5.4) of spine neck (R_n) and parent dendritic shaft (R_{sh}):

$$R_{sp} = R_n + R_{sh} \quad (5.4)$$

I can express the amplitude of the EPSP evoked at the dendritic shaft as Eq. 5.5:

$$V_{sh} = g_{head} E_{head} \frac{R_{sh}}{1 + g_{head} R_{sp}} \quad (5.5)$$

where g_{head} is the total input conductance of ion channels at the spine head and E_{head} is the reversal potential. Given that in the model g_{head} is much smaller than R_{sp} , I can simplify Eq. 5.5 to Eq. 5.6:

$$V_{sh} \approx g_{head} E_{head} R_{sh} \quad (5.6)$$

From Eq. 5.6, I see that V_{sh} depends on two variables: g_{head} and R_{sh} , as the reversal potential is always constant. The calculation of R_{sh}^{prox} and R_{sh}^{dist} is performed using the compute function provided by NEURON Impedance class (data not plotted). In the control condition, tapering of the tertiary dendrite produces a static R_{sh} that is twice as high distally vs proximally ($R_{sh}^{dist} = 2 * R_{sh}^{prox}$). The attenuated distance-dependence of dendritic shaft EPSP amplitude in the absence of NMDAR and VGCCs likely reflects a reduction in absolute shaft depolarization due to a decrease in g_{head} .

As the activation of a single spine depolarized distal dendritic shafts more robustly than proximal ones, it stands to reason that rapid activation of multiple neighboring spines will induce a larger depolarization in distal shafts, supporting their ability to sustain regenerative events. Indeed, sequential activation of 12 neighboring spines induce a depolarization on distal dendritic shafts (Fig. 5.7B, solid red lines), whose amplitude is twice as high as in the proximal dendrites (Fig. 5.7B, vertical double arrows). Such ample distal dendritic depolarization in turn boosts the activation of NMDAR and VGCCs in the stimulated spines. Although this boost only modestly enhances the peak EPSP amplitude at individual distal spines, it sustains the membrane potential of distal spine heads at a high voltage (above -30 mV) well after the stimulus, in contrast to the fast decay in proximal spines (Fig. 5.7B). The resulting plateau potential generated in distal dendrites then transfers, via cable properties of the dendrite to the soma where it is expressed as a long-lasting upstate (Fig. 5.7B, dashed green lines). These simulations expand the previous work to offer a model by which dendritic tapering slows the decay of synaptically-induced dendritic depolarizations by amplifying interspine cooperativity, consistent with studies in pyramidal neurons [Harnett et al., 2012].

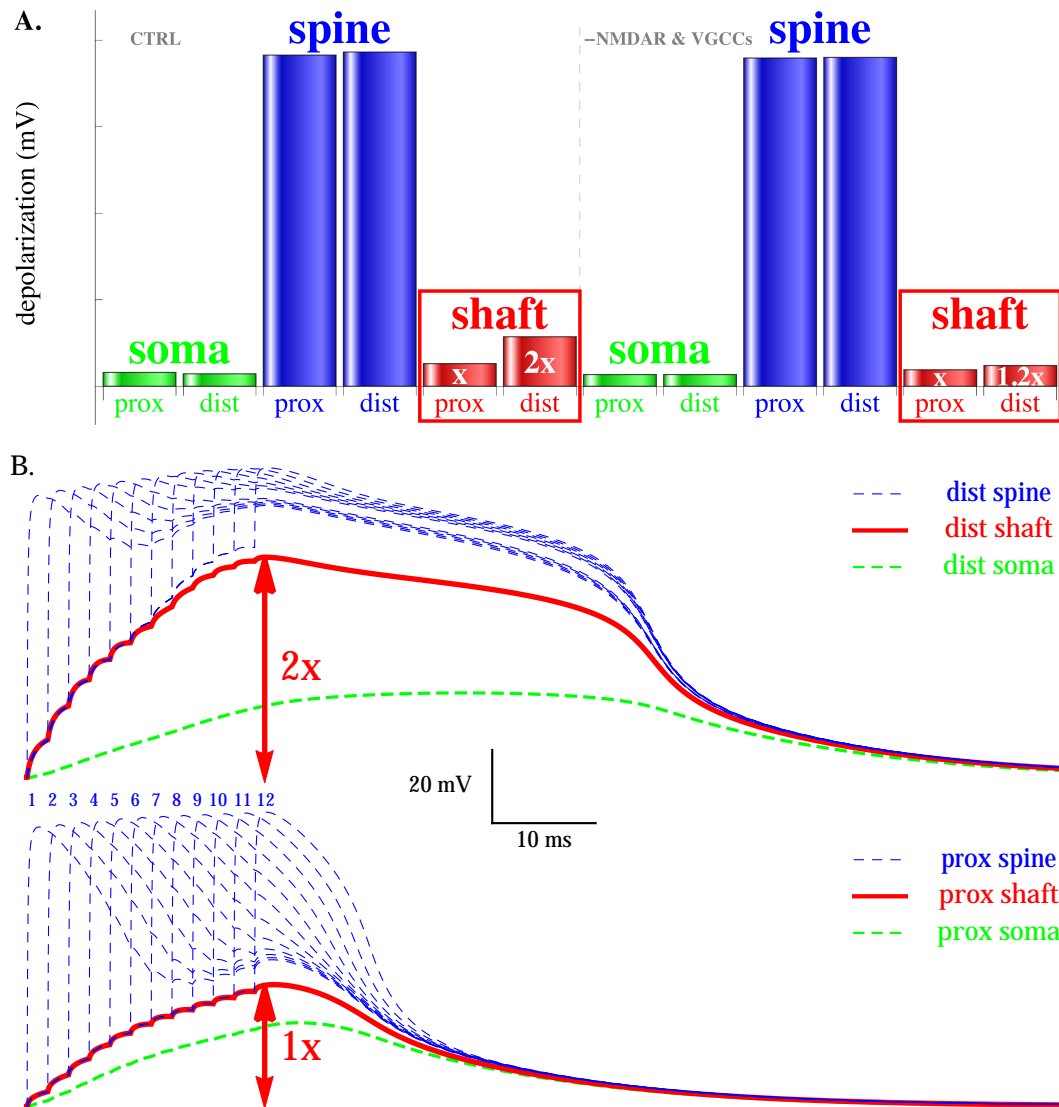


Figure 5.7: **Thin distal dendrite can support state transition.**

A: The EPSP amplitudes in the control conditions (left panel) and in the absence of NMDAR and VGCCs (right panel). The red rectangles highlight the ratio of distal to proximal shaft depolarization.

B: Membrane potential traces from soma (green), shaft (red) and spine heads (blue) of the modeled SPN in response to stimulation of 12 neighboring distal (top) or proximal (bottom) spines.

Association-based Dendritic Computation

Active dendrites are able to generate regenerative events and therefore serve as elementary computational units of information processing in the brain. Here I conceptualize this active SPN model as an association-based information processing unit capable of integrating distally-encoded regenerative events with temporally restricted proximally encoded cues. To begin testing this, the dendritic length stimulated to evoke a plateau potential is reduced by half (from 12 to 6 spines, stimulated twice each, maintaining 12 total stimuli), sharpening the spatial parameter. Just as in Fig. 5.5, this modification induces robust plateau potentials when delivered distally but not proximally (Fig. 5.7, blue vs. green). Neither stimulation pattern induces a somatic action potential. Integration of distal and proximal cues is then examined by distributing the 12 stimuli among distal and proximal spines. Stimulation of 6 neighboring proximal spines immediately followed by stimulation of 6 neighboring distal spines produces a long somatic plateau potential (Fig. 5.7, dashed red). Stimulation of 6 distal spines before 6 proximal spines, however, induces a plateau potential and initiated a somatic action potential (Fig. 5.7, solid red). These simulations raise the possibility that SPNs can associate discrete clusters of excitatory inputs based on the timed innervation of specific portions of their dendritic tree.

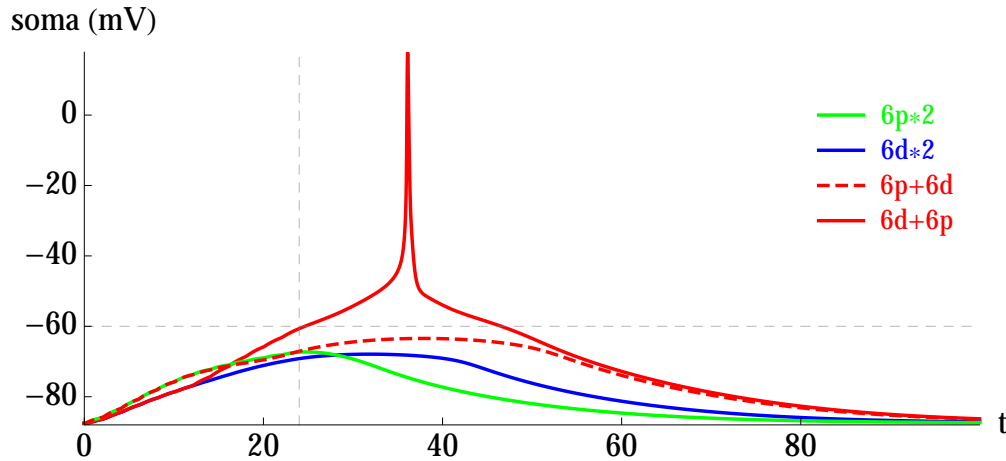


Figure 5.8: **Synaptically driven distal plateau potential facilitates the generation of action potentials by proximal inputs.** Somatic responses evoked by stimulating: 6 neighboring proximal spines twice each (green); 6 neighboring distal spines twice each (blue); 6 proximal spines followed by 6 distal spines (dashed red); 6 distal spines followed by 6 proximal spines (solid red). All spines are stimulated at 500 Hz.

The next obvious step is to perform the full permutation of protocol sequence of synaptic inputs distributed along the dendrite. The total number of input spine is still 12, but the proximal and distal input density are redistributed as color-tabled in Fig. 5.9 (left side) with different permutations of the sum of twelve. I observe that only when distal inputs come before the proximal inputs and the density is well-balanced, an action potential is observed, but not the other way around. It has been proposed that distal inputs encode an internal

representation of an object or a concept and proximal inputs represent the external sensory information. The model prediction shows that when the sensory input comes without any previous internal representation, there is absolutely no output spiking no matter how the limited neural resources are distributed. On the other hand, when the internal representation exists, then most of the input reshuffles can lead to an action.

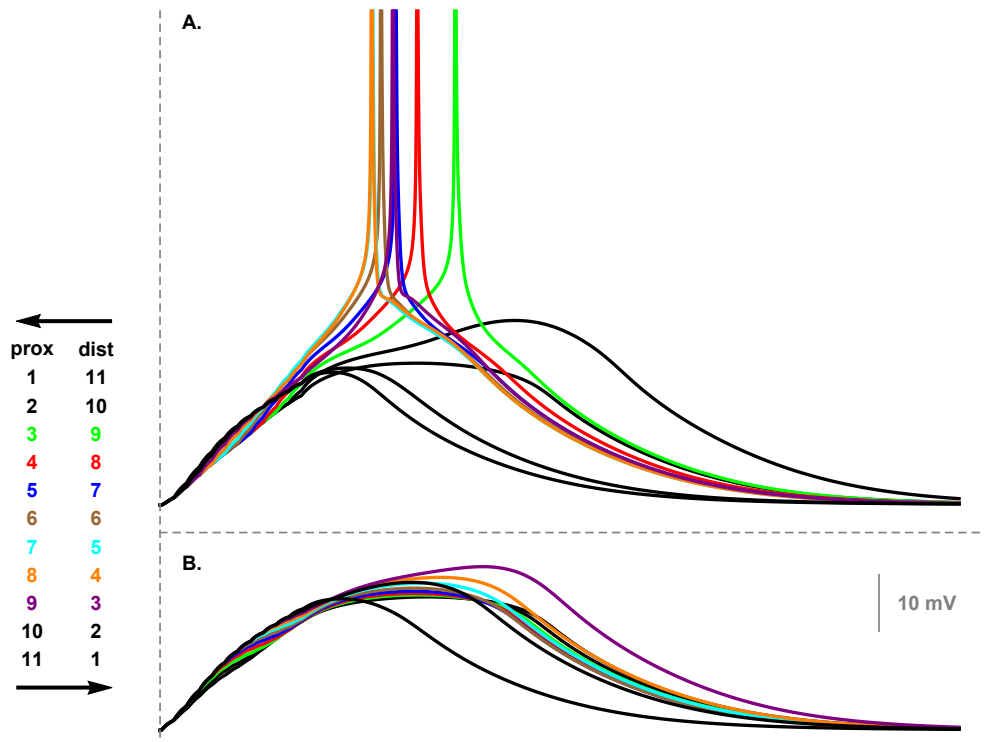


Figure 5.9: Synaptically driven distal plateau potential facilitates the generation of action potentials followed by proximal inputs. See text for details.

5.3 The Reduced Compartmental Model

5.3.1 Modeling Background and Motivation

The pioneering exploration of the computational capabilities of dendrites by Wilfred Rall has provided the theoretical framework for computational neuroscience. Many of his works are classics, from modeling the complex branching structures of dendritic trees to studying their contributions to the signal processing in the nervous system. One outstanding paper [Rall, 1964] is: *Theoretical significance of dendritic trees for neuronal input-output relations*.

It was the first theoretical paper to demonstrate neurons as computational units, that are able to detect the spatiotemporal direction of synaptic activation on the dendrites. Rall showed in the simulation that the farther the locations of stimulation are away from the soma, the lower and later the voltage peaks are observed at the soma. However, at the level of unitary somatic EPSP, this prediction is not compatible with our current knowledge on dendritic location-independence [Magee and Cook, 2000]. Moreover, at the level of evoked EPSPs by the activation of a group of adjacent neighboring spines in a rapid succession, Rall's prediction can also not hold true as the peak somatic voltages do not bear location-dependent differences [Plotkin et al., 2011].

Motivated by Rall's work [Rall, 1964], which demonstrated rich computational capabilities of dendrites such as the direction selectivity *without* assuming voltage-dependent channels, I set up the simulation study below to examine the conditions under which a reduced passive model can predict striatal upstate and direction sensitivity.

5.3.2 Model Description

The main equations of the model are described as follows:

1) the dynamics of the membrane potential V_m are calculated using an equivalent electrical circuit model which can be described as:

$$C_m \frac{dV_m}{dt} = -G_r(V_m - E_r) - G_e(E_e - E_r) - G_i(E_i - E_r) \quad (5.7)$$

where C_m is membrane capacitance. G_e and G_i are synaptic conductances with reversal potentials E_e and E_i . The conductance G_r and reversal potential E_r model leak currents.

2) two new variables \mathcal{E} and \mathcal{I} are introduced, along with the new normalized time constant τ_m , to abstract a unit-less representation excitatory and inhibitory synaptic inputs:

$$\mathcal{E} = \frac{G_e}{G_r}, \quad \mathcal{I} = \frac{G_i}{G_r}, \quad \tau_m = \frac{C_m}{G_r} \quad (5.8)$$

where \mathcal{E}^i and \mathcal{I}^i are designated inputs to the i -th dendritic section (see below).

3) built upon the circuit model (Eq. 5.7), this reduced model has 1 somatic compartment and 9 dendritic compartments on a single tree, as illustrated in Fig. 5.10. The membrane

potential of each numbered (i -th) compartment (V_m^i) is calculated using Eq. 5.9:

$$\tau_m \frac{dV_m^i}{dt} = -(1 + \mathcal{E}^i + \mathcal{I}^i + \Delta Z^2)V_m^i + \Delta Z^2(V_m^{i-1} + V_m^{i+1}) + \mathcal{E}^i \quad (5.9)$$

where the compartmental electronic distance ΔZ is set to 0.2 and the membrane time constant is. Boundary conditions are $V_m^{i=0} = V_m^{i=11} = 0$.

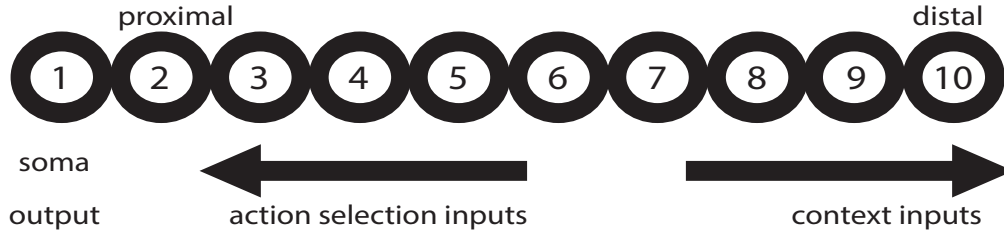


Figure 5.10: The reduced compartmental model.

Each circle represents a neuronal compartment and the model comprises 10 compartments, with one somatic compartment (noted as No.1), 4 proximal compartments which provide action cues and 4 distal compartments that encode context inputs.

I first validate the model by stimulating pairs of compartments along the dendrite with $\Delta\mathcal{E} = 1.0$ and $\Delta t/\tau = 0.25$. Fig. 5.11 shows that the effect of dendritic location given identical excitatory \mathcal{E} -pulse stimulation is that the peak somatic depolarization decreases with the increasing distance of stimulated dendritic compartment to the soma, consistent with Rall's original observation [Rall, 1964].

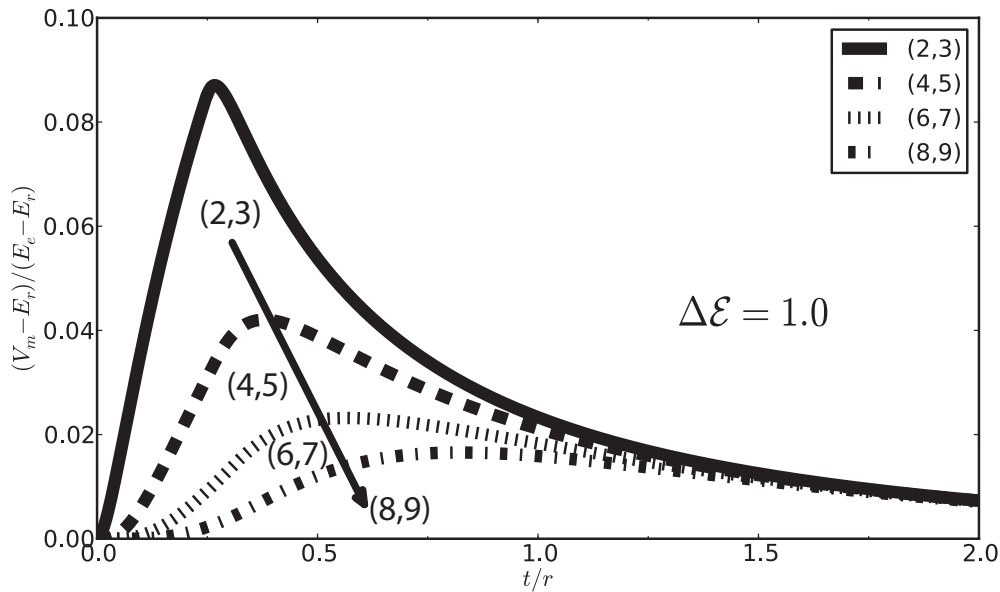


Figure 5.11: The somatic responses to the pairs of excitatory stimulation.

5.3.3 Simulation Results

Strong distal activation evokes up states

[Plotkin et al., 2011] used the technique of laser uncaging of glutamate to stimulate dendrites at different locations with varying distances from the soma. They investigated under which conditions such dendritic stimulation, which mimics synaptic stimulation, gives rise to state transitions as observed from intracellular recording [Wilson and Kawaguchi, 1996].

From their study, I extract four important observations:

- i) the somatically recorded membrane potentials triggered by both proximal and distal stimulation are similar in terms of the peak *amplitude*;
- ii) the peak somatic potential triggered by distal uncaging is *delayed* by approx. 50 ms compared to the peak triggered by proximal uncaging;
- iii) the membrane potential at the soma *decays* back to the resting voltage at almost the same time after both proximal and distal stimulation;
- iv) the duration of upstate is *longer* when triggered by distal compared to proximal stimulation (the time between the end of uncaging and a 50% voltage fall).

I first consider observation: i) how can somatic membrane potential rise to the same peak amplitude for both proximal and distal stimulation? I find that a location-dependence of excitatory stimulation strength \mathcal{E} is necessary to achieve this. Fig. 5.12a shows the somatic voltage in response to a proximal (dashed line) and distal excitatory stimulation (solid line). The strength of proximal stimulation is set to match experimental findings. An amplitude of 20 mV is shown to be achieved by stimulating on average 25 spines, but the threshold for evoking a sustained somatic depolarization is only about 11 spines from the distal region [Plotkin et al., 2011]. Therefore, I select 9 mV depolarization as the reference amplitude in this study, which is consistent with the threshold phenomenon in the striatal neurons (Joshua Plotkin, personal correspondence). As expected from the model, the distal compartments require a stronger stimulation than the proximal. In Fig. 5.12a, a distal stimulation of approx. $10\times$ the strength of the proximal is used to reach the same peak amplitude at the soma (2.0 vs. 19.0).

The delayed peak of somatic potential which follows naturally from the model, is not compatible with observation iii). The potential decays later to the resting level for distal stimulation (Fig. 5.12a). I find that the inhibitory stimulation is necessary for achieving a somatic voltage-decay back for distal stimulation at the same time as for the proximal one. Fig. 5.12b shows the result when applying a strong distal inhibitory stimulation after the somatic potential peaked. So far, I have demonstrated that key characteristics of striatal upstate can be produced with the model and my proposal is therefore an alternative to voltage-dependent channels in dendrites, but it requires a properly matched inhibition at distal sites.

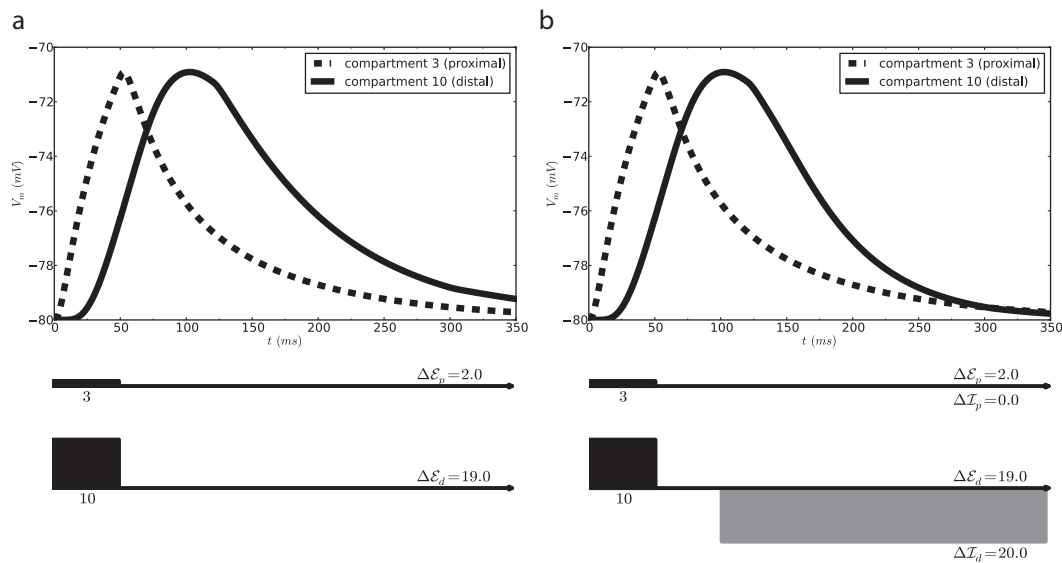


Figure 5.12: The model with strong distal stimulation, captures key features of state transitions observed in SPNs.

a) Somatic response evoked by placing on compartment 3 an \mathcal{E} -pulse with magnitude $\Delta\mathcal{E}_p = 2.0$ (dashed line), and on compartment 10 an \mathcal{E} -pulse with magnitude $\Delta\mathcal{E}_d = 19.0$ (solid line). The latter value was chosen such that the two peak responses are the same (here: approx. -71 mV). However, these simulations are only consistent with observations i) and ii) but not with the observation iii).

b) Same as in a), but with additional delayed distal inhibition, which makes the model prediction consistent with all four observations.

Revisiting directional sensitivity

I argue that Rall's most significant contribution in his 1964 paper was the discovery that a model neuron is sensitive to the temporal sequence of synaptic inputs and can act as a device computing the direction of motion [Rall, 1964]. This phenomenon was afterwards explored by [Torre and Poggio, 1978] and very recently supported by the experiment from [Branco et al., 2010], in which they used so-called IN and OUT protocols. These two experimental protocols represent respectively the sequential synaptic stimulation from distal location towards the soma (IN) and from proximal location to the distal (OUT) dendritic branch. In this paper, the notion of "directional sensitivity" was re-ignited and two distinct neuronal outputs under the protocols were communicated:

- v) IN protocol produces a larger somatic peak potential than the OUT by about 35%;
 - vi) OUT protocol evokes a higher somatic potential trace than the IN during the decay.
- (The numbering is continued from the observations i-iv).

I first simulate IN and OUT sequences using Rall's default parametrization (e.g., replicating his Fig.7 in [Rall, 1964]), shown in Fig. 5.13a. Here, the excitatory strength at each node is identical. I observe that the peak voltage in the IN protocol is higher than in the OUT protocol, which constitutes the direction-selectivity of Rall's model, but the value is almost twice as high for the OUT sequence and *not* around 35%. Besides, the somatic membrane potential during the decay phase is *not* higher in the OUT protocol as observed experimentally by [Branco et al., 2010].

I then simulate the model with the excitatory strengths that make somatic peak amplitudes identical for all dendritic compartments (Fig. 5.13a). I find that now the model predictions are in much better agreement with observations v) and vi). More specifically, the IN protocol produces a larger response at the soma peaking at -58.5 mV, which is 5.5 mV above the peak potential obtained by the OUT protocol (-64 mV), well matching a 35% increase (Fig. 5.13b). Furthermore, the OUT sequence now produces a larger potential during the decay phase than the IN sequence, which is due to the overall stronger excitatory activation in our parametrization. Note that I have derived the location-dependence of excitatory strength to evoke the same peak amplitude at soma (Fig. 5.12a), and not to match at the first place the direction-selectivity reported in [Branco et al., 2010].

Background depolarization set by distal inputs

It was suggested that context-dependent pattern recognition can be realized by distally-driven state transitions by which associative information processing of the proximal input can be performed [Plotkin et al., 2011]. Here I explore if such a computation can be performed in this reduced model, when the distal activation is strong (Fig. 5.12a).

I simulate three scenarios (see Fig. 5.14): *First*, using the exact parameters as in [Rall, 1964], two distal \mathcal{E} -pulses are delivered before one proximal \mathcal{E} -pulse (thin solid line). The strengths of all pulses are the same as in Rall's original work. The resulting somatic potential is slightly

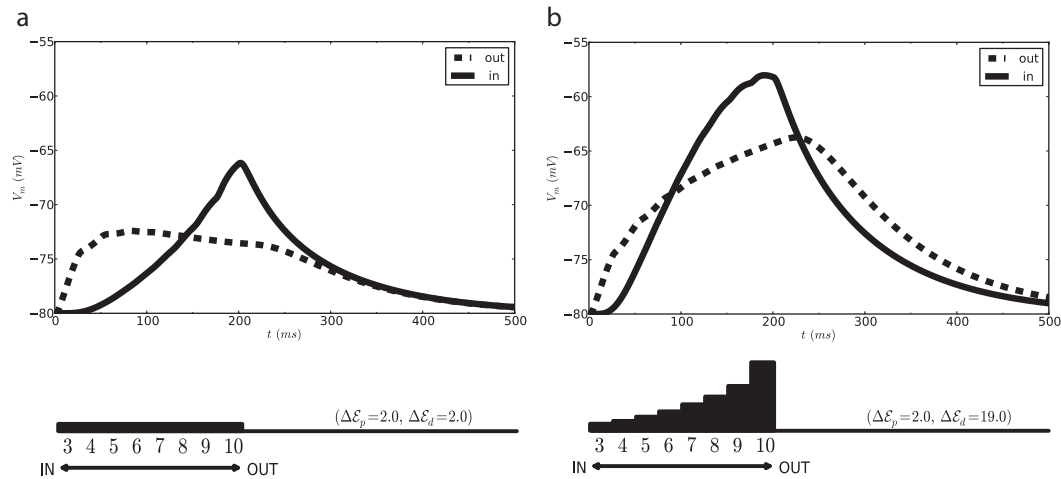


Figure 5.13: The direction selectivity evoked by different strengths of distal stimulation.

a) Stimulation protocol as used in Rall's original paper (Fig.7 in [Rall, 1964]).

The computed direction selectivity is *not* consistent with the observations v-vi.

b) Simulations of IN and OUT protocols, with excitatory strengths at each node evoking the same somatic peak response when applied alone.

above -70 mV (thin grey line), which is far from the voltage threshold for state transitions around -60 mV. *Second*, three consecutive proximal \mathcal{E} -pulses are applied, all of them with the same strength as in the first scenario (dashed line). Interestingly, the peak potential at the soma is only a few millivolts higher than in the first case. *Third*, similar to the first scenario, I simulate two distal compartments followed by a proximal stimulation (thick solid line). Now, however, I use the stimulation strengths I determined, namely with stronger activation for distal sites. This gives rise to a much larger depolarization than in the previous two cases. The soma is depolarized by 20 mV, close to the spike threshold -60 mV.

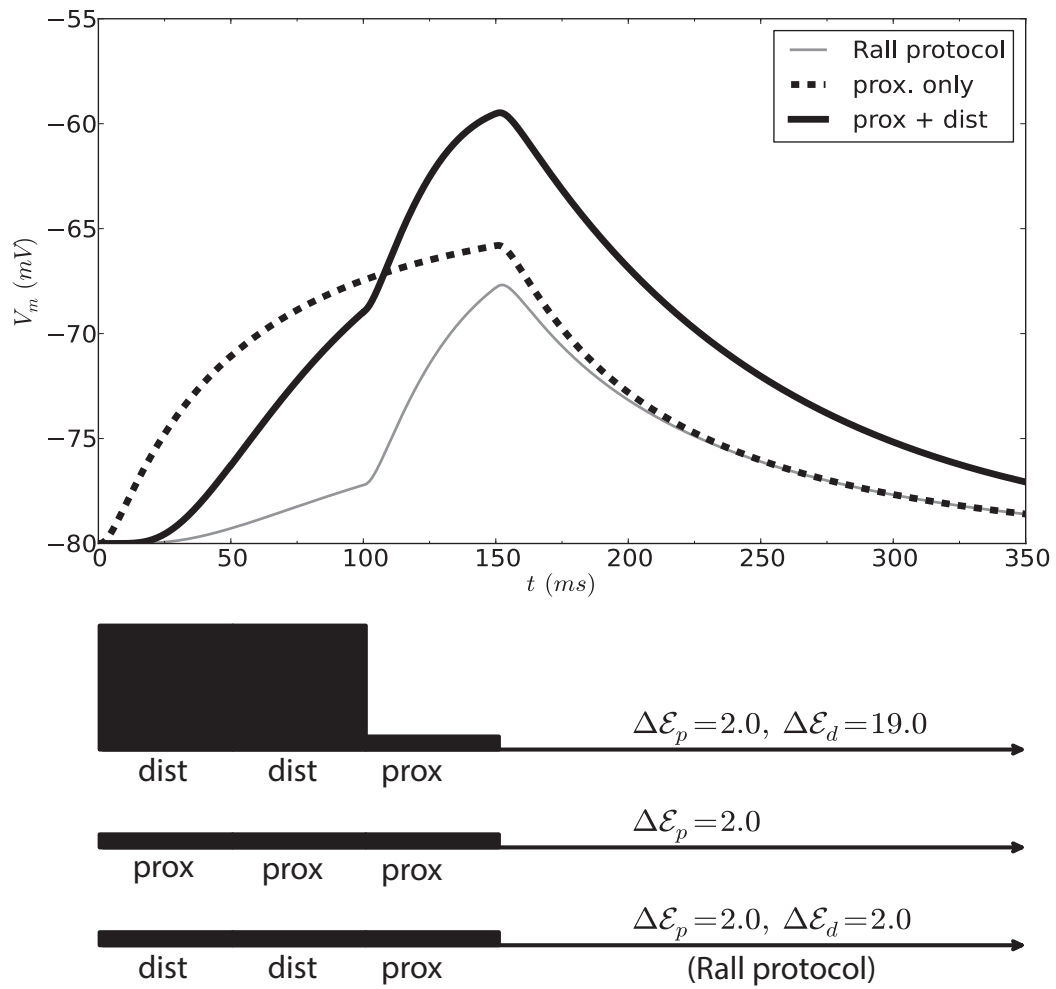


Figure 5.14: Effects of sequential distal/proximal depolarization on somatic response

prox + dist: first strong distal, then weak proximal stimulation (solid black line)

prox only: only weak proximal stimulation (dashed black line)

Rall protocol: first weak distal, then weak proximal stimulation (solid grey line)

5.4 Discussion

In this chapter, I demonstrate using a detailed compartmental SPN model that highly-tapered distal dendrites of SPNs can support local regenerative events while the proximal dendrites of larger diameters can not. The simulation results expand upon this, suggesting that the small diameter of distal dendrites only modestly affects the peak EPSP amplitude of stimulated spines, but robustly increases the amount of time neighboring stimulated spines reside above a possible “threshold” depolarization. The nature of this cooperativity indicates that the temporal fidelity of clustered excitatory inputs may be more faithfully preserved in the proximal than distal dendritic regions. It is thought that a major task of the striatum is to govern action selection. Part of this likely involves SPNs making meaningful associations between diverse inputs. Moreover, I discover that input patterns are indeed recognized only in the upstate while in the downstate the neuron as an associative classifier is to great extents switched off. Such simulation evidence reinforces the idea that synaptic inputs at *distal* dendritic locations could set the context for recognizing synaptic activation patterns of synapses *proximal* to the soma and such context-dependent information processing is fundamental to our brain, e.g., basal ganglia, for implementing algorithms like action selection and decision making. Furthermore, experimental studies can readily identify the active contributors of an observed phenomenon by advanced pharmacological methods, although the role of passive dendrites and their contributions to the striatal state transitions are yet not clear.

To clarify the contributions of intrinsic dendritic anatomy, I then investigate dendritic computations in a reduced compartmental model with passive dendrites. Extending Rall’s original work I consider the location-dependence of synaptic activations as free parameters, which are determined to match recorded somatic membrane potentials in striatal neurons undergoing synaptically driven transitions to upstates. I observe that when the distal activation is stronger than the proximal, the Rall model predicts key features of the upstate, which so far have been attested to involve voltage-dependent channels in dendrites. Assuming an additional delayed and strong distal inhibition further improves the model replication, in which the decay to resting voltage occurs with identical trajectories, independent of stimulation location. Besides accounting for key features of the upstate and thereby providing the substrate for context-dependent pattern recognition, the strong distal activations also make the Rall model’s predictions very similar to recent experimental findings on the synaptic direction selectivity as reported [Branco et al., 2010].

To summarize, the simulation results from both models demonstrate that: 1) the association-based dendritic computations, previously thought to require active dendrites, can be realized with passive dendrites. As a consequence, future experimental studies have to determine on a case-by-case basis the actual implementation of dendritic computations and distinguish between the single-cell model with active channels, properly matched location-dependent synaptic strengths, or a mixture of both; 2) this shall, however, not rule out or even replace models with voltage-dependent dendritic channels. The simulations presented in Fig. 5.9 describe a mechanism by which SPN distal dendrites may gate the generation of action

potentials triggered by proximally-synapsing inputs. This active property has several implications for striatal computations: i) only inputs converging in time and space (in sufficient numbers) on distal dendrites will lead to the generation of somatic upstates; ii) once an upstate is established, only sufficiently strong and appropriately timed proximal inputs will lead to action potential generation, ultimately gating information flow out of the striatum and inhibition or disinhibition of the basal ganglia output nuclei controlling action. Such property is very likely to be possessed also by other neuron subtypes that manifest the upstate phenomenon [Oikonomou et al., 2014], in particular, the cortical pyramidal neurons [Major et al., 2008] which is the focus of the next chapter.

Chapter 6

Differential Spine and Shaft Computations in a Pyramidal Neuron Model

In the previous chapter, I report that a detailed SPN model replicates striatal upstate phenomenon in the condition that the synaptic input arrives directly on the spine head and the length of spine neck regulates the upstate duration (Fig. 5.6). In other interpretations of this result, it is very likely that presynaptic terminals which directly target the dendritic shaft of SPNs (axo-dendritic synapses without spine neck) may result in functionally very segregated consequences in terms of neuronal integration from those which make contact to the spine head (axo-spinous synapses). Although experimental evidence for striatal synapses on this issue still awaits future investigation, cortical electrophysiology works have revealed some basic anatomical and functional characteristics of the differentiated axo-projections [Araya et al., 2006a]. However, a more integrative view of functional differences caused by the axo-dendritic and axo-spinous synapses of the cortical pyramidal neuron is currently missing.

In this chapter, I first parameterize a cortical pyramidal neuron model by putting spine and shaft synapses next to one another, carefully calibrated and validated the model in Sec 6.2. Then I investigate the model to understand the underlying mechanisms in the ensuing section. Finally, I present the simulation results from the model and derive the main predictions that are of immediate interest to the current experiment designs of studying both thalamocortical and thalamostriatal system.

6.1 Experimental Background and Modeling Motivation

Although an overwhelming majority of synaptic contacts are made directly onto axo-spinous (spine) synapses after a developmental transition, axo-shaft synapses persistently co-exist adjacent to either existing spines or newly-born ones, redistributing contacting boutons but not transforming themselves into spine synapses [Reilly et al., 2011]. It has become prevailing textbook-knowledge that most synaptic contacts occur on the spines in both cortical and subcortical areas of the brain. However, the ratio of shaft synapses to spines can be highly variable, depending on specific brain areas [Aoto et al., 2007]. In addition, latest studies on the organization of neural circuitry have discovered differential patterns of synaptic connectivity with either axo-shaft or axo-spinous synapses. For example there exists a predominant axo-shaft targeting of CM/Pf (Center Median/Parafascicular) synapses in the thalamostriatal connections [Smith et al., 2014], which is indicative of unknown functional roles played by shaft synapses. As the goal-directed movements can completely depend on the basal ganglia with the input from thalamus in the absence of cerebral cortex, such preferential connectivity formed exclusively by the axo-dendritic Cm/Pf synapses may play a bigger role than we thought before in carrying out independently a variety of evolutionarily conserved motor functions commanded by thalamus [Grillner and Robertson, 2015].

Recently, [Araya et al., 2006a] demonstrated that glutamate uncaging targeted directly onto dendritic shaft reliably evoked EPSPs that are comparable to those evoked by spines, suggesting that pyramidal dendrites could be abundant with axo-dendritic contacting sites located between spines. Furthermore, they investigated the integrative behaviors of the EPSPs generated by spine and shaft synapses, and found that the combined responses of spines sum linearly (about 100% of the expected arithmetic sum) and those of the shaft sum sublinearly (about 80%). However, the underlying mechanisms are not clear.

It is noteworthy that Araya et al. [Araya et al., 2006a] didn't interrogate distal dendrites, nevertheless subsequent studies on the same cell type have made remarkable advances and demonstrated that distal spines can take advantage of dendritic impedance gradients to overcome the relatively larger electrotonic distance, thereby implementing a rate coding [Branco and Häusser, 2011]. In such context, the integrative property of distal shaft synapses remains largely unknown. Besides, a *raison d'être* for shaft synapses, especially the potential functional implication of their dendritic integration, has not yet been identified. Moreover, both the role of distal shaft synapses in the control of action potential output [Williams and Stuart, 2003] and back-propagation [Tsay and Yuste, 2002] also awaits further explorations.

6.2 Model Description

Simulations are performed with NEURON [Hines and Carnevale, 1997] using a reconstructed layer 2/3 pyramidal neuron taken from [Branco and Häusser, 2011]. The focused dendritic branch (marked red in Fig. 6.1A) has a total length of about $100\ \mu\text{m}$ with the proximal tip $40\ \mu\text{m}$ and the distal tip $140\ \mu\text{m}$ away from soma. 51 spines are put on the branch with an interspinal distance of $2\ \mu\text{m}$ and 50 shaft inputs are inserted respectively between every two spines. It has been observed that synaptic strengths along a dendritic branch are inversely correlated with spine neck length [Araya et al., 2006b], an important morphological variable regulated in an activity-dependent manner [Araya et al., 2014]. This feature, nevertheless, was rarely incorporated into the neuronal simulations studying synaptic integration. Based on the convincing evidence from Yuste Lab, individual spine-evoked EPSPs in this model are parameterized by a function of neck length (nl) derived from the plotted data in [Araya et al., 2006b] which can be described simply by an inverse linear function Eq. 6.1, plotted with the blue line and blue dots in Fig. 6.1B:

$$v_{epsp}^{sp}(nl) = 1.14222 - 0.461111nl \quad (6.1)$$

Although the natural variability of spine morphologies in the cortical pyramidal neuron is ideally best characterized by a skewed distribution [Arellano et al., 2007], it is acknowledged that the synaptic strengths follow also a normal distribution [Forti et al., 1997]. Thus by parametrizing the peak conductances of glutamatergic receptors I distribute individual spine-evoked EPSP using Eq. 6.1 together with a Gaussian probability of $1.0\ \mu\text{m}$ mean and $0.2\ \mu\text{m}$ standard deviation of neck length (marked blue shadow in Fig. 6.1B) and neck diameter is fixed in all simulations. For the reason that this study is designed to explore the impact of dendritic impedance gradient on synaptic integration, the location dependence of EPSP Efficacy on synapse location is intentionally eliminated [Williams and Stuart, 2002]. As a consequence, spines don't represent any correlation of dendritic location with evoked EPSPs and the same principle was applied to distribute shaft-evoked EPSPs as plotted with red dots and circles in Fig. 6.1B.

6.3 Results

6.3.1 Replication of Integrative Behaviors by Spine and Shaft Synapses

I simulate exact same experimental protocols used in [Araya et al., 2006a] to validate the model. In the dendritic region of a distance to soma between 20 and $80\ \mu\text{m}$, 1-5 spine and shaft synapses are selected and stimulated with an inter-uncaging interval of $5\ \text{ms}$. The peak amplitudes of combined spine-evoked EPSPs are nearly all identical to the expected arithmetic sums of individual EPSPs (green dashed line and points in Fig. 6.2A), matching a strictly linear input-output relation (black dashed line in Fig. 6.2A). In contrast, the peak amplitudes generated by the combined shaft-evoked EPSPs (red dashed line and points in Fig. 6.2A) are all located below the linear line. Consistent with the experimental findings, spine-evoked EPSPs sum linearly with nearly 100% linearity percentage (the ratio of the predicted value to the expected sum of individuals) and shaft-evoked ones integrate with

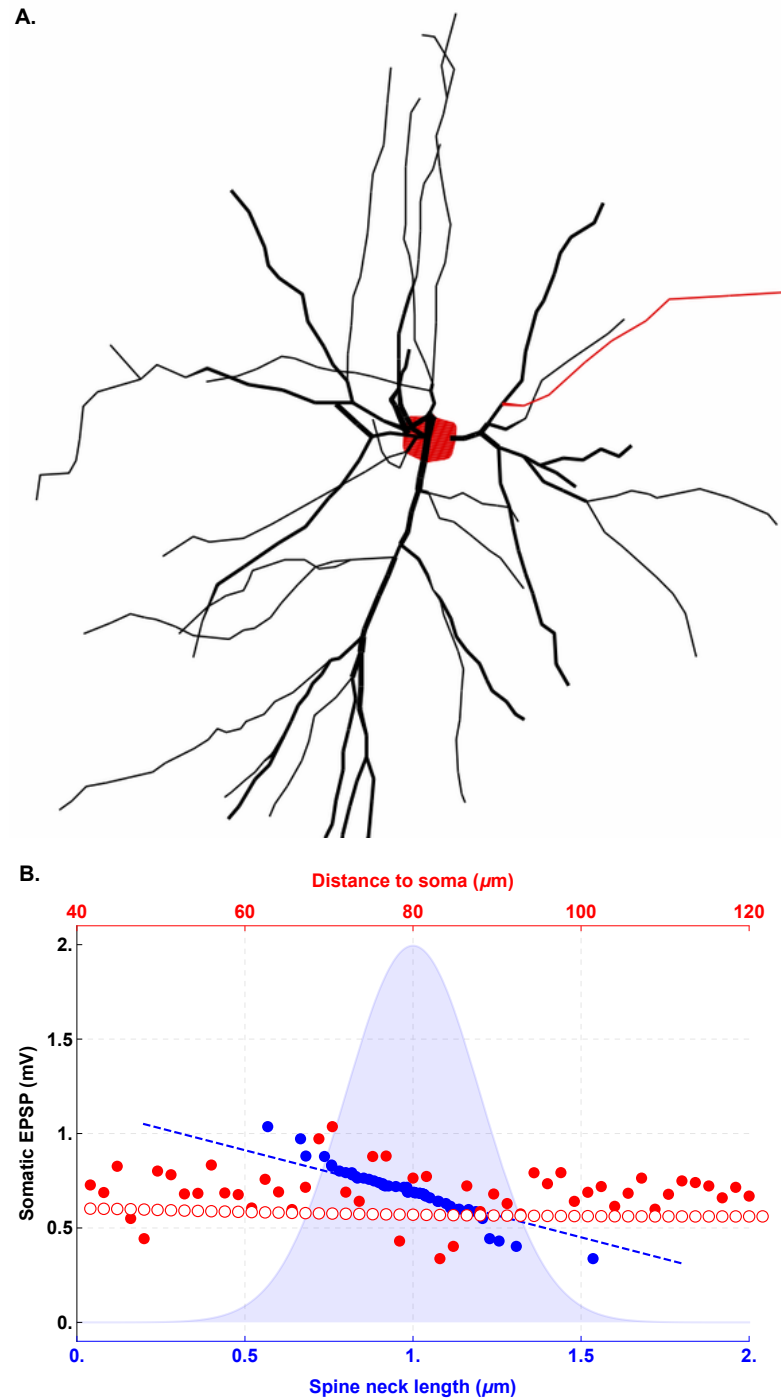


Figure 6.1: **Model construction and distribution of evoked EPSPs by spine and shaft synapses.**

A. Morphology of a reconstructed pyramidal neuron model. The marked big red point is the somatic compartment and the marked red thin line is the focused dendritic branch on which synaptic inputs are put.

B. The blue dots represent spine-evoked EPSPs using a linear regression model estimated from Fig.2C in [Araya et al., 2006b]. The light blue shadow is a normal distribution with a mean of $0.5 \mu\text{m}$ and a standard deviation of $0.2 \mu\text{m}$ in “Spine neck length”. The red dots are the same dataset used for plotting blue dots but plotted versus “Distance to soma”. The red circles are shaft-evoked EPSPs plotted versus “Distance to soma”.

80% (Fig. 6.2B, left bars). The only inconsistency between the model prediction and the data from [Araya et al., 2006a] lies in the calibration of the linearity percentage in area. The shaft area does not bear any reductive behavior for the tested input numbers ranging from 2 to 5. Based on the illustration of Fig. 6.2C, the integral areas taken from the actual combined EPSPs are bigger than the arithmetic sums of both shaft-evoked and spine-evoked EPSPs (Fig. 6.2B, right bars). Taken together, this model faithfully replicates the main findings in [Araya et al., 2006a] given identical spatiotemporal protocols, thereby qualifying for being further utilized to explore plausible mechanism underlying differential modes of synaptic integration by spine and shaft synapses.

6.3.2 Underlying Mechanism of Linear and Sublinear Summation

[Araya, 2014] stated in this latest review that the precise mechanisms which promote the subthreshold linear summation of spine synapses remain unknown, which calls for both future experimental examination and theoretical exploration. NMDARs are well known to boost synaptic responses, thus I examine whether they are as well essential to maintain spine linearity. When NMDAR activity is completely inhibited in the shaft, the linearity percentage of 60% is significantly below the experimentally-reported value 80% (Fig. 6.3A, dashed magenta line and dots), suggesting that the sublinearity is due in part to the progressively diminishing ionic driving force of shaft synapses and NMDAR investment compensates to some extent for such intrinsic property of passive filtering of dendrites. Then I reduce NMDAR density to 50% in the spine head mimicking a partial blockade or down-regulation of such compensatory effect provided by NMDAR conductance. The results show that linear summation of spines is disrupted by such biophysical alteration and the synaptic responses integrated sublinearly similar to their shaft counterparts (Fig. 6.3A, dashed blue line and dots). In addition, Fig. 6.3C shows that NMDAR activity almost drops to the same level in the spine as what's in the shaft after five synaptic events (marked by a cyan rectangle), thereby not being able to sustain linear summation. Furthermore, I also find that despite larger peak amplitude and summed area of NMDAR activity in the spine head (NMDAR-50%) than in the shaft (Fig. 6.3B), the resulting linearity percentage is similar. Taken together, such NMDAR-dependent mechanism is consistent with the observation that application of APV produced a sublinearity of the combined EPSPs in cultured pyramidal neurons [Cash and Yuste, 1998] and the summary of NMDAR data suggests that aside from intrinsic dendritic filtering, a low-level activity in the shaft and a reducing activity in the spine, insufficient for counterbalancing dendritic filtering, could explain for the sublinear integrative behaviors of their evoked responses (Fig. 6.3D). Such phenomenon reminisces the notion that it is definitely required for NMDAR-mediated spines to work cooperatively to not only generate synaptic amplification [Harnett et al., 2012], but also to produce linear summation.

6.3.3 Dependence of Synaptic Integration upon Three Variables

Recent experimental work in a pyramidal model [Branco and Häusser, 2011] demonstrated that a single dendrite shifts its computational strategies from temporal integration to rate coding, empowered by an impedance gradient along the branch. Part of their data illus-

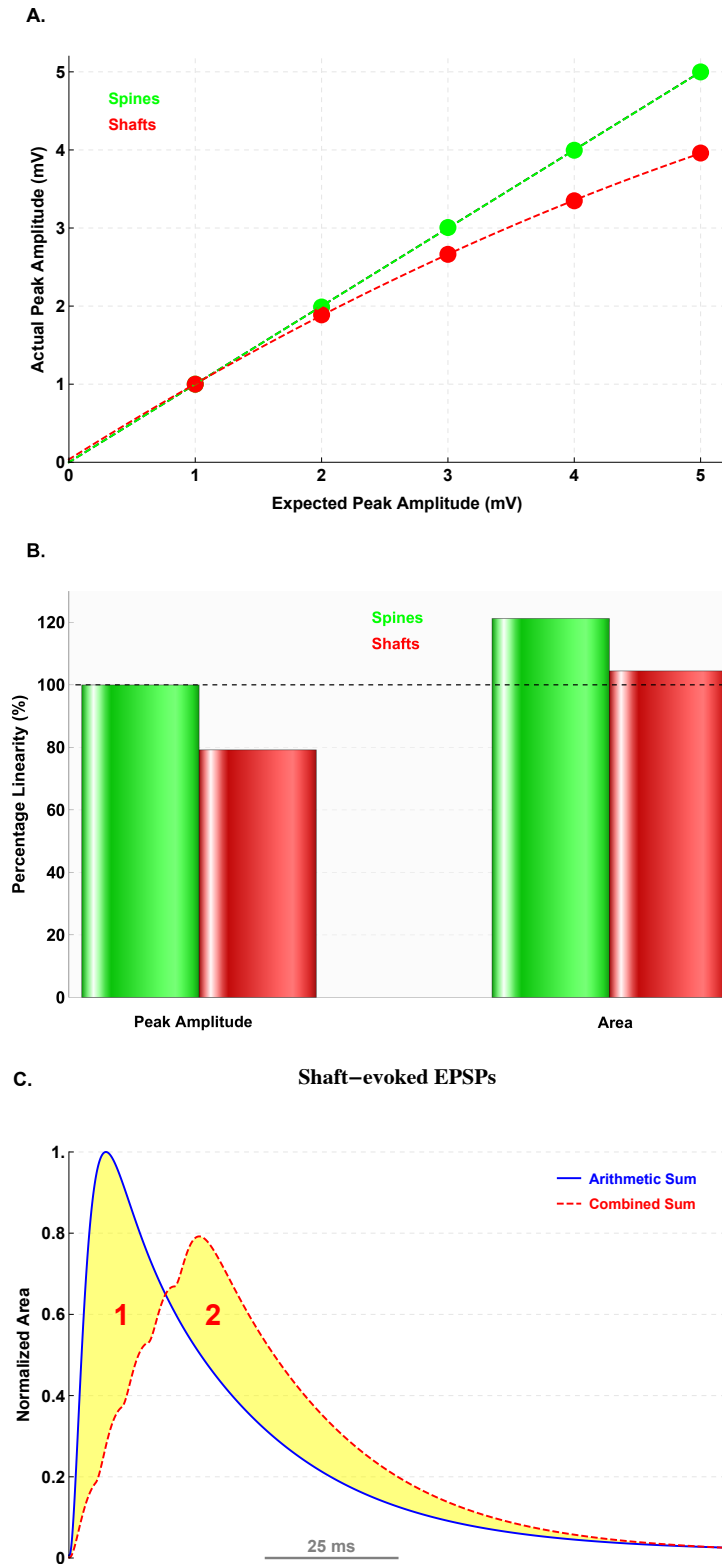


Figure 6.2: Replication of spine linear and shaft sublinear summation reported in [Araya et al., 2006a]. **A.** Plot of the actual vs. the expected peak amplitudes of combined EPSPs, scaled to have a unitary EPSP of 1mV. **B.** Plot of the percentage linearity, calculated by taking the ratio of the peak amplitude or area of combined EPSPs to the expected values given 5 synaptic events. **C.** Plot of two somatic membrane potential trajectories given 5 synaptic events of shaft synapses: blue curve represents the arithmetic sum of individual EPSPs and red curve represents the combined sum.

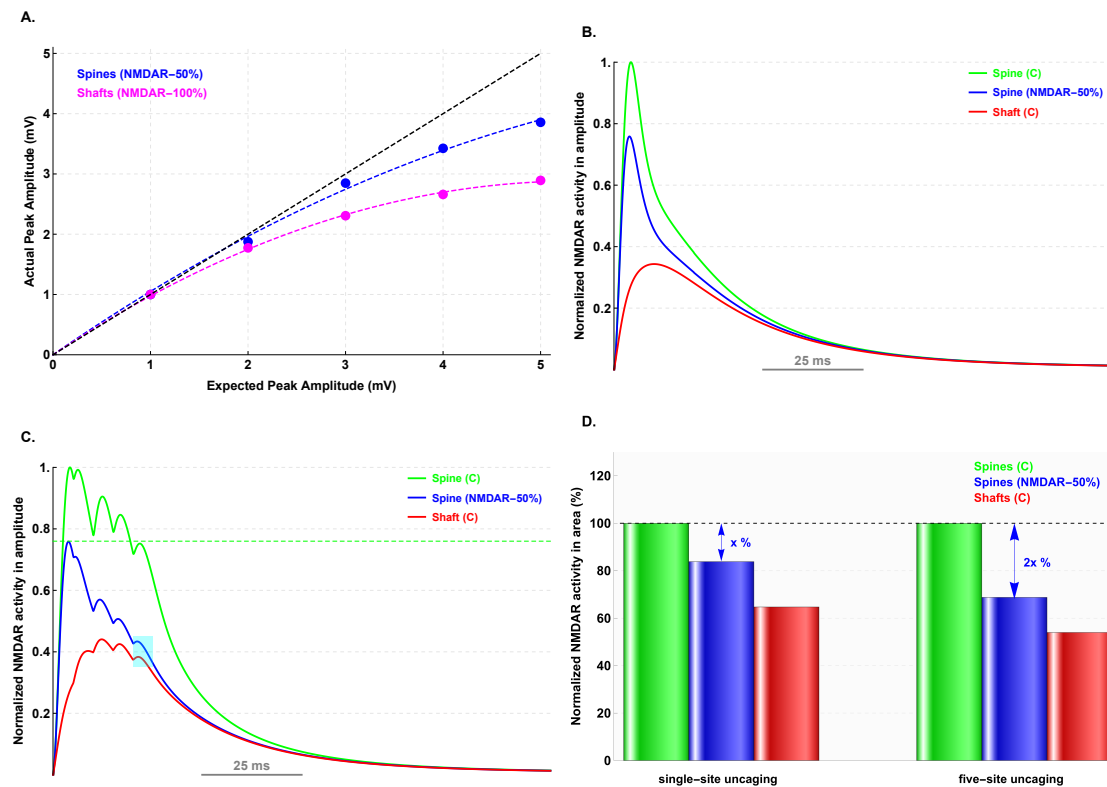


Figure 6.3: NMDAR-dependent mechanism for sublinear integration.

A. Spine responses sum sublinearly given a 50% NMDAR blockade and the shaft sum even more sublinearly without NMDARs.

B. Differential NMDAR activities with a single synaptic event: spine control (green), spine 50% NMDAR (blue) and shaft control (red).

C. Same as in B, but given five synaptic events.

D. Summary of normalized NMDAR activities in area.

trated that stimulating two adjacent spines at relatively distal locations resulted in a linear percentage of the combined EPSPs significantly above 100%. Therefore, in contract to this observation, the claim made in [Araya et al., 2006a] apparently requires a re-evaluation, stating that spine linear summation is not affect by the dendritic location. Thus I use the validated model to simulate the protocols used in the Fig.3 of [Araya et al., 2006a] and explore how the three experimental variables namely interspinal distance, distance to soma and neck length could influence synaptic summation of both spine and shaft synapses.

In all sets of simulation, 3 inputs are selected based on different variable profiles. First, interspinal distance is varied from $2\ \mu\text{m}$ to $20\ \mu\text{m}$, the summation over this variable range lies all in the zone where linearity percentage is between 97% and 103% (Fig. 6.4A). Likewise, spine neck length also doesn't seem to significantly alter the linear profile of integration (Fig. 6.4B). Nevertheless, as expected, the impedance gradient in the stimulated branch results in a linearized summation of shaft-evoked EPSPs from the proximal tip to the distal (Fig. 6.4C) and a supralinear integration of spines in the distal region (Fig. 6.4D). I argue that the examination of the inputs located $100\ \mu\text{m}$ away from soma was lacking in [Araya et al., 2006a] and this missing piece of knowledge may explain the differential conclusions drawn from the respective studies.

6.3.4 Synaptic Amplification by Shaft Synapses

[Branco and Häusser, 2011] also demonstrated that stimulating less than 8 spines is sufficient to reveal the differential coding schemes implemented by the proximal and distal dendrites. What remains unknown is how shaft synapses may also transform information differently in such context. I select respectively 8 to 12 inputs between $20\text{-}80\ \mu\text{m}$ (proximal sites) and beyond $100\ \mu\text{m}$ (distal sites). At the proximal region, spines perform linear integration and the shaft sublinear (Fig. 6.5A). At the distal region, spine synapses bring about nonlinear computing with a very low supralinear threshold. More precisely, just two spines could generate a linearity percentage of 250%. Interestingly, shaft synapses are also capable of producing supralinear summation but with a much higher threshold, namely 5 inputs are required to excite the dendrite to spike (Fig. 6.5B). Moreover, unlike by the proximal situation in which the peak amplitude of the combined EPSPs resulted by the shaft is always lower than by the spine due to the sublinear summation, once certain threshold is crossed, shaft synapses amplify somatic membrane potential more effectively than spines.

In Fig. 6.5B, two interesting characteristics are illustrated of combined distal shaft EPSPs: i) *higher amplification after crossing the threshold* - given convergent distal inputs, membrane potentials on the spine head and on the shaft can reach a comparable level of saturated depolarization, in this case, up to 60 mV (Fig. 6.6A). However, the depolarization in the individual spine head saturates rapidly due to the high impedance provided by the neck. In addition, spine neck functions as a voltage divider, resulting in a relatively lower dendritic depolarization than the shaft evoked voltage which transfers directly to the soma without such divisive effect. Worth noting that the absolute higher distal shaft amplification is not

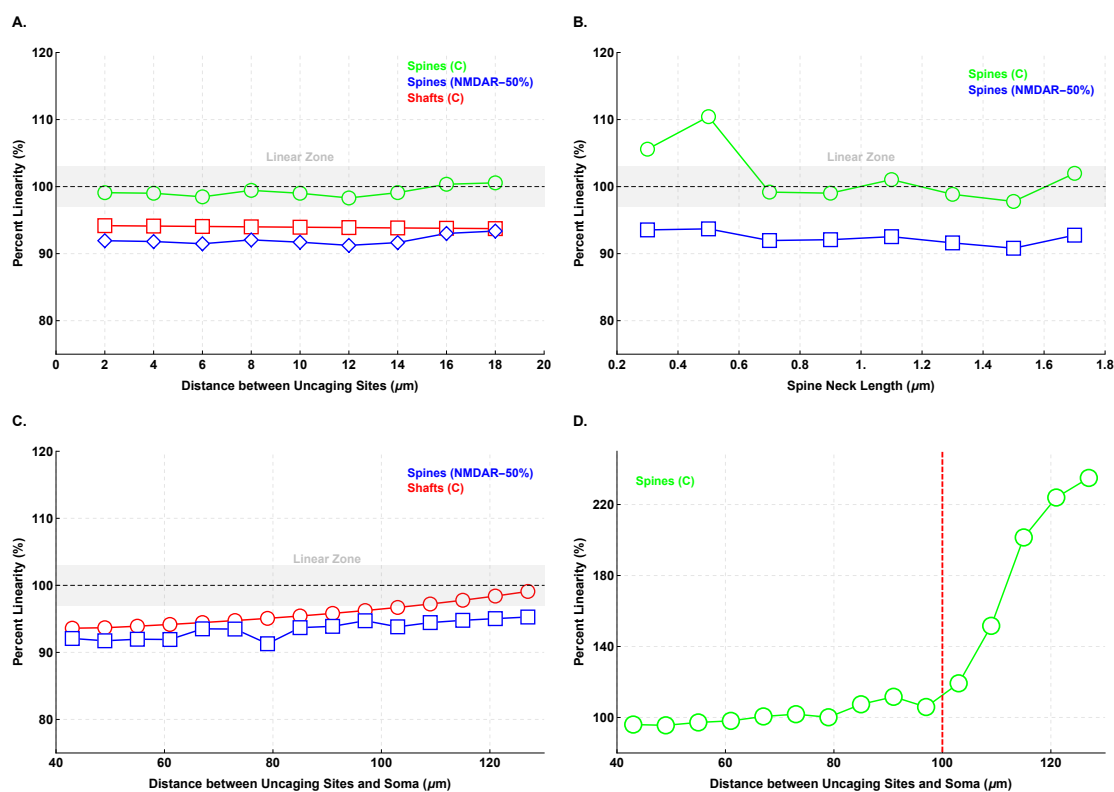


Figure 6.4: Effects of three experimental variables on synaptic integrations.

- A. Synaptic summation is not affected by the distance between synaptic sites.
- B. Spine neck length does not significantly alter the linear property of spine summation.
- C. The summation of shaft-evoked EPSPs is dependent of distance between the stimulated sites and soma. At more distal region, the summation becomes linear.
- D. The integration of spine-evoked becomes supralinear at more distal region.

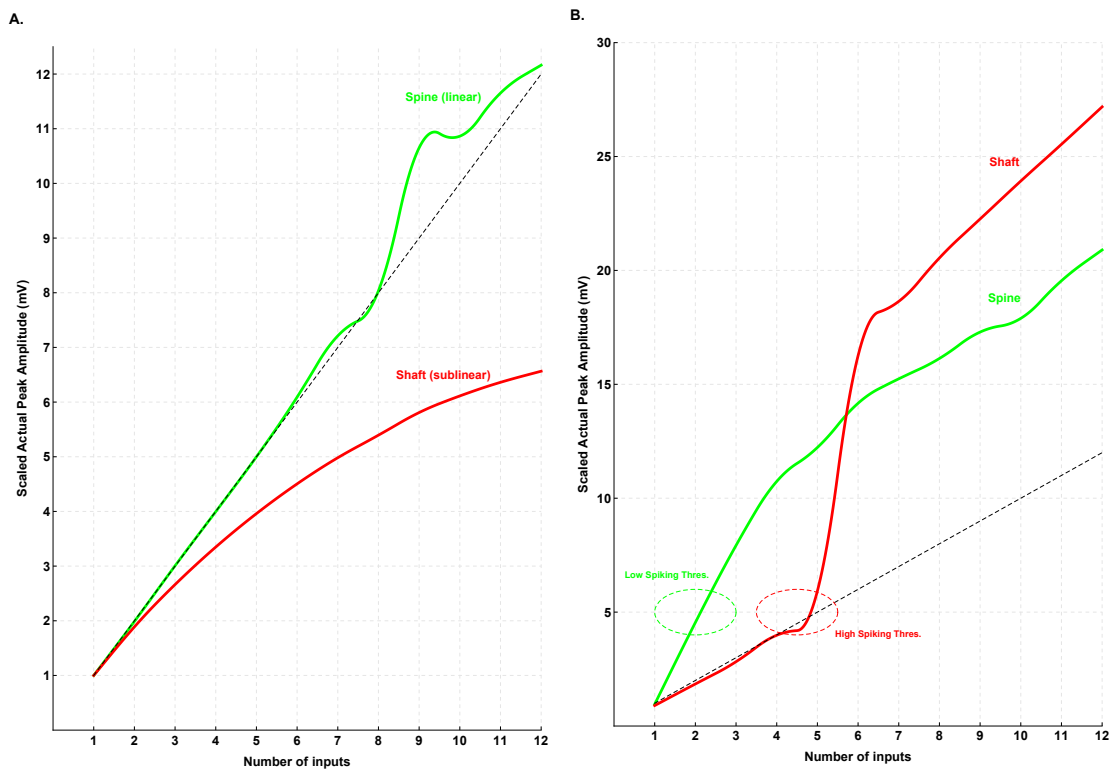


Figure 6.5: **Functional implication of an impedance-gradient mediated integration of spine and shaft synapses.** A. At proximal sites (60 μm), synaptic inputs sum linearly in spines and sublinearly in shafts. B. At distal sites (120 μm), spines integrate supralinearly (green) with a low input-number threshold (2 inputs) and shaft synapses (red) sum as well supralinearly with a higher input-number threshold (5 inputs).

ascribed to a larger average EPSP, in fact the average spine EPSP is even 20% higher than the shaft in the current model (Fig. 6.1B). ii) *higher threshold for supralinear integration* - the impedance of distal dendrite is larger than the proximal enabling local compartment to gradually engage more voltage-gated channels such as calcium and NMDAR. Our observation shows that the calcium current in the distal dendrite does not accumulate in a supralinear fashion (data not plotted). It is the nonlinear nature of NMDAR that gives rise to the spiking behavior, allowing for detecting more salient synaptic events and regulating the shaft spiking threshold (Fig. 6.6B).

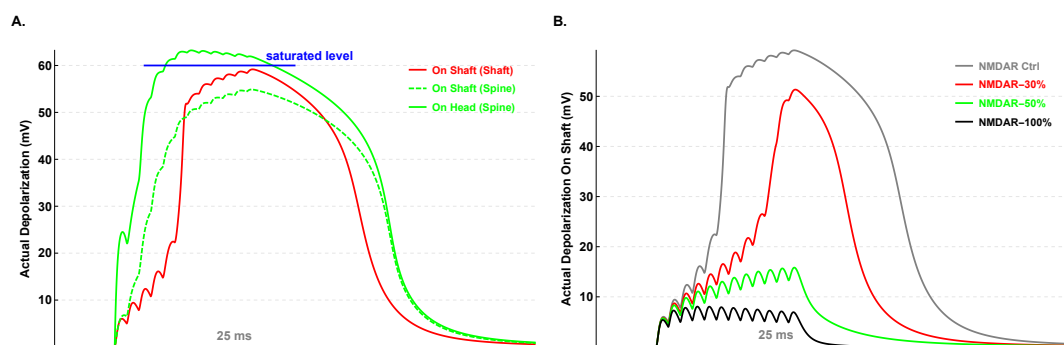


Figure 6.6: Mechanisms of distal shaft amplification.

A. The voltage trajectories in the spine head and distal dendritic shaft.

B. The voltage trajectories in distal dendritic shaft, simulated with 4 different percentages of NMDAR density.

6.4 Discussion

Due to technical limitations, it is experimentally challenging to accurately identify synaptic contacts located on the shaft, and then investigate the integrative properties of the evoked EPSPs using electrophysiology methods. Thus it is not surprising that the relevant literature is scarce, in which individual synapses were precisely uncaged along a dendrite and activated in a variety of spatiotemporal patterns.

In this study, I take advantage of numerical simulation and explored potential computational modes of shaft synapses. The model faithfully replicates 100% linearized summation of spines and 80% sublinearized summation of shaft terminals [Araya et al., 2006a]. Expanding upon this, the results reveal a presence of synaptic amplification initiated distally by axo-dendritic synapses, a phenomenon previously thought only achievable with the spine [Harnett et al., 2012]. The modeled location-dependent shaft synaptic integration enriches a single neuron with additional computational capacities: i) sublinear integration underlies information processing of pyramidal neurons [Longordo et al., 2013], a cluster of proximal shaft synapses can independently perform such computation without a balanced recruitment of inhibition; ii) unlike in other cell types [Plotkin et al., 2011], supralinear integration of distal regenerative synaptic responses is achieved by spines without a proper threshold-detecting mechanism [Branco and Häusser, 2011]. The distal shaft synapse can improve this by linearizing the combined output of sparsely scattered synaptic events.

In young animals, the percentage of shaft contacts is relatively high. How the spatiotemporally structured axo-dendritic input patterns are transformed into axonal spike generation remains largely elusive as the related research is currently limited to anatomical and molecular analysis. The presented results discovers a novel form of shaft-governed synaptic amplification that could motivate further study on the functional properties of axo-dendritic synapses.

Chapter 7

Concluding Remarks

The six papers presented in this thesis aim for better comprehension of single neuron computation under various modeling conditions. The two parts seem very irrelevant to one another at first glance, in that not only different modeling approaches are adopted but also different combinations of nonlinear elements are taken to address specific questions. However, with a closer look, such decision is made based upon how the particular scientific question can be best addressed and both parts converge on the central theme of the thesis and contribute to an advanced understanding of how the variations in the observed neuronal responses are attributable to either intrinsic features in the cellular property (duration of action potential) using phenomenological models or anatomical characteristics in the cellular structure (type and location of synaptic contacts on the dendrite) using compartmental models with the respective configuration of presynaptic input protocols.

In this chapter, I summarize again the major findings of the individual chapters, outline future works towards building a versatile model of the striatal principal neuron, link the detailed cellular modeling with synaptic plasticity and demonstrate a cellular implementation of bayesian computation.

7.1 Summary

One theme of the presented research is to make use of the most simplified nonlinear models of neuronal dynamics (e.g. Integrate-and-Fire model) and phenomenological models of synaptic plasticity empowered by simplistic STDP windows to address the question: how a model neuron responds to converging presynaptic inputs with a considerable amount of quantity given various kinds of learning rules and diverse configurations of input statistics? The first publication [Zheng and Schwabe, 2011a] is dedicated to characterize the differential rate coding of a single neuron that learns with STDP rules given perturbative presynaptic statistics of spike trains, to adapt the postsynaptic spiking activity and adjust the synaptic pattern (interpreted as synaptic memory). The nonlinear subcellular devices utilized by the model neuron are synaptic plasticity and artificial spiking threshold which are then simulated under the Song framework [Song et al., 2000]. The results show that even with such minimal combination of nonlinearity, model neurons can operate in different dynamical regimes (elevated or transient rate increase) and display distinct behaviors of memory conservations (mild or severe memory loss). In addition, I relate the abnormal presynaptic activity to what has been observed in seizures and study the effect of an increased GABAergic reversal potential reported in epilepsy [Barmashenko et al., 2011]. Surprisingly, increased reversal potentials can benefit the robustness of memory, which may provide an additional previously unknown homeostatic mechanism for protecting memory from perturbations [Zheng and Schwabe, 2011b]. The simulation results contribute to the prediction that in model neurons, paroxysmal activity could easily override memories without other homeostatic mechanisms, therefore pathological brain states may be even more disruptive than previously thought when learning mechanisms are also taken into account.

The results from the study of the phenomenological STDP models, particularly the resulting synaptic weight distribution shaped by the learning rules, motivated me then to investigate a previously-overlooked question in the field of spike-timing dependent plasticity: How the detailed shape of STDP window near the transition from potentiation to depression could affect neuronal dynamics of the identical neuron model? Distinct from the study which proposed a positive shift inspired by either slow kinetics of NMDA receptors [Babadi and Abbott, 2010] or axonal delay [Morrison et al., 2007], I argue that the window shall be negatively shifted due to the variability of durations of action potential [Zheng and Schwabe, 2013b] and such justification is indeed supported by various published experimental observations. The equilibration of synaptic weight patterns and the regulation of postsynaptic spiking displayed via model neurons are then characterized in greater detail, in the publication [Zheng and Schwabe, 2014]. When driven by noise inputs, the effect of long AP durations in down-regulating the postsynaptic firing rate is very evident by both additive and mixed modes (much prominent in the additive mode). As every single action potential is extremely costly in terms of its natural metabolic process, this behavior is desired to reduce unnecessary biological cost and preserve physiological energy. Meanwhile, when driven by salient signal inputs, model neurons respond quickly and stay in an active spiking state while the induction of competition between synapses is preserved.

This dSTDP model provides yet an alternative solution to the dilemma that strong competition between synapses cannot co-exist with the stability of synaptic weight dynamics [Gilson and Fukai, 2011].

The other theme of this thesis takes a completely different approach by focusing on the exploration of the information processing of single model neurons with a much richer combination of nonlinear units, incorporating active dendrites, spines and natural spiking behaviors. The modeled striatal principal neuron is validated by somatic current clamp and dendritic glutamate uncaging protocols, which is the *first* model published [Zheng et al., 2014] in the striatal modeling literature that can replicate both the response to current injections and the distally-evoked state transitions. The results emphasize the role of functional compartmentalization in thin dendrites in support of generating dendritic plateau potentials through an enhancement of the cooperativity among the neighboring spines. In another paper, [Zheng and Schwabe, 2013a] demonstrates a similar characteristic through exploring the contribution of dendritic anatomy to upstate generation from a purely passive perspective. The main discovery made by the active spiny SPN model is that although dendritic plateau potentials do not themselves cause action potentials which may interrupt the basic information processing in SPNs, nevertheless they provide conditions for reliable signal transformation from cortex or thalamus. In other words, it sets the *probability threshold* to transform proximal inputs into postsynaptic spikes (see details in Sec 7.4). Aside from modeling SPNs, using the same compartmental modeling approach, the potential functional differences of axo-dendritic and axo-spinous synapses in gating the dendritic information flow is studied in a pyramidal neuron in an accepted manuscript [Zheng and Schwabe, 2015], which provides a number of instructive results in relation to the stratal function, by raising the possibility that axo-dendritic synapses of SPNs from thalamic innervations are very likely to entail the generation of state transitions.

7.2 Towards a Versatile Model of SPN

The SPN model presented in [Zheng et al., 2014] has made a sizable progress towards a versatile model of striatal output neuron by relating the synaptically and dendritically evoked local regenerative events to its influence on the somatic readout of action potential generation. Nevertheless, future interactions between experimentalists and modelers are required to further address and investigate a wide array of fundamental neurophysiological questions concerning the striatal function.

First, sodium channels can contribute to the differential regulation of bAP-evoked excitatory potentials in the dendrites (Fig.2 in [Day et al., 2008]). This observation is *not* manifest in the current model, as each individual channel is uniformly distributed along the dendritic compartments with equal density. In addition, the study in CA1 pyramidal neurons revealed a cell-to-cell or branch-to-branch dichotomy in action-potential back-propagation and such difference is thought to be partly attributed to a delicately-differentiated invest-

ment of sodium channels [Golding et al., 2001]. This observed dichotomy is worth an investigation in the SPN model because it might strongly influence the local read-out of synaptic and dendritic coincidence detection. Moreover, one of the notable features of sodium channel-dominated strong dendritic excitability is that it changes the number of synaptic inputs necessary for dendritic spikes, thereby controlling the conditional probability of relevant nonlinear events [Jarsky et al., 2005]. Such hypothesis is already testable in the model of current version. Furthermore, sodium channels amplify spine-evoked excitatory potentials and this effect is postsynaptic [Araya et al., 2007]. Although [Plotkin et al., 2011] has shown that TTX do not modulate the dynamics of state transition, its role in shifting the amplitude distribution of unitary synaptic events is yet to be examined.

Second, the four voltage-dependent potassium channels invested in the compartments have their respective contributions to the membrane potential dynamics of the modeled SPN. **KIR** channels determine the level of resting potential and globally constrain the neuronal excitability. Even a tiny bit of increase of the channel density could lower the downstate voltage thereby effectively down-regulating the neuronal response to any form of excitatory drives. For the reason that it is of such symbolic importance, the channel kinetics shall be investigated in the striatal cells using the transitional ramp protocol, although the current implementation works “fine” by inferring model parameters from other animal models. **Kv4** channels respond very alertly to the excitatory synaptic inputs and modulate the extent of invasion of back-propagating action potentials. Besides, they also determines the onset of the first spike under current clamp protocol and shape the hyper-polarization after each somatic firing. High-magnification images of protein labeling revealed a clear expression of Kv4.2-channel in both dendrites and spines. However, in the current spine model, Kv4 is *not* included in the channel pool and its regulatory effect in the enhancement of calcium signaling is *not* present in my model, although being clearly demonstrated in [Day et al., 2008]. It seems to me that the density needs to be set to a fairly large value to see some dampening effect in lowering the local depolarization in the spine head. **Kv1** channels regulate somatic, but not dendritic, excitability in SPNs [Shen et al., 2004]. Strategically placing the channel non-uniformly in the somatic and dendritic compartments is an immediate next step for the modeling study. I hypothesize that re-balanced Kv1 and Kv4 channels in the dendrites can extend the duration of state transitions once initiated. **KRP** channels are only placed in the soma and the parameters are tuned to provide a reasonable inter-spike interval during somatic spiking. Currently, there is no evidence about how it might influence the properties of dendritic computation. **SK** channels (calcium-sensitive potassium channels) are excluded from the model for simplicity and as well due to the reality that the related experimental evidence in the striatal neurons is fuzzy, mainly in respect of synaptic plasticity, not dendritic integration [Nazzaro et al., 2012]. Nevertheless, it is evident that SK-type channels participate in a local feedback loop within a spinous compartmentalization [Higley and Sabatini, 2008]. From my own modeling, I did once witness the effect of SK channels in regulating the duration of distally-evoked upstate from a model in which R-type calcium channel is the dominant factor, not NMDAR channel.

More specifically, without SK channels placed in the spine head, synaptically-evoked distal upstates could have biologically unrealistic lengths up to several seconds. This observation reinforces the notion that the regulatory channels like SK-type may probably not be a part of the basic computational toolkit, but yet an important member of fundamental regulatory toolkit to keep a normal biological functionality of the spine head, e.g. in this case, to prevent excessive calcium entry into a spine that could lead to an impairment of the normal intra-spine molecular signaling.

Third, if say sodium and potassium channels equip the SPNs to perform elementary non-linear dendritic integration, somatic pulse generation and regulation of synaptic plasticity [Johnston et al., 2003], calcium channels could have even more profound implications for all these functions. High-threshold voltage-dependent calcium channels have been identified in the previous SPN studies: N-type, Q-type, R-type and L-type (particularly Cav1.2) [Churchill and Macvicar, 1998]. For the reason that N-type and Q-type are primarily expressed in the presynaptic axonal terminal (personal communication with Joshua Plotkin), these two channels are not incorporated into the model. Analogously, no significant change of state transitions to uncaging glutamate was observed by applying bath application of L-type blockers [Plotkin et al., 2011], thus L-type was also excluded from the model. T-type (low-threshold) and R-type channels were reported to co-regulate with NMDAR channels, the onset and duration of distal upstates. One aspect inconsistent with the original modeling in [Plotkin et al., 2011] is that placing T-type in the spine head, *not* the dendrite, modulates the amplitude and duration of distally-evoked regenerative events. There are two mechanisms in the current model that could help account for this discrepancy: 1) the main contribution of T-type is hypothesized to provide additional depolarization occurring in the dendritic shaft. However, this effect could readily be achieved with the parametrization of distal tapering of dendritic diameter; 2) the unitary synaptic amplitude in the current model is too large, making T-type less influential in the dendrites (see next paragraph for discussion). Nevertheless, placing T-type channels in the dendrites does increase the excitability of neuronal response to current injection. Fig. 7.1A illustrates that T-type elevates the responsiveness of SPN model to the identical injected current. Interestingly, such elevation can be subject to the existence of SK channels. The elevated level of SK density can diminish the contribution from calcium currents, thereby making the neuron less excitable (Fig. 7.1B). Besides, T-type channel has also been recently reported to interact with the voltage-dependent potassium channel. More specifically, the signaling complex formed by T-type and Kv4 channels efficiently couples calcium influx to K^+ channel-interacting proteins (KChIP3) and adapts the kinetic dynamics of Kv4 [Anderson et al., 2010]. In comparison, the contribution of R-type is relatively minimal (Fig. 7.1C), probably due to its rapid deactivation with time constants of a few hundred *microseconds* [Foehring et al., 2000]. Figuring out an appropriate parameter space that reflects the complex interaction between calcium and calcium-sensitive potassium channels, can definitely add another dimension to the model fidelity, it is, however, out of the scope of this thesis.

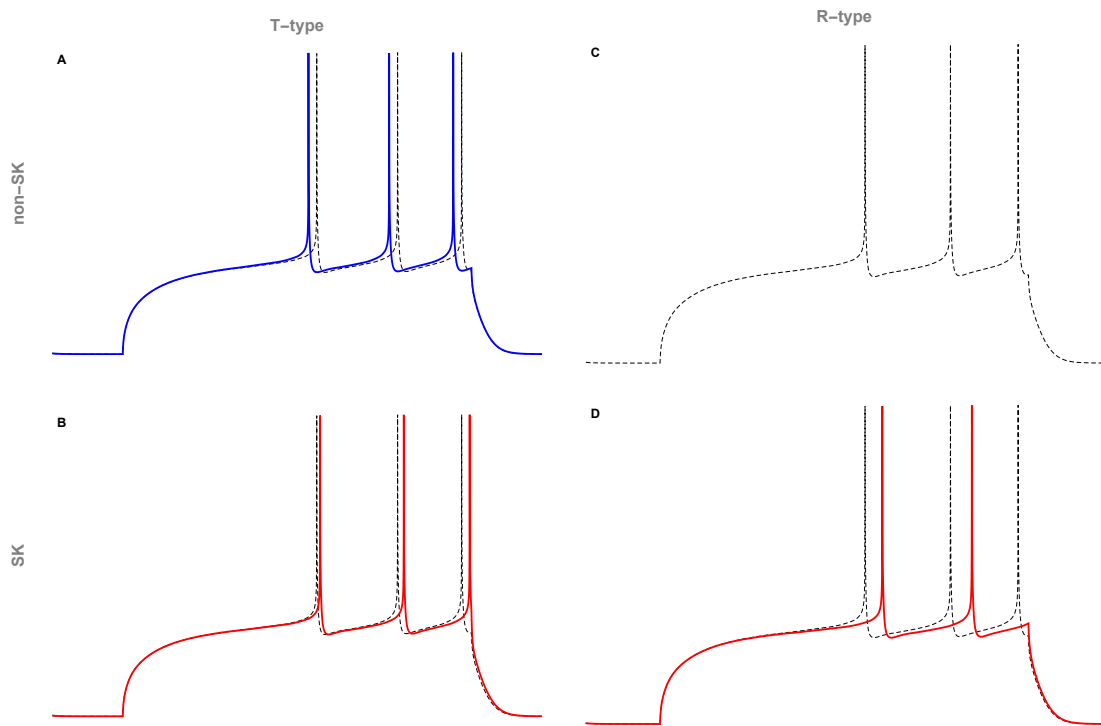


Figure 7.1: Simple illustration of an interaction between calcium and SK channels.

A. Given that the density of SK channel in the model is zero, the investment of T-type calcium channels increases the neuronal excitability by advancing the first spike under current injection protocol (blue curve) in contrast to the control condition in which the density of T-type is also set to zero (black curve).

B. Same as in A, the density of SK channel is a non-zero value and the current induced by SK delays the first spike (red curve).

C. Same as in A, instead R-type calcium channels are placed in the model with the same density, this does not affect the somatic spiking.

D. Same as in C, adding SK channels delays the first spike (red curve).

Fourth, the evoked individual EPSP generated by the model is between 2.0mV and 2.5mV (Fig. 5.6A), which is larger than the evoked excitatory potential of 1mV by a single pulse of glutamate uncaging used in [Plotkin et al., 2011]. The larger somatic EPSP amplitude in the current model does create undesirable artifacts, although it does a pretty good job in replicating the upstate phenomenon and providing a reasonable account for the underlying dendritic passive mechanism. One of the artifacts is that the amplitude and duration of state transition depend “linearly” on the number of activated synaptic inputs as shown in Fig.7.2A. It is not in agreement with the observation, in which about 10 spines are required to be activated in rapid succession to reach a threshold for evoking the somatic plateau potential [Plotkin et al., 2011]. Therefore, attempts were made to find a better solution for this issue. By tuning the somatic response of a single synaptic input to 1mV, the current model can perfectly reproduce the threshold-gated initiation of plateau potential at the distal dendrite as in Fig.7.2B. It will be very interesting to see how this 1mV-model responds to the prox-dist protocols studied in [Zheng et al., 2014].

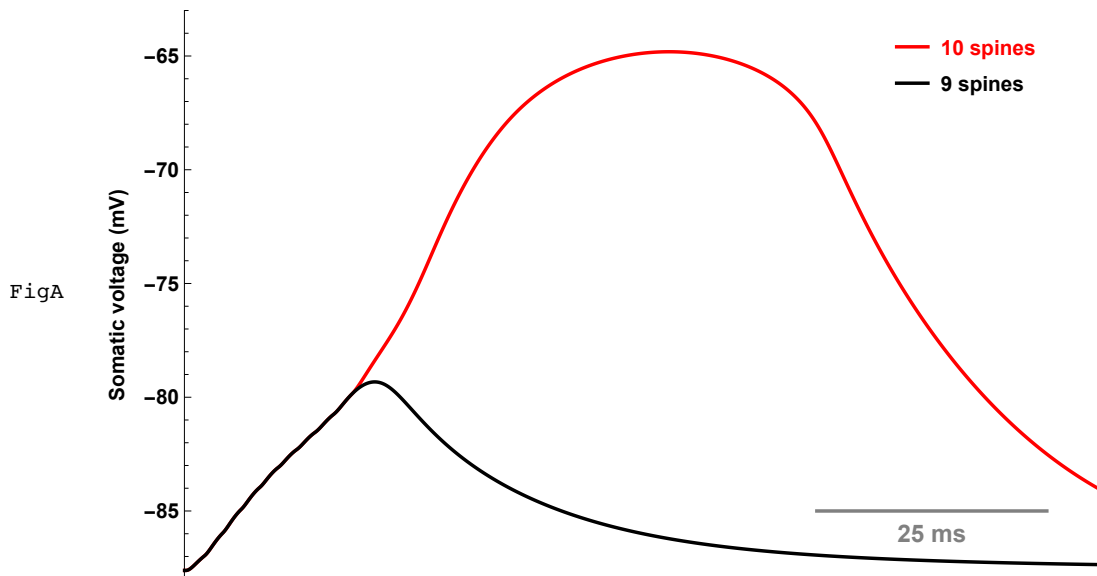


Figure 7.2: **The threshold behavior of distal upstate is achieved in a 1mV model.**

A. The somatic plateau potential generated by the SPN model presented in Sec 5.2.1.

B. Same as in A, but by simulated the model that produces 1mV somatic EPSPs.

Finally, the ultimate goal of modeling single striatal spiny projection neurons is to exploit the simulation as an important computational means to assist in studying the circuit-specific deficits of related diseases and to put together the fragmentary advances made in animal models in our quest to understand the consequences of the mechanisms that drive pathology at the cellular level. The progress towards achieving this goal could be accelerated by differentiating the two types of SPNs into separated modeling collections. The use of bacterial artificial chromosome (BAC) transgenic mice has made it apparent that the two types of neurons, dSPNs and iSPNs, differ significantly in their intrinsic excitability, especially the size and morphological properties [Surmeier et al., 2014]. Thanks to the generosity of

Surmeier Lab, the morphological and geometrical data that are indispensable for the model separation has been made available to me. I am excited to further work on the parameterization of a balanced expression of synaptic channels in the spines and distance-dependent ion-channel distribution [Ashhad and Narayanan, 2013] that enable the models with capability to replicate the dendritically-evoked state transitions and differences in the membrane properties.

Besides, SPN dendrites are too thin to yield to traditional electrode-based recording. Emerging advanced tools such as optogenetics and uncaging have made it possible to directly interrogate dendritic territories, but so far still mostly limited to ‘one sub-dendritic scan at a time’ (personal communication with Joshua Plotkin). The accurate quantitative models, as exemplified in Fig. 5.9, provide necessary computational techniques to incorporate new experimental findings and help unravel the enigmatic characteristics of dendrites in shaping the adaptive striatal input-output transformation [Segev and London, 2000]. Moreover, in addition to the excitatory synaptic input, local GABAergic input to SPNs also change in the disease states. Recent theoretical work has provided new and testable insights into the principle of how the synaptic inhibition by GABAergic inputs impinging directly on the dendrites. In contrary to the “proximal on-path theory”, distal “off-path” inhibition could more effectively control the neuronal output by cooling down the proximal excitable hotspots [Gidon and Segev, 2012]. The structural complexity from neighboring SPNs and network heterogeneity from diverse groups of interneurons, complicates the effects of GABAergic alteration in SPNs [Plotkin and Surmeier, 2015] and thus the compartmental models may give hope, for example, to examine the effects of the aforementioned distal “off-path” inhibition in cooling off the nonlinear feature of state transitions. Furthermore, small network models may also gain additional insights from detailed compartmental modeling. Only a few percent of dSPNs (presumably equivalent a small network of dSPNs) can completely inhibit the downstream output from SNr and a small group of bursting iSPNs can prominently elevate the activity of SNr [Lindahl et al., 2013]. The simulated IaF models might offer qualitatively correct predictions about how the basal ganglia output nuclei is controlled by the direct and indirect pathways. However, if the timing matters for properly controlled discharge of self-pacing GP neurons [Chan et al., 2005] and dendritic plateau potentials is critical for spike time control in the presence of inhibitory input [Shai et al., 2014], then separated collections of detailed SPN models can be desirable.

Conclusively, dSPNs and iSPNs are not just simple connectors between thalamocortical regions and basal ganglia, they receive dopaminergic modulatory inputs that have completely opposite effects on every aspect of their neuronal integrative dynamics. The future workout that divides the striatal neurons into clean dSPN and iSPN versions, investigates the impact of inhomogeneous channel distribution on the dendrite and explores the interaction between calcium and calcium-activated channels, could anticipate improvements on the existing attempts conducted in [Gertler et al., 2008], study the dopaminergic modulation on the respective type [Moyer et al., 2007] and guide future experiments that are expensive.

7.3 Synaptic Plasticity and Dendritic Plateau Potentials

The longstanding paradox, that SPNs must have unidirectional synaptic plasticity due to the distinct expressions of dopamine receptors, has been elegantly resolved by [Shen et al., 2008], which demonstrated nicely that bidirectional changes of synaptic strength can be induced in SPNs given standard STDP protocols. In this dissertation, I didn't have sufficient amount of time to undertake projects that address either how synaptic plasticity can potentially exert a wide range of effects on the information transformation of a single SPN or how dendritic plateau potentials can mediate synaptic plasticity in conjunction with the voltage-dependent synaptic learning [Gambino et al., 2014]. Nevertheless, the paradigm used in [Zheng and Schwabe, 2014] to study the emergent properties of STDP and the NEURON framework presented in [Zheng et al., 2014] to investigate the computational function of a single dendritic branch, has equipped us to simulate various behaviors of local cellular input processing, affected by synaptic changes. It seems that nonlinear short-term neuronal dynamics typically arise from activation of sufficiently clustered synapses in space and time [Branco and Häusser, 2010]. Thus, one of the intriguing questions is then how the induction of synaptic plasticity on an existing local circuitry can bring about a conditional alteration of dendritic processing? In Fig. 7.2, I illustrated that only 10 distal spines, not 9, are able to reach the threshold for the plateau potential. Simulated with the identical parameterization, the number of the synaptic input for reaching such threshold can be reduced to 9 spines with an increase of the synaptic weight by 30%, as in Fig. 7.2. Moreover, [Plotkin and Surmeier, 2015] stressed that the plasticity of neuronal excitability is far from entirely being synaptic. The input threshold for distally-evoked plateau potential may be comparably lower in iSPNs than in dSPNs, which requires both experimental and computational examinations in the future. Given that directly testing the consequences of STDP-induced clustered potentiation or depression remains challenging, adding synaptic learning to SPN models can offer a glimpse into the unexplored areas of striatal physiology.

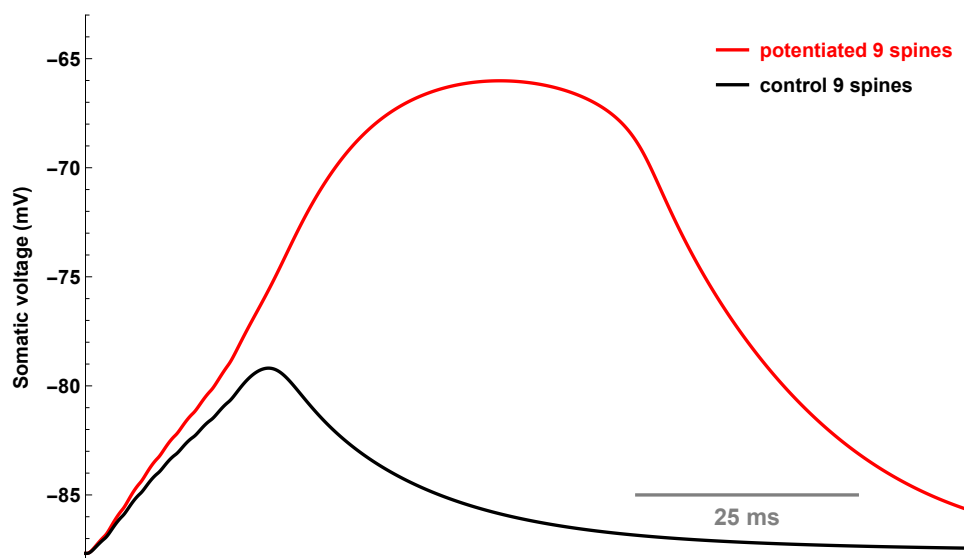


Figure 7.3: Synaptic potentiation of converged distal inputs reduces the threshold for the dendritic plateau potential. 9 unpotentiated distal spines are not capable of generating an upstate (black). When potentiated by 30%, the same amount of input ensemble evokes an upstate (red).

7.4 Cellular Implementation of Bayesian Computation

In the beginning of the thesis, a Bayesian Belief Network was applied to calculate the discrete posteriors about unknown mechanisms of synaptic plasticity. Besides its broad applications, the bayesian idea has also been profoundly re-shaping our understanding about the neural underpinning of behaviors, that our brain is itself probabilistic, forms internal belief distributions of practically every possible given variable and performs bayesian-like neural computation with uncertainty and probability [Ma and Jazayeri, 2014]. Much influenced by the doctrine that one can study the nature of a cell and understand the nature of a human because in the biological reality a human is merely a fractal image of the cell, I speculate that a single neuron must also have at its disposal a representation of conditional and non-conditional probability associated with any specific variable in the living world.

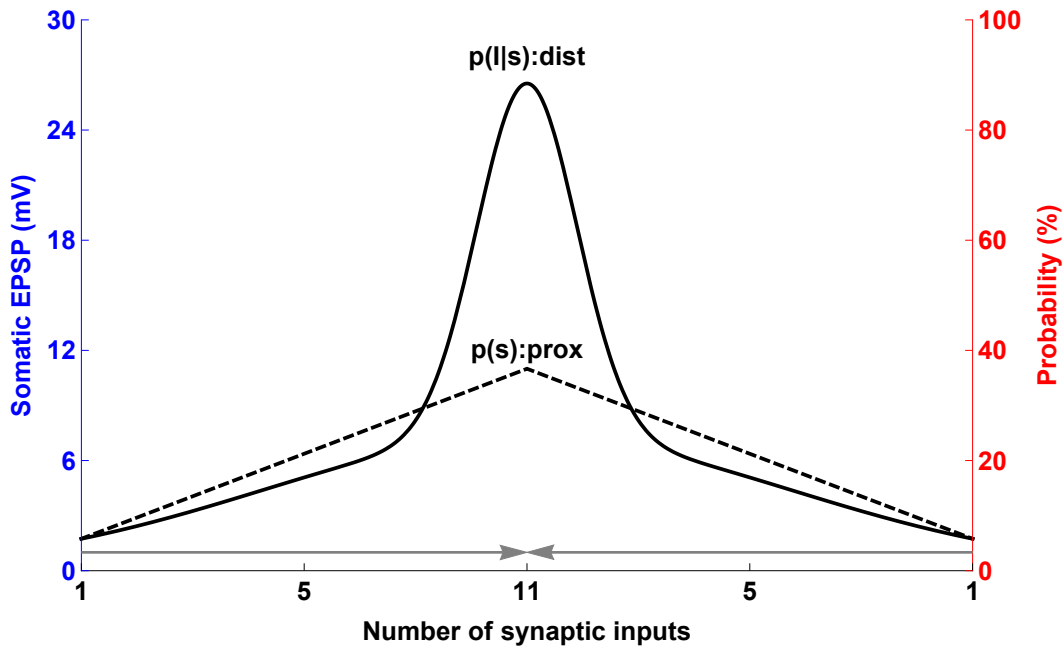


Figure 7.4: SPN dendritic compartments represent bayesian substrates for inferences.

The response of distal dendrites to the synaptic activation is highly nonlinear, which makes them good candidates to represent the significance of internal signals generated by local and global neural networks. In contrast, the response of proximal dendrites is linear and suitable to transform faithfully the external stimuli from the environment.

I find that the SPN model could provide exactly the substrate for that kind of computation. Hypothetically, the conditional distribution of activation of the internal knowledge I given an input variable s that relates to a sensory cue, can be denoted as $p(I|s)$, and the prior distribution of s that represents all the possible values of this sensory cue, can be denoted as $p(s)$. The posterior distribution $p(s|I)$ which is the response probability of s given I can be then computed simply by the Bayes' theorem:

$$p(s|I) = \frac{p(I|s)p(s)}{p(I)} \quad (7.1)$$

where the denominator $p(I)$ operates as a normalization factor.

As the response of local dendritic activation is *not* direction-dependent [Plotkin et al., 2011], the distal and proximal compartments can exploit the membrane potential trace (left y-axis) to create the statistical models (right y-axis), respectively for $p(I|s)$ and $p(s)$ as illustrated in Fig.7.4. Such hypothetical probabilistic approach reflects that the dendritic compartments of a SPN may derive explicit probability functions to combine evidences from the sensory input and the internal state of the brain to calculate the neural readout of $p(s|I)$.

How a single neuron integrates feed-forward sensory signals from the external world with the internally-organized neural activity is not yet well-understood [Peyrache et al., 2015]. The ubiquity of dendritic plateau potentials found in diverse cell types is thought to underpin a prominent source of internal signals [Major et al., 2008] and provide the underlying mechanism of enhancing the stimulus selectivity of input signals [Smith et al., 2013]. The probabilistic brain constantly carries out tasks like cognitive reasoning and decision-making process involving knows or unknowns with the Bayesian approach [Pouget et al., 2013], individual nerve cells must somehow contribute to such process using their nonlinear computing devices. Fig.7.4 indicates that a large intrinsic part of such single neuron computation may exploit distal dendrites to represent the probabilistic distributions of internal neural states which heavily depend on the cell type, the type of synapse and the dendritic location of synaptic innervation [Zheng and Schwabe, 2015].

Bibliography

- [BNT, 2007] (2007). <http://code.google.com/p/bnt>.
- [Abbott and Nelson, 2000] Abbott, L. F. and Nelson, S. B. (2000). Synaptic Plasticity: Taming the Beast. *Nature Neuroscience*, 3 Suppl:1178–1183.
- [Abraham, 2008] Abraham, W. C. (2008). Metaplasticity: Tuning Synapses and Networks for Plasticity. *Nature Reviews Neuroscience*, 9(5):387–399.
- [Anderson et al., 2010] Anderson, D., Mehaffey, W. H., Iftinca, M., Rehak, R., Engbers, J. D. T., Hameed, S., Zamponi, G. W., and Turner, R. W. (2010). Regulation of Neuronal Activity by Cav3-Kv4 Channel Signaling Complexes. *Nature Neuroscience*, 13(3):333–337.
- [Ansorg and Schwabe, 2010] Ansorg, R. and Schwabe, L. (2010). Domain-specific modeling as a pragmatic approach to neuronal model descriptions. In Yao, Y., Sun, R., Poggio, T., Liu, J., Zhong, N., and Huang, J., editors, *Brain Informatics*, volume 6334 of *Lecture Notes in Computer Science*, pages 168–179. Springer Berlin Heidelberg.
- [Aoto et al., 2007] Aoto, J., Ting, P., Maghsoodi, B., Xu, N., Henkemeyer, M., and Chen, L. (2007). Postsynaptic ephrinB3 promotes shaft glutamatergic synapse formation. *The Journal of Neuroscience*, 27(28):7508–7519.
- [Araya, 2014] Araya, R. (2014). Input transformation by dendritic spines of pyramidal neurons. *Frontiers in Neuroanatomy*, 8:141.
- [Araya et al., 2006a] Araya, R., Eiselthal, K. B., and Yuste, R. (2006a). Dendritic spines linearize the summation of excitatory potentials. *Proceedings of the National Academy of Sciences of the United States of America*, 103(49):18799–18804.
- [Araya et al., 2006b] Araya, R., Jiang, J., Eiselthal, K. B., and Yuste, R. (2006b). The spine neck filters membrane potentials. *Proceedings of the National Academy of Sciences of the United States of America*, 103(47):17961–17966.
- [Araya et al., 2007] Araya, R., Nikolenko, V., Eiselthal, K. B., and Yuste, R. (2007). Sodium channels amplify spine potentials. *Proceedings of the National Academy of Sciences*, 104(30):12347–12352.

- [Araya et al., 2014] Araya, R., Vogels, T. P., and Yuste, R. (2014). Activity-dependent dendritic spine neck changes are correlated with synaptic strength. *Proceedings of the National Academy of Sciences of the United States of America*, 111(28):E2895–904.
- [Arellano et al., 2007] Arellano, J. I., Benavides-Piccione, R., DeFelipe, J., and Yuste, R. (2007). Ultrastructure of dendritic spines: correlation between synaptic and spine morphologies. *Frontiers in Neuroscience*, 1(1):131–143.
- [Artola et al., 1990] Artola, A., Bröcher, S., and Singer, W. (1990). Different voltage-dependent thresholds for inducing long-term depression and long-term potentiation in slices of rat visual cortex. *Nature*, 347(6288):69–72.
- [Ashhad and Narayanan, 2013] Ashhad, S. and Narayanan, R. (2013). Quantitative interactions between the A-type K⁺ current and inositol trisphosphate receptors regulate intraneuronal Ca²⁺ waves and synaptic plasticity. *The Journal of Physiology*, 591(7):1645–1669.
- [Babadi and Abbott, 2010] Babadi, B. and Abbott, L. F. (2010). Intrinsic stability of temporally shifted spike-timing dependent plasticity. *PLoS Comput. Biol.*, 6(11):e1000961.
- [Bailey and Kandel, 2008] Bailey, C. H. and Kandel, E. R. (2008). Synaptic remodeling, synaptic growth and the storage of long-term memory in Aplysia. *Progress in Brain Research*, 169:179–198.
- [Barinaga, 1995] Barinaga, M. (1995). Dendrites shed Their Dull Image. *Science*, 268(5208):200–201.
- [Barmashenko et al., 2011] Barmashenko, G., Hefft, S., Aertsen, A., Kirschstein, T., and Köhling, R. (2011). Positive shifts of the GABAA receptor reversal potential due to altered chloride homeostasis is widespread after status epilepticus. *Epilepsia*, 52(9):1570–1578.
- [Bi and Poo, 1998] Bi, G. Q. and Poo, M. M. (1998). Synaptic modifications in cultured hippocampal neurons: dependence on spike timing, synaptic strength, and postsynaptic cell type. *The Journal of Neuroscience*, 18(24):10464–10472.
- [Biddell and Johnson, 2013] Biddell, K. and Johnson, J. (2013). A biophysical model of cortical glutamate excitation of medium spiny neurons in the dorsal lateral striatum. In *2013 IEEE 56th International Midwest Symposium on Circuits and Systems (MWSCAS)*, pages 964–966.
- [Bienenstock et al., 1982] Bienenstock, E. L., Cooper, L. N., and Munro, P. W. (1982). Theory for the development of neuron selectivity: orientation specificity and binocular interaction in visual cortex. *The Journal of Neuroscience*, 2(1):32–48.

- [Billings and van Rossum, 2009] Billings, G. and van Rossum, M. C. W. (2009). Memory retention and spike-timing-dependent plasticity. *Journal of Neurophysiology*, 101(6):2775–2788.
- [Bliss and Lømo, 1973] Bliss, T. V. and Lømo, T. (1973). Long lasting potentiation of synaptic transmission in the dentate area of the anaesthetized rabbit following stimulation of the perforant path. *The Journal of Physiology*, 232(2):331–356.
- [Bloodgood et al., 2009] Bloodgood, B. L., Giessel, A. J., and Sabatini, B. L. (2009). Biphasic synaptic Ca influx arising from compartmentalized electrical signals in dendritic spines. *PLoS Biol.*, 7(9):e1000190.
- [Bloodgood and Sabatini, 2007] Bloodgood, B. L. and Sabatini, B. L. (2007). Nonlinear Regulation of Unitary Synaptic Signals by CaV 2.3 Voltage-Sensitive Calcium Channels Located in Dendritic Spines. *Neuron*, 53(2):249–260.
- [Bower and Buckmaster, 2008] Bower, M. R. and Buckmaster, P. S. (2008). Changes in granule cell firing rates precede locally recorded spontaneous seizures by minutes in an animal model of temporal lobe epilepsy. *Journal of Neurophysiology*, 99(5):2431–2442.
- [Branco et al., 2010] Branco, T., Clark, B. A., and Häusser, M. (2010). Dendritic discrimination of temporal input sequences in cortical neurons. *Science*, 329(5999):1671–1675.
- [Branco and Häusser, 2010] Branco, T. and Häusser, M. (2010). The single dendritic branch as a fundamental functional unit in the nervous system. *Current Opinion in Neurobiology*, 20(4):494–502.
- [Branco and Häusser, 2011] Branco, T. and Häusser, M. (2011). Synaptic integration gradients in single cortical pyramidal cell dendrites. *Neuron*, 69(5):885–892.
- [Brette and Gerstner, 2005] Brette, R. and Gerstner, W. (2005). Adaptive exponential integrate-and-fire model as an effective description of neuronal activity. *Journal of Neurophysiology*, 94(5):3637–3642.
- [Caporale and Dan, 2008] Caporale, N. and Dan, Y. (2008). Spike timing-dependent plasticity: a Hebbian learning rule. *Annual Review Neuroscience*, 31:25–46.
- [Carnevale and Hines, 2006] Carnevale, N. T. and Hines, M. L. (2006). *The NEURON Book*. Cambridge University Press.
- [Cash and Yuste, 1998] Cash, S. and Yuste, R. (1998). Input summation by cultured pyramidal neurons is linear and position-independent. *The Journal of Neuroscience*, 18(1):10–15.
- [Castellani et al., 2009] Castellani, G. C., Bazzani, A., and Cooper, L. N. (2009). Toward a microscopic model of bidirectional synaptic plasticity. *Proceedings of the National Academy of Sciences of the United States of America*, 106(33):14091–14095.

- [Chan et al., 2005] Chan, C. S., Surmeier, D. J., and Yung, W.-H. (2005). Striatal information signaling and integration in globus pallidus: timing matters. *Neuro-Signals*, 14(6):281–289.
- [Churchill and Macvicar, 1998] Churchill, D. and Macvicar, B. A. (1998). Biophysical and pharmacological characterization of voltage-dependent Ca^{2+} channels in neurons isolated from rat nucleus accumbens. *Journal of Neurophysiology*, 79(2):635–647.
- [Clopath et al., 2010] Clopath, C., Büsing, L., Vasilaki, E., and Gerstner, W. (2010). Connectivity reflects coding: a model of voltage-based STDP with homeostasis. *Nature Neuroscience*, 13(3):344–352.
- [Clopath and Gerstner, 2010] Clopath, C. and Gerstner, W. (2010). Voltage and Spike Timing Interact in STDP - A Unified Model. *Frontiers in Synaptic Neuroscience*, 2:25.
- [Cooper, 2010] Cooper, L. N. (2010). STDP: Spiking, Timing, Rates and Beyond. *Frontiers in Synaptic Neuroscience*, 2:14.
- [Cormier et al., 2001] Cormier, R. J., Greenwood, A. C., and Connor, J. A. (2001). Bidirectional synaptic plasticity correlated with the magnitude of dendritic calcium transients above a threshold. *Journal of Neurophysiology*, 85(1):399–406.
- [Cui et al., 2013] Cui, G., Jun, S. B., Jin, X., Pham, M. D., Vogel, S. S., Lovinger, D. M., and Costa, R. M. (2013). Concurrent activation of striatal direct and indirect pathways during action initiation. *Nature*, 494(7436):238–242.
- [Day et al., 2008] Day, M., Wokosin, D., Plotkin, J. L., Tian, X., and Surmeier, D. J. (2008). Differential excitability and modulation of striatal medium spiny neuron dendrites. *The Journal of Neuroscience*, 28(45):11603–11614.
- [Delgado et al., 2010] Delgado, J. Y., Gómez-González, J. F., and Desai, N. S. (2010). Pyramidal neuron conductance state gates spike-timing-dependent plasticity. *The Journal of Neuroscience*, 30(47):15713–15725.
- [Deng et al., 2013] Deng, P.-Y., Rotman, Z., Blundon, J. A., Cho, Y., Cui, J., Cavalli, V., Zakharenko, S. S., and Klyachko, V. A. (2013). FMRP regulates neurotransmitter release and synaptic information transmission by modulating action potential duration via BK channels. *Neuron*, 77(4):696–711.
- [Destexhe et al., 1994a] Destexhe, A., Mainen, Z. F., and Sejnowski, T. J. (1994a). An efficient method for computing synaptic conductances based on a kinetic model of receptor binding. *Neural Computation*, 6(1):14–18.
- [Destexhe et al., 1994b] Destexhe, A., Mainen, Z. F., and Sejnowski, T. J. (1994b). Synthesis of models for excitable membranes, synaptic transmission and neuromodulation using a common kinetic formalism. *Journal of Computational Neuroscience*, 1(3):195–230.

- [Dobrunz and Stevens, 1999] Dobrunz, L. E. and Stevens, C. F. (1999). Response of hippocampal synapses to natural stimulation patterns. *Neuron*, 22(1):157–166.
- [Doi et al., 2010] Doi, S., Inoue, J., and Pan, Z. (2010). The hodgkin–huxley theory of neuronal excitation. In *Computational Electrophysiology*, volume 2 of *A First Course in “In Silico Medicine”*, pages 37–54. Springer Japan.
- [Esteban et al., 2003] Esteban, J. A., Shi, S.-H., Wilson, C., Nuriya, M., Huganir, R. L., and Malinow, R. (2003). PKA phosphorylation of AMPA receptor subunits controls synaptic trafficking underlying plasticity. *Nature Neuroscience*, 6(2):136–143.
- [Faeder et al., 2009] Faeder, J. R., Blinov, M. L., and Hlavacek, W. S. (2009). Rule-based modeling of biochemical systems with BioNetGen. *Methods in Molecular Biology (Clifton, N.J.)*, 500:113–167.
- [Feldman, 2012] Feldman, D. E. (2012). The spike-timing dependence of plasticity. *Neuron*, 75(4):556–571.
- [Foehring et al., 2000] Foehring, R. C., Mermelstein, P. G., Song, W.-J., Ulrich, S., and Surmeier, D. J. (2000). Unique properties of R-type calcium currents in neocortical and neostriatal neurons. *Journal of Neurophysiology*, 84(5):2225–2236.
- [Forti et al., 1997] Forti, L., Bossi, M., Bergamaschi, A., Villa, A., and Malgaroli, A. (1997). Loose-patch recordings of single quanta at individual hippocampal synapses. *Nature*, 388(6645):874–878.
- [Froemke et al., 2005] Froemke, R. C., Poo, M.-m., and Dan, Y. (2005). Spike-timing-dependent synaptic plasticity depends on dendritic location. *Nature*, 434(7030):221–225.
- [Fuenzalida et al., 2010] Fuenzalida, M., Fernández de Sevilla, D., Couve, A., and Buño, W. (2010). Role of AMPA and NMDA receptors and back-propagating action potentials in spike timing-dependent plasticity. *Journal of Neurophysiology*, 103(1):47–54.
- [Gambino et al., 2014] Gambino, F., Pagès, S., Kehayas, V., Baptista, D., Tatti, R., Carleton, A., and Holtmaat, A. (2014). Sensory-evoked LTP driven by dendritic plateau potentials in vivo. *Nature*, 515(7525):116–119.
- [Gerstner et al., 1997] Gerstner, W., Kreiter, A. K., Markram, H., and Herz, A. V. (1997). Neural codes: firing rates and beyond. *Proceedings of the National Academy of Sciences*, 94(24):12740–12741.
- [Gertler et al., 2008] Gertler, T. S., Chan, C. S., and Surmeier, D. J. (2008). Dichotomous anatomical properties of adult striatal medium spiny neurons. *The Journal of Neuroscience*, 28(43):10814–10824.

- [Gidon and Segev, 2012] Gidon, A. and Segev, I. (2012). Principles governing the operation of synaptic inhibition in dendrites. *Neuron*, 75(2):330–341.
- [Gilson and Fukai, 2011] Gilson, M. and Fukai, T. (2011). Stability versus neuronal specialization for STDP: long-tail weight distributions solve the dilemma. *PLoS One*, 6(10):e25339.
- [Gold and Bear, 1994] Gold, J. I. and Bear, M. F. (1994). A model of dendritic spine Ca^{2+} concentration exploring possible bases for a sliding synaptic modification threshold. *Proceedings of the National Academy of Sciences*, 91(9):3941–3945.
- [Golding et al., 2001] Golding, N. L., Kath, W. L., and Spruston, N. (2001). Dichotomy of action-potential backpropagation in CA1 pyramidal neuron dendrites. *Journal of Neurophysiology*, 86(6):2998–3010.
- [Goodman and Brette, 2008] Goodman, D. and Brette, R. (2008). Brian: a simulator for spiking neural networks in python. *Frontiers in Neuroinformatics*, 2:5.
- [Gray and McCormick, 1996] Gray, C. M. and McCormick, D. A. (1996). Chattering cells: superficial pyramidal neurons contributing to the generation of synchronous oscillations in the visual cortex. *Science*, 274(5284):109–113.
- [Grillner and Robertson, 2015] Grillner, S. and Robertson, B. (2015). The basal ganglia downstream control of brainstem motor centres—an evolutionarily conserved strategy. *Current Opinion in Neurobiology*, 33C:47–52.
- [Grunditz et al., 2008] Grunditz, A., Holbro, N., Tian, L., Zuo, Y., and Oertner, T. G. (2008). Spine neck plasticity controls postsynaptic calcium signals through electrical compartmentalization. *The Journal of Neuroscience*, 28(50):13457–13466.
- [Gulledge et al., 2012] Gulledge, A. T., Carnevale, N. T., and Stuart, G. J. (2012). Electrical advantages of dendritic spines. *PLoS One*, 7(4):e36007.
- [Hao and Oertner, 2012] Hao, J. and Oertner, T. G. (2012). Depolarization gates spine calcium transients and spike-timing-dependent potentiation. *Current Opinion in Neurobiology*, 22(3):509–515.
- [Harnett et al., 2012] Harnett, M. T., Makara, J. K., Spruston, N., Kath, W. L., and Magee, J. C. (2012). Synaptic amplification by dendritic spines enhances input cooperativity. *Nature*, 491(7425):599–602.
- [Hayashi et al., 2000] Hayashi, Y., Shi, S.-H., Esteban, J. A., Piccini, A., Poncer, J.-C., and Malinow, R. (2000). Driving AMPA receptors into synapses by LTP and CaMKII: requirement for GluR1 and PDZ domain interaction. *Science*, 287(5461):2262–2267.
- [Hebb, 1949] Hebb, D. O. (1949). *The Organization of Behavior: A Neuropsychological Theory*. Wiley.

- [Higley and Sabatini, 2008] Higley, M. J. and Sabatini, B. L. (2008). Calcium signaling in dendrites and spines: practical and functional considerations. *Neuron*, 59(6):902–913.
- [Hines and Carnevale, 1997] Hines, M. L. and Carnevale, N. T. (1997). The NEURON simulation environment. *Neural Computation*, 9(6):1179–1209.
- [Hines and Carnevale, 2001] Hines, M. L. and Carnevale, N. T. (2001). NEURON: a tool for neuroscientists. *The Neuroscientist*, 7(2):123–135.
- [Hines et al., 2004] Hines, M. L., Morse, T., Migliore, M., Carnevale, N. T., and Shepherd, G. M. (2004). ModelDB: A Database to Support Computational Neuroscience. *Journal of Computational Neuroscience*, 17(1):7–11.
- [Hodgkin and Huxley, 1952] Hodgkin, A. L. and Huxley, A. F. (1952). A quantitative description of membrane current and its application to conduction and excitation in nerve. *The Journal of Physiology*, 117(4):500–544.
- [Hoffman et al., 1997] Hoffman, D. A., Magee, J. C., Colbert, C. M., and Johnston, D. (1997). K^+ channel regulation of signal propagation in dendrites of hippocampal pyramidal neurons. *Nature*, 387(6636):869–875.
- [Holbro et al., 2010] Holbro, N., Grunditz, A., Wiegert, J. S., and Oertner, T. G. (2010). AMPA receptors gate spine Ca^{2+} transients and spike-timing-dependent potentiation. *Proceedings of the National Academy of Sciences*, 107(36):15975–15980.
- [Izhikevich, 2003] Izhikevich, E. M. (2003). Simple model of spiking neurons. *IEEE Transactions on Neural Networks*, 14(6):1569–1572.
- [Izhikevich, 2004] Izhikevich, E. M. (2004). Which model to use for cortical spiking neurons? *IEEE Transactions on Neural networks*, 15(5):1063–1070.
- [Izhikevich and Desai, 2003] Izhikevich, E. M. and Desai, N. S. (2003). Relating STDP to BCM. *Neural Computation*, 15(7):1511–1523.
- [Jahr and Stevens, 1990] Jahr, C. E. and Stevens, C. F. (1990). A quantitative description of NMDA receptor-channel kinetic behavior. *The Journal of Neuroscience*, 10(6):1830–1837.
- [Jarsky et al., 2005] Jarsky, T., Roxin, A., Kath, W. L., and Spruston, N. (2005). Conditional dendritic spike propagation following distal synaptic activation of hippocampal CA1 pyramidal neurons. *Nature Neuroscience*, 8(12):1667–1676.
- [Johnston et al., 2003] Johnston, D., Christie, B. R., Frick, A., Gray, R., Hoffman, D. A., Schexnayder, L. K., Watanabe, S., and Yuan, L.-L. (2003). Active dendrites, potassium channels and synaptic plasticity. *Philosophical Transactions of the Royal Society of London. Series B, Biological Sciences*, 358(1432):667–674.

- [Kampa et al., 2004] Kampa, B. M., Clements, J., Jonas, P., and Stuart, G. J. (2004). Kinetics of Mg^{2+} unblock of NMDA receptors: implications for spike-timing dependent synaptic plasticity. *The Journal of Physiology*, 556(2):337–345.
- [Kampa and Stuart, 2006] Kampa, B. M. and Stuart, G. J. (2006). Calcium spikes in basal dendrites of layer 5 pyramidal neurons during action potential bursts. *The Journal of Neuroscience*, 26(28):7424–7432.
- [Kawaguchi and Kubota, 1993] Kawaguchi, Y. and Kubota, Y. (1993). Correlation of physiological subgroupings of nonpyramidal cells with parvalbumin and calbinding immunoreactive neurons in layer V of rat frontal cortex. *Journal of Neurophysiology*, 70:387–396.
- [Keller et al., 2008] Keller, D. X., Franks, K. M., Bartol, Jr, T. M., and Sejnowski, T. J. (2008). Calmodulin activation by calcium transients in the postsynaptic density of dendritic spines. *PLoS One*, 3(4):e2045.
- [Kelso et al., 1986] Kelso, S. R., Ganong, A. H., and Brown, T. H. (1986). Hebbian synapses in hippocampus. *Proceedings of the National Academy of Sciences*, 83(14):5326–5330.
- [Kempster et al., 2001] Kempster, R., Gerstner, W., and van Hemmen, J. L. (2001). Intrinsic stabilization of output rates by spike-based Hebbian learning. *Neural Computation*, 13(12):2709–2741.
- [Kepecs et al., 2002] Kepecs, A., van Rossum, M. C. W., Song, S., and Tegner, J. (2002). Spike-timing-dependent plasticity: common themes and divergent vistas. *Biological Cybernetics*, 87(5-6):446–458.
- [Knoblauch et al., 2012] Knoblauch, A., Hauser, F., Gewaltig, M.-O., Körner, E., and Palm, G. (2012). Does spike-timing-dependent synaptic plasticity couple or decouple neurons firing in synchrony? *Frontiers in Computational Neuroscience*, 6.
- [Kobayashi et al., 2009] Kobayashi, R., Tsubo, Y., and Shinomoto, S. (2009). Made-to-order spiking neuron model equipped with a multi-timescale adaptive threshold. *Frontiers in Computational Neuroscience*, 3:9.
- [Koch and Zador, 1993] Koch, C. and Zador, A. (1993). The function of dendritic spines: devices subserving biochemical rather than electrical compartmentalization. *The Journal of Neuroscience*, 13(2):413–422.
- [Kotaleski and Blackwell, 2010] Kotaleski, J. H. and Blackwell, K. T. (2010). Modelling the molecular mechanisms of synaptic plasticity using systems biology approaches. *Nature Reviews Neuroscience*, 11(4):239–251.
- [Kreitzer, 2009] Kreitzer, A. C. (2009). Physiology and pharmacology of striatal neurons. *Annual Review Neuroscience*, 32:127–147.

- [Kumar and Kotaleski, 2014] Kumar, A. and Kotaleski, J. H. (2014). <http://www.bcf.uni-freiburg.de/events/conferences-workshops/20140409-cns-workshop-2014>.
- [Langley et al., 1987] Langley, P., Simon, H. A., Bradshaw, G. L., and Zytkow, J. M. (1987). *Scientific Discovery: Computational Explorations of the Creative Processes*. The MIT Press, Cambridge, MA.
- [Le Novere, 2006] Le Novere, N. (2006). Model storage, exchange and integration. *BMC Neuroscience*, 7 Suppl 1:S11.
- [Lee et al., 2009] Lee, S.-J. R., Escobedo-Lozoya, Y., Szatmari, E. M., and Yasuda, R. (2009). Activation of CaMKII in single dendritic spines during long-term potentiation. *Nature*, 458(7236):299–304.
- [Lee Rodgers and Nicewander, 1988] Lee Rodgers, J. and Nicewander, W. A. (1988). Thirteen ways to look at the correlation coefficient. *The American Statistician*, 42(1):59–66.
- [Lerner and Kreitzer, 2012] Lerner, T. N. and Kreitzer, A. C. (2012). RGS4 is required for dopaminergic control of striatal LTD and susceptibility to parkinsonian motor deficits. *Neuron*, 73(2):347–359.
- [Lindahl et al., 2013] Lindahl, M., Sarvestani, I. K., Ekeberg, Ö., and Kotaleski, J. H. (2013). Signal enhancement in the output stage of the basal ganglia by synaptic short-term plasticity in the direct, indirect, and hyperdirect pathways. *Frontiers in Computational Neuroscience*, 7.
- [Lisman and Spruston, 2005] Lisman, J. and Spruston, N. (2005). Postsynaptic depolarization requirements for LTP and LTD: a critique of spike timing-dependent plasticity. *Nature Neuroscience*, 8(7):839–841.
- [Lisman and Spruston, 2010] Lisman, J. and Spruston, N. (2010). Questions about STDP as a General Model of Synaptic Plasticity. *Frontiers in Synaptic Neuroscience*, 2:140.
- [Longordo et al., 2013] Longordo, F., To, M.-S., Ikeda, K., and Stuart, G. J. (2013). Sub-linear integration underlies binocular processing in primary visual cortex. *Nature Neuroscience*, 16(6):714–723.
- [Lu et al., 2009] Lu, W., Shi, Y., Jackson, A. C., Bjorgan, K., Doring, M. J., Sprengel, R., Seeburg, P. H., and Nicoll, R. A. (2009). Subunit composition of synaptic AMPA receptors revealed by a single-cell genetic approach. *Neuron*, 62(2):254–268.
- [Ma and Jazayeri, 2014] Ma, W. J. and Jazayeri, M. (2014). Neural coding of uncertainty and probability. *Annual Review Neuroscience*, 37:205–220.
- [Maass and Sontag, 2000] Maass, W. and Sontag, E. (2000). Neural systems as nonlinear filters. *Neural Computation*, 12(8):1743–1772.

- [Magee and Cook, 2000] Magee, J. C. and Cook, E. P. (2000). Somatic EPSP amplitude is independent of synapse location in hippocampal pyramidal neurons. *Nature Neuroscience*, 3(9):895–903.
- [Magee and Johnston, 1995] Magee, J. C. and Johnston, D. (1995). Synaptic activation of voltage-gated channels in the dendrites of hippocampal pyramidal neurons. *Science*, 268(5208):301–304.
- [Magee and Johnston, 1997] Magee, J. C. and Johnston, D. (1997). A synaptically controlled, associative signal for Hebbian plasticity in hippocampal neurons. *Science*, 275(5297):209–213.
- [Magistretti and Alonso, 1999] Magistretti, J. and Alonso, A. (1999). Slow Voltage Dependent Inactivation of a Sustained Sodium Current in Stellate Cells of Rat Entorhinal Cortex Layer II. *Annals of the New York Academy of Sciences*, 868(1):84–87.
- [Major et al., 2008] Major, G., Polsky, A., Denk, W., Schiller, J., and Tank, D. W. (2008). Spatiotemporally graded NMDA spike/plateau potentials in basal dendrites of neocortical pyramidal neurons. *Journal of Neurophysiology*, 99(5):2584–2601.
- [Malinow and Malenka, 2002] Malinow, R. and Malenka, R. C. (2002). AMPA receptor trafficking and synaptic plasticity. *Annual Review Neuroscience*, 25:103–126.
- [Manninen et al., 2010] Manninen, T., Hituri, K., Kotaleski, J. H., Blackwell, K. T., and Linne, M.-L. (2010). Postsynaptic signal transduction models for long-term potentiation and depression. *Frontiers in Computational Neuroscience*, 4:152.
- [Margolis et al., 2008] Margolis, E. B., Mitchell, J. M., Ishikawa, J., Hjelmstad, G. O., and Fields, H. L. (2008). Midbrain dopamine neurons: projection target determines action potential duration and dopamine D(2) receptor inhibition. *The Journal of Neuroscience*, 28(36):8908–8913.
- [Markram et al., 2011] Markram, H., Gerstner, W., and Sjöström, P. J. (2011). A history of spike-timing-dependent plasticity. *Frontiers in Synaptic Neuroscience*, 3.
- [Markram et al., 1997] Markram, H., Lübke, J., Frotscher, M., and Sakmann, B. (1997). Regulation of synaptic efficacy by coincidence of postsynaptic APs and EPSPs. *Science*, 275(5297):213–215.
- [Markram and Tsodyks, 1996] Markram, H. and Tsodyks, M. (1996). Redistribution of synaptic efficacy between neocortical pyramidal neurons. *Nature*, 382(6594):807–810.
- [Martina and Jonas, 1997] Martina, M. and Jonas, P. (1997). Functional differences in Na⁺ channel gating between fast-spiking interneurons and principal neurons of rat hippocampus. *The Journal of Physiology*, 505(3):593–603.

- [Matsuda, 1991] Matsuda, H. (1991). Magnesium gating of the inwardly rectifying K⁺ channel. *Annual Review of Physiology*, 53:289–298.
- [Matsuzaki et al., 2001] Matsuzaki, M., Ellis-Davies, G. C., Nemoto, T., Miyashita, Y., Iino, M., and Kasai, H. (2001). Dendritic spine geometry is critical for AMPA receptor expression in hippocampal CA1 pyramidal neurons. *Nature Neuroscience*, 4(11):1086–1092.
- [Matsuzaki et al., 2004] Matsuzaki, M., Honkura, N., Ellis-Davies, G. C., and Kasai, H. (2004). Structural basis of long-term potentiation in single dendritic spines. *Nature*, 429(6993):761–766.
- [Mattioni and Le Novere, 2013] Mattioni, M. and Le Novere, N. (2013). Integration of biochemical and electrical signaling-multiscale model of the medium spiny neuron of the striatum. *PLoS One*, 8(7):e66811.
- [McCormick et al., 1985] McCormick, D. A., Connors, B. W., Lighthall, J. W., and Prince, D. A. (1985). Comparative electrophysiology of pyramidal and sparsely spiny stellate neurons of the neocortex. *Journal of Neurophysiology*, 54(4):782–806.
- [McCulloch and Pitts, 1943] McCulloch, W. S. and Pitts, W. (1943). A logical calculus of the ideas immanent in nervous activity. *The Bulletin of Mathematical Biophysics*, 5(4):115–133.
- [Mermelstein et al., 1998] Mermelstein, P. G., Song, W. J., Tkatch, T., Yan, Z., and Surmeier, D. J. (1998). Inwardly rectifying potassium (IRK) currents are correlated with IRK subunit expression in rat nucleus accumbens medium spiny neurons. *The Journal of Neuroscience*, 18(17):6650–6661.
- [Migliore et al., 1999] Migliore, M., Hoffman, D. A., Magee, J. C., and Johnston, D. (1999). Role of an A-type K⁺ conductance in the back-propagation of action potentials in the dendrites of hippocampal pyramidal neurons. *Journal of Computational Neuroscience*, 7(1):5–15.
- [Morishita et al., 2001] Morishita, W., Connor, J. H., Xia, H., Quinlan, E. M., Shenolikar, S., and Malenka, R. C. (2001). Regulation of synaptic strength by protein phosphatase 1. *Neuron*, 32(6):1133–1148.
- [Morrison et al., 2007] Morrison, A., Aertsen, A., and Diesmann, M. (2007). Spike-timing-dependent plasticity in balanced random networks. *Neural Computation*, 19(6):1437–1467.
- [Moyer et al., 2007] Moyer, J. T., Wolf, J. A., and Finkel, L. H. (2007). Effects of dopaminergic modulation on the integrative properties of the ventral striatal medium spiny neuron. *Journal of Neurophysiology*, 98(6):3731–3748.

- [Nazzaro et al., 2012] Nazzaro, C., Greco, B., Cerovic, M., Baxter, P., Rubino, T., Trusel, M., Parolaro, D., Tkatch, T., Benfenati, F., Pedarzani, P., and Tonini, R. (2012). SK channel modulation rescues striatal plasticity and control over habit in cannabinoid tolerance. *Nature Neuroscience*, 15(2):284–293.
- [Nevian and Sakmann, 2006] Nevian, T. and Sakmann, B. (2006). Spine Ca^{2+} signaling in spike-timing-dependent plasticity. *The Journal of Neuroscience*, 26(43):11001–11013.
- [Ngezahayo et al., 2000] Ngezahayo, A., Schachner, M., and Artola, A. (2000). Synaptic activity modulates the induction of bidirectional synaptic changes in adult mouse hippocampus. *The Journal of Neuroscience*, 20(7):2451–2458.
- [Nisenbaum et al., 1996] Nisenbaum, E. S., Wilson, C. J., Foehring, R. C., and Surmeier, D. J. (1996). Isolation and characterization of a persistent potassium current in neostriatal neurons. *Journal of Neurophysiology*, 76(2):1180–1194.
- [Noguchi et al., 2005] Noguchi, J., Matsuzaki, M., Ellis-Davies, G. C. R., and Kasai, H. (2005). Spine-neck geometry determines NMDA receptor-dependent Ca^{2+} signaling in dendrites. *Neuron*, 46(4):609–622.
- [Nowak et al., 1984] Nowak, L., Bregestovski, P., Ascher, P., Herbert, A., and Prochiantz, A. (1984). Magnesium gates glutamate-activated channels in mouse central neurones. *Nature*, 307(5950):462–465.
- [Oikonomou et al., 2014] Oikonomou, K. D., Singh, M. B., Sterjanaj, E. V., and Antic, S. D. (2014). Spiny neurons of amygdala, striatum, and cortex use dendritic plateau potentials to detect network UP states. *Frontiers in Cellular Neuroscience*, 8:292.
- [O’Reilly et al., 2012] O’Reilly, J. X., Jbabdi, S., and Behrens, T. E. J. (2012). How can a bayesian approach inform neuroscience? *European Journal of Neuroscience*, 35(7):1169–1179.
- [Peyrache et al., 2015] Peyrache, A., Lacroix, M. M., Petersen, P. C., and Buzsaki, G. (2015). Internally organized mechanisms of the head direction sense. *Nature Neuroscience*, 18(4):569–575.
- [Plotkin et al., 2011] Plotkin, J. L., Day, M., and Surmeier, D. J. (2011). Synaptically driven state transitions in distal dendrites of striatal spiny neurons. *Nature Neuroscience*, 14(7):881–888.
- [Plotkin and Surmeier, 2015] Plotkin, J. L. and Surmeier, D. J. (2015). Corticostriatal synaptic adaptations in Huntington’s disease. *Current Opinion in Neurobiology*, 33C:53–62.
- [Polsky et al., 2004] Polsky, A., Mel, B. W., and Schiller, J. (2004). Computational subunits in thin dendrites of pyramidal cells. *Nature Neuroscience*, 7(6):621–627.

- [Pouget et al., 2013] Pouget, A., Beck, J. M., Ma, W. J., and Latham, P. E. (2013). Probabilistic brains: knowns and unknowns. *Nature Neuroscience*, 16(9):1170–1178.
- [Rall, 1964] Rall, W. (1964). Theoretical significance of dendritic trees for neuronal input-output relations. In Reiss, R. and Alto, P., editors, *Neural Theory and Modeling*. Stanford University Press.
- [Rall, 1977] Rall, W. (1977). *Core Conductor Theory and Cable Properties of Neurons*, volume 1, pages 39–97. American Physiological Society.
- [Reilly et al., 2011] Reilly, J. E., Hanson, H. H., and Phillips, G. R. (2011). Persistence of excitatory shaft synapses adjacent to newly emerged dendritic protrusions. *Molecular and Cellular Neurosciences*, 48(2):129–136.
- [Salinas and Sejnowski, 2001] Salinas, E. and Sejnowski, T. J. (2001). Correlated neuronal activity and the flow of neural information. *Nature Reviews Neuroscience*, 2(8):539–550.
- [Schiller et al., 2000] Schiller, J., Major, G., Koester, H. J., and Schiller, Y. (2000). NMDA spikes in basal dendrites of cortical pyramidal neurons. *Nature*, 404(6775):285–289.
- [Segev and London, 2000] Segev, I. and London, M. (2000). Untangling dendrites with quantitative models. *Science*, 290(5492):744–750.
- [Segev and Rall, 1988] Segev, I. and Rall, W. (1988). Computational study of an excitable dendritic spine. *Journal of Neurophysiology*, 60(2):499–523.
- [Segev et al., 1994] Segev, I., Rinzel, J., and Shepherd, G. M., editors (1994). *The Theoretical Foundations of Dendritic Function: The Selected Papers of Wilfrid Rall with Commentaries (Computational Neuroscience)*. The MIT Press; 1 Edition.
- [Sejnowski, 2003] Sejnowski, T. J. (2003). The once and future Hebb synapse. *Canadian Psychology*, 44(1):17.
- [Shai et al., 2014] Shai, A. S., Koch, C., and Anastassiou, C. A. (2014). Spike-timing control by dendritic plateau potentials in the presence of synaptic barrages. *Frontiers in Computational Neuroscience*, 8.
- [Shen et al., 2008] Shen, W., Flajolet, M., Greengard, P., and Surmeier, D. J. (2008). Dichotomous dopaminergic control of striatal synaptic plasticity. *Science*, 321(5890):848–851.
- [Shen et al., 2004] Shen, W., Hernandez-Lopez, S., Tkatch, T., Held, J. E., and Surmeier, D. J. (2004). Kv1.2-containing K⁺ channels regulate subthreshold excitability of striatal medium spiny neurons. *Journal of Neurophysiology*, 91(3):1337–1349.
- [Shouval et al., 2002] Shouval, H. Z., Bear, M. F., and Cooper, L. N. (2002). A unified model of NMDA receptor-dependent bidirectional synaptic plasticity. *Proceedings of the National Academy of Sciences*, 99(16):10831–10836.

- [Sjöström et al., 2001] Sjöström, P. J., Turrigiano, G. G., and Nelson, S. B. (2001). Rate, timing, and cooperativity jointly determine cortical synaptic plasticity. *Neuron*, 32(6):1149–1164.
- [Smith et al., 2012] Smith, A. M., Xu, W., Sun, Y., Faeder, J. R., and Marai, G. E. (2012). RuleBender: integrated modeling, simulation and visualization for rule-based intracellular biochemistry. *BMC Bioinformatics*, 13 Suppl 8:S3.
- [Smith et al., 2013] Smith, S. L., Smith, I. T., Branco, T., and Häusser, M. (2013). Dendritic spikes enhance stimulus selectivity in cortical neurons in vivo. *Nature*, 503(7474):115–120.
- [Smith et al., 2014] Smith, Y., Galvan, A., Ellender, T. J., Doig, N., Villalba, R. M., Huerta-Ocampo, I., Wichmann, T., and Bolam, J. P. (2014). The thalamostriatal system in normal and diseased states. *Frontiers in Systems Neuroscience*, 8.
- [Song and Abbott, 2001] Song, S. and Abbott, L. F. (2001). Cortical development and remapping through spike timing-dependent plasticity. *Neuron*, 32(2):339–350.
- [Song et al., 2000] Song, S., Miller, K. D., and Abbott, L. F. (2000). Competitive Hebbian learning through spike-timing-dependent synaptic plasticity. *Nature Neuroscience*, 3(9):919–926.
- [Song et al., 2005] Song, S., Sjöström, P. J., Reigl, M., Nelson, S., and Chklovskii, D. B. (2005). Highly Nonrandom Features of Synaptic Connectivity in Local Cortical Circuits. *PLoS Biol.*, 3(3):e68.
- [Sparkes et al., 2010] Sparkes, A., Aubrey, W., Byrne, E., Clare, A., Khan, M. N., Liakata, M., Markham, M., Rowland, J., Soldatova, L. N., Whelan, K. E., Young, M., and King, R. D. (2010). Towards Robot Scientists for autonomous scientific discovery. *Automated Experimentation*, 2:1.
- [Spruston et al., 1995] Spruston, N., Schiller, Y., Stuart, G., and Sakmann, B. (1995). Activity-dependent action potential invasion and calcium influx into hippocampal CA1 dendrites. *Science*, 268(5208):297–300.
- [Stanley et al., 2012] Stanley, G. B., Jin, J., Wang, Y., Desbordes, G., Wang, Q., Black, M. J., and Alonso, J.-M. (2012). Visual orientation and directional selectivity through thalamic synchrony. *The Journal of Neuroscience*, 32(26):9073–9088.
- [Stuart and Sakmann, 1994] Stuart, G. J. and Sakmann, B. (1994). Active propagation of somatic action potentials into neocortical pyramidal cell dendrites. *Nature*, 367(6458):69–72.
- [Surmeier et al., 2014] Surmeier, D. J., Graves, S. M., and Shen, W. (2014). Dopaminergic modulation of striatal networks in health and Parkinson’s disease. *Current Opinion in Neurobiology*, 29C:109–117.

- [Svoboda et al., 1996] Svoboda, K., Tank, D. W., and Denk, W. (1996). Direct measurement of coupling between dendritic spines and shafts. *Science*, pages 716–718.
- [Tkatch et al., 2000] Tkatch, T., Baranauskas, G., and Surmeier, D. J. (2000). Kv4.2 mRNA abundance and A-type K(+) current amplitude are linearly related in basal ganglia and basal forebrain neurons. *The Journal of Neuroscience*, 20(2):579–588.
- [Tønnesen et al., 2014] Tønnesen, J., Katona, G., Rózsa, B., and Nägerl, U. V. (2014). Spine neck plasticity regulates compartmentalization of synapses. *Nature Neuroscience*, 17(5):678–685.
- [Torre and Poggio, 1978] Torre, V. and Poggio, T. (1978). A synaptic mechanism possibly underlying directional selectivity to motion. *Proceedings of the Royal Society of London. Series B. Biological Sciences*, 202(1148):409–416.
- [Traub et al., 2003] Traub, R. D., Buhl, E. H., Gloveli, T., and Whittington, M. A. (2003). Fast rhythmic bursting can be induced in layer 2/3 cortical neurons by enhancing persistent Na⁺ conductance or by blocking BK channels. *Journal of Neurophysiology*, 89(2):909–921.
- [Truccolo et al., 2011] Truccolo, W., Donoghue, J. A., Hochberg, L. R., Eskandar, E. N., Madsen, J. R., Anderson, W. S., Brown, E. N., Halgren, E., and Cash, S. S. (2011). Single-neuron dynamics in human focal epilepsy. *Nature Neuroscience*, 14(5):635–641.
- [Tsay and Yuste, 2002] Tsay, D. and Yuste, R. (2002). Role of dendritic spines in action potential backpropagation: a numerical simulation study. *Journal of Neurophysiology*, 88(5):2834–2845.
- [Tsodyks and Markram, 1997] Tsodyks, M. V. and Markram, H. (1997). The neural code between neocortical pyramidal neurons depends on neurotransmitter release probability. *Proceedings of the National Academy of Sciences*, 94(2):719–723.
- [Turrigiano, 2008] Turrigiano, G. G. (2008). The self-tuning neuron: synaptic scaling of excitatory synapses. *Cell*, 135(3):422–435.
- [Urakubo et al., 2008] Urakubo, H., Honda, M., Froemke, R. C., and Kuroda, S. (2008). Requirement of an Allosteric Kinetics of NMDA Receptors for Spike Timing-Dependent Plasticity. *The Journal of Neuroscience*, 28(13):3310–3323.
- [Van Rossum et al., 2000] Van Rossum, M. C., Bi, G. Q., and Turrigiano, G. G. (2000). Stable Hebbian learning from spike timing-dependent plasticity. *The Journal of Neuroscience*, 20(23):8812–8821.
- [Wang et al., 1991] Wang, X.-J., Rinzel, J., and Rogawski, M. A. (1991). A model of the T-type calcium current and the low-threshold spike in thalamic neurons. *Journal of Neurophysiology*, 66(3):839–850.

- [Wheeler et al., 1996] Wheeler, D. B., Randall, A., and Tsien, R. W. (1996). Changes in action potential duration alter reliance of excitatory synaptic transmission on multiple types of Ca^{2+} channels in rat hippocampus. *The Journal of Neuroscience*, 16(7):2226–2237.
- [Wiegert and Oertner, 2011] Wiegert, J. S. and Oertner, T. G. (2011). Shapeshifting for memory. *e-Neuroforum*, 2(1):6–12.
- [Williams and Stuart, 2002] Williams, S. R. and Stuart, G. J. (2002). Dependence of EPSP efficacy on synapse location in neocortical pyramidal neurons. *Science*, 295(5561):1907–1910.
- [Williams and Stuart, 2003] Williams, S. R. and Stuart, G. J. (2003). Role of dendritic synapse location in the control of action potential output. *Trends in Neurosciences*, 26(3):147–154.
- [Wilson, 1992] Wilson, C. J. (1992). Dendritic morphology, inward rectification, and the functional properties of neostriatal neurons. In *Single Neuron Computation*, pages 141–171.
- [Wilson and Kawaguchi, 1996] Wilson, C. J. and Kawaguchi, Y. (1996). The origins of two-state spontaneous membrane potential fluctuations of neostriatal spiny neurons. *The Journal of Neuroscience*, 16(7):2397–2410.
- [Wolf et al., 2005] Wolf, J. A., Moyer, J. T., Lazarewicz, M. T., Contreras, D., Benoit-Marand, M., O'Donnell, P., and Finkel, L. H. (2005). NMDA/AMPA ratio impacts state transitions and entrainment to oscillations in a computational model of the nucleus accumbens medium spiny projection neuron. *The Journal of Neuroscience*, 25(40):9080–9095.
- [Yuste, 2013] Yuste, R. (2013). Electrical compartmentalization in dendritic spines. *Annual Review Neuroscience*, 36:429–449.
- [Yuste, 2015] Yuste, R. (2015). The discovery of dendritic spines by cajal. *Frontiers in Neuroanatomy*, 9(18).
- [Yuste and Bonhoeffer, 2001] Yuste, R. and Bonhoeffer, T. (2001). Morphological changes in dendritic spines associated with long-term synaptic plasticity. *Annual Review Neuroscience*, 24(1):1071–1089.
- [Zador, 2000] Zador, A. M. (2000). The basic unit of computation. *Nature Neuroscience*, 3:1167–1167.
- [Zhang et al., 2008] Zhang, Y.-P., Holbro, N., and Oertner, T. G. (2008). Optical induction of plasticity at single synapses reveals input-specific accumulation of αCaMKII . *Proceedings of the National Academy of Sciences*, 105(33):12039–12044.

- [Zheng and Schwabe, 2011a] Zheng, Y. and Schwabe, L. (2011a). Knowledge representation meets simulation to investigate memory problems after seizures. In Hu, B., Liu, J., Chen, L., and Zhong, N., editors, *Brain Informatics*, volume 6889 of *Lecture Notes in Computer Science*, pages 76–87. Springer Berlin Heidelberg.
- [Zheng and Schwabe, 2011b] Zheng, Y. and Schwabe, L. (2011b). Robustness of stdp-induced memory to perturbations of presynaptic activity: a simulation study. *BMC Neuroscience*, 12(Suppl 1),P290.
- [Zheng and Schwabe, 2013a] Zheng, Y. and Schwabe, L. (2013a). Dendritic computations in a rall model with strong distal stimulation. In Mladenov, V., Koprinkova-Hristova, P., Palm, G., Villa, A., Appollini, B., and Kasabov, N., editors, *Artificial Neural Networks and Machine Learning – ICANN 2013*, volume 8131 of *Lecture Notes in Computer Science*, pages 304–311. Springer Berlin Heidelberg.
- [Zheng and Schwabe, 2013b] Zheng, Y. and Schwabe, L. (2013b). Shaping synaptic learning by the duration of the postsynaptic action potential. In *Neural Networks (IJCNN), The 2013 International Joint Conference on*, pages 1–5.
- [Zheng and Schwabe, 2014] Zheng, Y. and Schwabe, L. (2014). Shaping synaptic learning by the duration of postsynaptic action potential in a new STDP model. *PLoS One*, 9(2):e88592.
- [Zheng and Schwabe, 2015] Zheng, Y. and Schwabe, L. (2015). Synaptic amplification by axo-dendritic synapses in a pyramidal neuron model. In *Neural Networks (IJCNN), The 2015 International Joint Conference on*. Accepted.
- [Zheng et al., 2014] Zheng, Y., Schwabe, L., and Plotkin, J. L. (2014). Location-dependent dendritic computation in a modeled striatal projection neuron. In Wermter, S., Weber, C., Duch, W., Honkela, T., Koprinkova-Hristova, P., Magg, S., Palm, G., and Villa, A., editors, *Artificial Neural Networks and Machine Learning – ICANN 2014*, volume 8681 of *Lecture Notes in Computer Science*, pages 741–748. Springer International Publishing.

Theses

1. Single neurons transform input spike trains into output spike sequences. The underlying neuronal computation relies on the cooperation between an array of nonlinear subcellular computational units: dendrite, spine, synapse and synaptic plasticity.
2. The cable equation and compartmental modeling provide an accurate approach to investigating the functional roles of these units in single neuron computation.
3. A compartmental model of striatal principal neuron (SPN) is validated by replicating the experiment of synaptically-driven state transitions.
4. The SPN model predicts that the interaction between dendritic sub-branches implements associative computation, depending on two cellular anatomical ingredients.
5. A compartmental model of cortical pyramidal neuron is built to study the integrative properties of two classes of excitatory synapses (axo-spinous and axo-shaft synapses) and replicate *in-vitro* findings to a reasonable level.
6. The cortical model unifies two contradictory statements in the literature and predicts that distal shaft synapses can achieve higher amplification than spine synapses.
7. The phenomenological approach is taken to study the emergent properties of single neuron computation given a neuron learns to adapt its spiking dynamics and shape weight distribution with spike-timing dependent plasticity (STDP) window.
8. A new phenomenological model that incorporates an AP-dependent learning window simulates the potential effects of action potential (AP) dynamics on STDP. The results suggest that AP duration is another key factor for insensitizing the postsynaptic neural firing and for controlling the shape of synaptic weight distribution.
9. The results described in this thesis provide strong and testable predictions, which if experimentally validated, could offer new insights into the functional consequences of the fundamental computational units of the brain such as shaft synapses that have not yet been investigated.

Liste der wissenschaftlichen Veröffentlichungen und Fachvorträge auf Tagungen

- | | |
|-----------------------------|---|
| JOURNAL
PUBLICATIONS | <ol style="list-style-type: none"> 1. Zheng, Youwei and Schwabe, Lars “Shaping synaptic learning by the duration of postsynaptic action potential in a new STDP model.” <i>PLoS One</i>, 9(2):e88592, 2014. DOI: 10.1371/journal.pone.0088592 |
| CONFERENCE
PROCEEDINGS | <ol style="list-style-type: none"> 1. Zheng, Youwei and Schwabe, Lars “Knowledge Representation Meets Simulation to Investigate Memory Problems after Seizures.” <i>Brain Informatics 2011</i>, 76-87. DOI: 10.1007/978-3-642-23605-1_11 2. Zheng, Youwei and Schwabe, Lars “Dendritic Computations in a Rall Model with Strong Distal Stimulation.” <i>ICANN 2013</i>, 304-311. DOI: 10.1007/978-3-642-40728-4_38 3. Zheng, Youwei and Schwabe, Lars “Shaping synaptic learning by the duration of the postsynaptic action potential.” <i>IJCNN 2013</i>, 1-5. DOI: 10.1109/IJCNN.2013.6706960 4. Zheng, Youwei; Schwabe, Lars and Plotkin, L. Joshua “Location-Dependent Dendritic Computation in a Modeled Striatal Projection Neuron.” <i>ICANN 2014</i>, 741-748. DOI: 10.1007/978-3-319-11179-7_93 5. Zheng, Youwei and Schwabe, Lars “Synaptic amplification by axo-shaft synapses in a pyramidal neuron model.” <i>IJCNN 2015</i>, 1-6. DOI: 10.1109/IJCNN.2015.7280356 |
| ABSTRACTS | <ol style="list-style-type: none"> 1. Zheng, Youwei and Schwabe, Lars “Robustness of STDP-induced memory to perturbations of presynaptic activity: a simulation study.” <i>BMC Neuroscience</i>, 12(Suppl 1):P290, 2011. DOI: 10.1186/1471-2202-12-S1-P290 |
| BOOK CHAPTERS | <ol style="list-style-type: none"> 1. Schwabe, Lars and Zheng, Youwei “Towards Model-Based Brain Imaging with Multi-Scale Modeling.” <i>Neuroimaging - Methods</i>, Peter Bright (Ed.), InTech, 2012. DOI: 10.5772/24693 |
| CONFERENCE
PRESENTATIONS | <ul style="list-style-type: none"> • Poster, The 20th Annual Computational Neuroscience Meeting
Stockholm, Sweden, Jul 2011 • Oral, The 2011 International Conference on Brain Informatics
Lanzhou, China, Sep 2011 • Poster, The 41st Annual Society for Neuroscience Meeting
Washington D.C., USA, Nov 2011 • Oral, The 2013 International Joint Conference on Neural Networks
Dallas, USA, August 2013 • Poster, The 2013 International Conference on Artificial Neural Network
Sofia, Bulgaria, Sep 2013 • Oral, The 2014 International Conference on Artificial Neural Network
Hamburg, Germany, Sep 2014 • Oral, The 2015 International Joint Conference on Neural Networks
Killarney, Ireland, Jul 2015 |

YOUWEI ZHENG

Persönliche Daten

Name

Youwei Zheng

Anschrift

Max-Planck-Str. 1
Nr. 4.08.4

E-Mail

youwei.zheng@uni-rostock.de

geb.

14.07.1986
Shanghai, China

Berufliche Laufbahn

September 2009 – Februar 2010

Diehl Aerospace GmbH
Praktikant: Softwareentwickler

März 2008 – August 2008

InnoGames GmbH
Praktikant: Softwareentwickler

Ausbildung

März 2010 – Present

Universität Rostock
Doktorand

Oktober 2012 – August 2014

Feinberg School of Medicine, Northwestern University
Predoctoral Visiting Scholar

November 2011 – Februar 2012

European Bioinformatics Institute
Predoctoral Visiting Scholar

Oktober 2008 – Februar 2010

Universität Rostock
Master of Science
Computational Engineering

März 2007 – September 2008

Fachhochschule Lübeck
Diplom-Ingenieur (FH)
Information Technology

September 2004 – Februar 2007

East China University of Science and Technology
Bachelor
Electrical Engineering

